2017

Landscape response to Quaternary climate change

Sally Anne Carney

Landscape response to Quaternary climate change

Abstract
The depth of erosion occurring in river catchments may be influenced by prevailing climatic conditions. In order to understand how future climate may influence erosion and soil availability, it is paramount to investigate to what extent erosion has responded to climate in the past. Marine sediments derived from continental catchments document conditions of erosion depth while also recording the history of chemical weathering and system energy. This study incorporates marine sediments from antipodal catchments, the Var River Catchment (southeast France) and the Hokitika River Catchment (western New Zealand South Island), with ages of up to 75ka and 120ka, respectively.

Geochemical and mineralogical techniques were utilized to establish an understanding of the response of catchment-wide erosion and the extent of chemical weathering to climatic variability. Mineralogical analysis was performed via X-ray diffraction, and geochemical techniques included U isotope analysis and major and trace element quantification. Grain size distribution of sediments was analysed to act as a potential proxy for fluvial system energy and to constrain the results of U isotope analysis. Brunauer–Emmett–Teller analysis was performed to measure the surface area of sieved and leached samples, and to subsequently derive comminution and residence ages of sediments.

Analyses indicated a reversal of erosion and weathering responses in the two antipodal catchments, and an inability to determine erosion response to short-lived climatic variability. In the Var, The Last Glacial Maximum and subsequent deglaciation phase coincides with deep and fast erosion and subsequent transition into the Holocene correlates with the onset of increased chemical weathering, shallowing in erosion and increase residence times of sediments. Conversely, in the Hokitika, glacial periods correlate with slightly shallower and slow erosion relative to interglacial periods, though erosion is consistently deep and fast during the past 120 ka due to the prevailing precipitation trends.

Degree Type
Thesis

Degree Name
BSc Hons

Department
School of Earth & Environmental Science

Advisor(s)
Anthony Dosseto

Keywords
uranium isotopes, erosion, quaternary

Landscape response to Quaternary climate change

An investigation of two antipodal orogens using uranium isotopes

Sally Anne Carney

18th October 2017

Submitted in part fulfilment of the requirements of the Honours degree of Bachelor of Science (Advanced)(Honours) in the School of Earth and Environmental Sciences, University of Wollongong 2017.

The information in this thesis is entirely the result of investigations conducted by the author, unless otherwise acknowledged and has not been submitted in part, or otherwise, for any other degree or qualification.

Sally Anne Carney

18th October 2017

Acknowledgements

There are several people who have contributed to positively to my Honours experience. Firstly, to my supervisor Assoc. Prof. Anthony Dosseto, thank you for the many opportunities you have provided by introducing me to the geochemistry world, be it in the lab or the field! Your guidance, enthusiasm and patience over the course of this year have been invaluable.

To Jose Abrantes, Chris Richardson, Lili Yu and Christian Ercolani, thank you for your assistance with both sample preparation and analysis. I would especially like to thank Patrick Wilcox for the immense contribution made to the sample preparation of the Hokitika sediments, and my Var lab rats Nick Fitzpatrick and Bryce Sherborne-Higgins. My appreciation also extends to Dr Alexander Francke, whose help in the lab and company in Canberra and Wellington provided a great addition to my Honours year.

To Matt, thank you for being a great friend to do Honours alongside, and for always giving your honest opinion and support. To my housemates, thanks for all the high stakes choccy-orange wagers, Bachie evenings and most importantly, swift action during car fires. You guys have made this year so enjoyable and provided so many laughs. Anwen, thank you especially for always looking out for me!

To my family and friends, thank you for your encouragement and support this year, especially during the final stages. Jord, thanks especially for the emotional-support donuts and always being there to chat. Finally, to Gwil, thank you for giving me perspective and encouragement when I need it, and for never saying no to a burrito.

Abstract

The depth of erosion occurring in river catchments may be influenced by prevailing climatic conditions. In order to understand how future climate may influence erosion and soil availability, it is paramount to investigate to what extent erosion has responded to climate in the past. Marine sediments derived from continental catchments document conditions of erosion depth while also recording the history of chemical weathering and system energy. This study incorporates marine sediments from antipodal catchments, the Var River Catchment (southeast France) and the Hokitika River Catchment (western New Zealand South Island), with ages of up to 75ka and 120ka, respectively.

Geochemical and mineralogical techniques were utilized to establish an understanding of the response of catchment-wide erosion and the extent of chemical weathering to climatic variability. Mineralogical analysis was performed via X-ray diffraction, and geochemical techniques included U isotope analysis and major and trace element quantification. Grain size distribution of sediments was analysed to act as a potential proxy for fluvial system energy and to constrain the results of U isotope analysis. Brunauer–Emmett–Teller analysis was performed to measure the surface area of sieved and leached samples, and to subsequently derive comminution and residence ages of sediments.

Analyses indicated a reversal of erosion and weathering responses in the two antipodal catchments, and an inability to determine erosion response to short-lived climatic variability. In the Var, The Last Glacial Maximum and subsequent deglaciation phase coincides with deep and fast erosion and subsequent transition into the Holocene correlates with the onset of increased chemical weathering, shallowing in erosion and increase residence times of sediments. Conversely, in the Hokitika, glacial periods correlate with slightly shallower and slow erosion relative to interglacial periods, though erosion is consistently deep and fast during the past 120 ka due to the prevailing precipitation trends.

Table of Contents

List of Figures

List of Tables

1 Introduction

Soil resources are essential for the sustainability of ecosystems and human civilizations. Investigations into the response of soil erosion to past climatic variability may allow for an understanding of the potential future response of soil erosion to future climate change. Although geological evidence for catchment-wide erosion is difficult to obtain, recent advancements in the use of uranium isotope proxies has led to developments in palaeo-erosion proxies (Dosseto & Schaller, 2016). Erosion in a local mountainous catchment may respond to many forcing variables, such as precipitation, seismic activity and vegetation changes. The overlying climatic conditions, which are recorded by palaeoclimatic proxies, may also trigger different modes of erosion, such as creep, mass wasting and abrasion by glaciers.

Previous studies of palaeo-erosional trends in river catchments have investigated a wide range of environments. In general, a positive relationship between periods of high rainfall and erosion is inferred, although this differs between catchments and environments. In the Himalayas, increases in sediment yield and erosion occurred during intensified monsoon conditions, as a function of increased landslide activity (Bookhagen et al., 2005). Similar trends are evident in the Andes and Taiwan (Trauth et al., 2000; Trauth et al., 2003; Hu et al. 2012). Not all studies have indicated a positive relationship between rainfall and erosion (Langbein & Schumm, 1958); Knox, 1972; Blum & Valastro, 1989; Acosta et al., 2015). During humid periods of the Holocene in the United States, decreased erosion has been inferred from silt deposited by poorly energetic rivers (Knox, 1972; Blum & Valastro, 1989). In various climatic zones in the US, sediment yields decrease above a given threshold as a result of increased vegetation density and slope stability caused by greater precipitation (Langbein & Schumm, 1958). Lower denudation rates observed for steeper hillslopes in humid areas in East Africa have also been attributed to dense vegetation, relative to sparsely vegetated, shallower slopes (Acosta et al., 2015). Erosion does not respond to climate change in a linear fashion (Tucker & Slingerland, 1997; Simpson & Castelltort, 2012). As a result of this non-linear relationship, it is imperative to directly quantify how erosion has varied during the past.

Uranium isotopes have recently been used as a tool to infer palaeo-erosion depth of sediments derived from river catchments, due to developments in analytical advances in mass spectrometry (Martin et al., 2015, Suresh et al., 2013, Dosseto, 2015). Uranium isotopes are also applied to sediments to infer the amount of time sediments spend in the catchment through comminution ages and residence times. These applications allow for the reconstruction of the speed and depth of erosion. Mineralogy and elemental ratios are used as proxies for reconstructing chemical weathering histories of catchment soils, which may be related to erosion trends.

The response of erosion to climatic variability in mountainous catchments has been limited to date. Marine sediments derived from mountainous catchments are ideal for investigating the relationship between erosion and climatic variation in the late Quaternary. Two antipodal catchments, the Var River Catchment in southeast France and Hokitika River Catchment in the South Island of New Zealand are investigated in this study. These sediments provide a record of hillslope erosion and sediment transport in alpine regions over the past 70,000 and 210,000 years, respectively. These sites provide convenient foundations on which to construct this study, as their high relief results in reduced lag time between the erosion of soils and deposition in the marine system.

Aims and Objectives

The aim of this study is to investigate how landscapes have responded to climatic variability throughout the late Quaternary period in two mountainous catchments. This is achieved through the development of palaeo-erosion and chemical weathering trends, based on uranium isotope proxies, and elemental and mineralogical abundances, respectively. This study also aims to quantify sediment residence times of sediments through uranium isotopes and surface area characteristics, to enhance understanding of sediment transport in catchments. Environmental reconstruction is achieved through the analysis of marine sediments derived from catchments draining the Southern Alps of New Zealand and the Alps of France.

2 Literature Review

2.1 Late Quaternary palaeoclimate

The purpose of this section is to establish the context of this study. This section reviews climatic variation throughout the late Quaternary, soil production, erosion, transport and deposition characteristics, and the palaeoclimatic indicators that allow for the interpretation of past climate and environments.

2.1.1 An overview of palaeoclimate

The climate of the late Quaternary period is characterised by the alternation of glacial and interglacial periods repeating every 100,000 years since 0.9Ma. Such phases are punctuated by lower periodicity hot and cold events operating on 19ka and 41ka cycles (Bonneau, 2014). These climatic cycles are predominantly controlled by variations in insolation, facilitated by changes in parameters of Earth's orbit. These parameters, including eccentricity, obliquity and axial precession, are referred to as Milankovitch cycles (Imbrie et al., 1992, 1993). Changes in oceanic, atmospheric and cryospheric feedback systems also influence variability of Earth's climate.

Climatic variation is recorded by palaeoclimatic proxies in various media (Figure 2.1; 2.2). Oxygen isotope compositions of ice and seawater, denoted by $\delta^{18}O$, are recorded in polar regions and marine sediments, respectively. Past warm stages are indicated by an increase in the $\delta^{18}O$ of polar ice and by an inverse decrease in the $\delta^{18}O$ of marine sediments. Conversely, cold periods are indicated by a decrease in the $\delta^{18}O$ of ice and increase in marine sediments. Variations in $\delta^{18}O$ are caused by the preferential uptake of the lighter isotope ^{16}O into ice sheets in the H_2O molecule, resulting in a heavier oxygen isotope composition in seawater. Foraminifera, microorganisms composed of calcium carbonate, incorporate oxygen into their shells from the surrounding seawater, and therefore also record the $\delta^{18}O$ of the seawater at the time of formation. The ratios of ^{18}O and ^{16}O are also recorded in calcite crystals during the formation of speleothems. Variations in $\delta^{18}O$ during the Quaternary period have resulted in the subdivision of this period into intervals referred to as Marine Isotope Stages (MIS). Marine Isotope Stages are numbered, with evenly numbered stages representing cold periods and odd-numbered stages representing warm intervals (Figure 2.1).

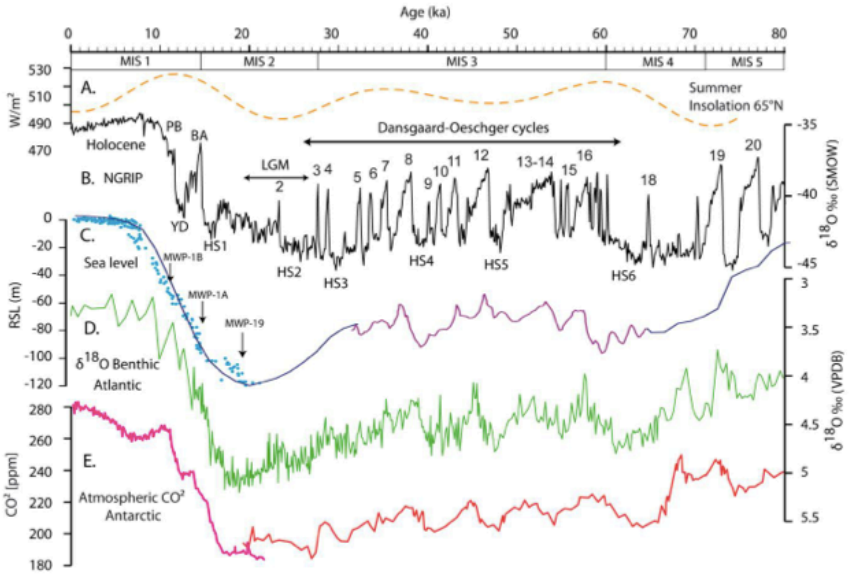

Figure 2.1 Climate records of the past 80ka in the Northern Hemisphere. A. Insolation curve at 65°N. B. $\delta^{18}O$ of Greenland NGRIP ice core. C. Sea level curve. D. $\delta^{18}O$ of benthic foraminifera in the Atlantic. E. Atmospheric CO_2 concentration derived from the Antarctic Dome C core. MWP: Melt water Pulse. MIS: Marine Isotopic Stage. LGM: Last Glacial Maximum. HS: Heinrich stadial events. YD: Younger Dryas; BA: Bølling-Allerød; PB: Préboréal. Dansgaard-Oeschger cycles are noted from 2 to 20 on the B curve. Adapted from Bonneau, 2014.

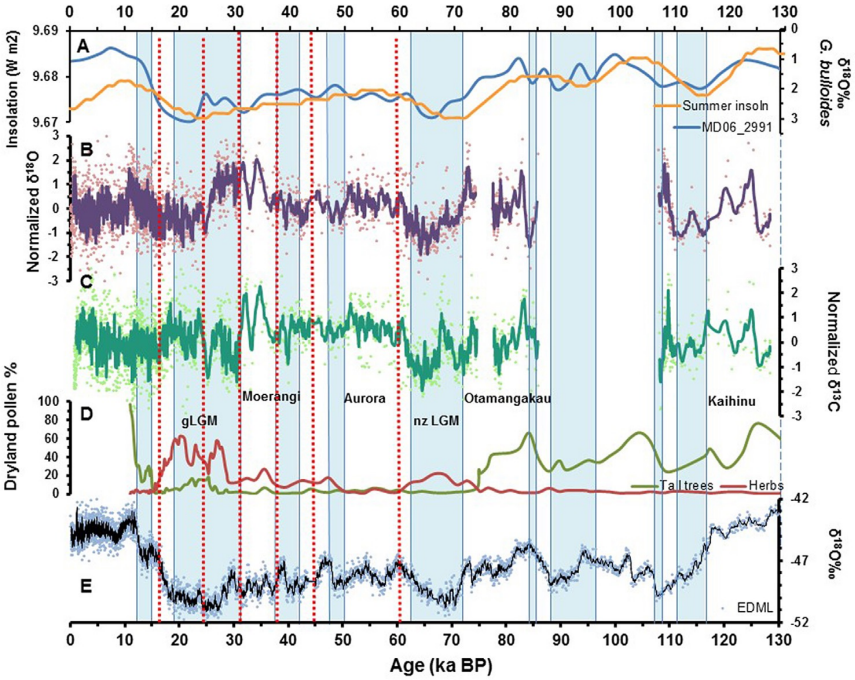

Figure 2.2 Palaeoclimatic records in New Zealand from 130 ka. A. Integrated summer insolation at 45°S (yellow curve) and $\delta^{18}O$ from planktonic foraminifera from marine core MD06-2991 (blue curve). B. Normalised $\delta^{18}O$ from New Zealand speleothems. C. Normalised $\delta^{13}C$ from New Zealand speleothems. D. Tall forest tree and herbfield pollen from Okarito Pahiki core. E. $\delta^{18}O$ record from the EPICA DML ice core (Antarctica). Blue columns represent the main cool intervals in the Southern Alps. White columns represent warm intervals with local names of intervals. Red dashed vertical lines indicate the timing of Heinrich events 1 to 6. From Williams et al., 2015.

Other tools further to oxygen isotopes have been used to reconstruct palaeoclimate (Figure 2.1; 2.2). Relative pollen abundance in sediments allows for reconstruction of palaeo-vegetation, and further provides indicators of climate on the basis of the climatic preferences of the vegetation represented (Ryan et al., 2012). Summer insolation intensity is largely related to variation in Earth's orbital parameters, and has been used to reconstruct climatic conditions (Huybers and Eisenman, 2006). Cosmogenic exposure ages of boulders deposited on glacial moraines provide evidence for the extent and timing of glacial events (Shulmeister et al., 2010).

Analysis of ice core records from both polar regions revealed the *bi-polar see-saw effect*, which describes the alternation of climatic conditions between hemispheres (Blunier and Brook, 2001; EPICA Community Members, 2006; Barker et al., 2009). For example, Antarctic cooling events correspond with the onset of warming Dansgaard-Oeschger events in the northern hemisphere (Figure 2.3). Conversely, when the northern hemisphere enters stadial conditions, warming in the southern hemisphere occurs. This phase relationship has been attributed to changes in the intensity of transfer of heat and freshwater flux via the Atlantic Meridional Overturning Circulation (AMOC), by which a stronger AMOC leads to increased transfer of heat from the Southern Ocean to the Northern Atlantic. As the Var and Hokitika study sites are located in the Northern and Southern hemispheres respectively, it is necessary to consider the influence of the bi-polar see-saw effect on the timing of the same events in both hemispheres. However, work by Williams et al. (2015) has indicated that the see-saw does not have a pronounced effect on the lag between northern hemispheric events and events in New Zealand, as it is not often discerned in local records and events frequently coincide closely with northern hemispheric equivalent events. Though the see-saw is sometimes evident, it has been postulated that the effect diminishes with increasing distance from the poles (Williams et al., 2015).

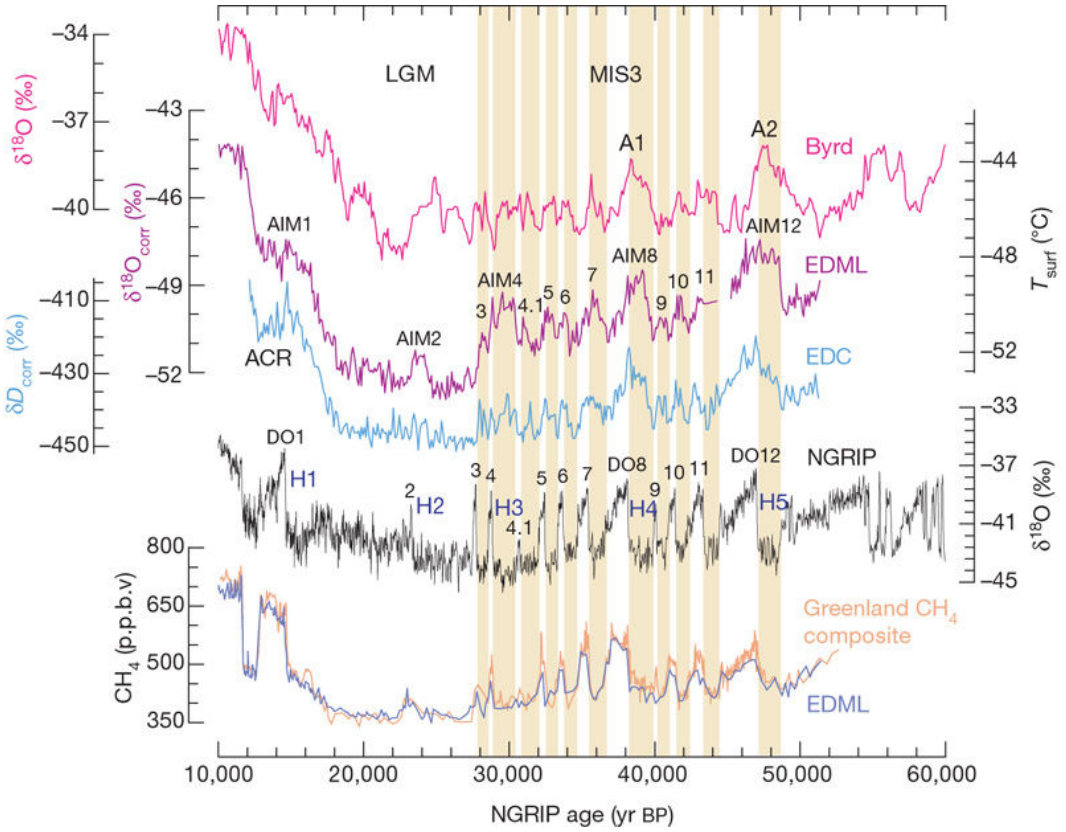

Figure 2.3 100-year averages of $\delta^{18}O$ in ice cores in both hemispheres over the last 60 ka. EDML, EDC and Byrd ice cores in the southern hemisphere are compared with the NGRIP $\delta^{18}O$ record from Northern Greenland. Yellow bars indicate the Greenland stadial periods related to respective Antarctic temperature increases. Heinrich events and Dansgaard-Oeschger events are indicated by H1 to H5 and DO1 to DO12 on the NGRIP curve. AIM: Antarctic Isotope Maximum. ACR: Antarctic Cold Reversal. The y-axis on the right side indicates approximate temperature changes in the EDML core. From EPICA Community Members, 2006.

2.1.2 A Synthesis of late Quaternary palaeoclimate

A profusion of climatic variability has occurred during the late Quaternary in both hemispheres (Figure 2.1, 2.2). In keeping with the age-restraints of the sediment records used in this study, this section will provide an overview of Northern Hemisphere and Southern Hemisphere climate for the past 70 ka and 210ka, respectively. Due to the large amount of available climate proxy data for the local New Zealand region, climatic characterization for this region is much more specific than Northern Hemisphere climatic reconstruction.

New Zealand palaeoclimate

MIS 7: 240ka to 190ka

Marine Isotope Stage 7 is an interglacial interval characterized by a decrease in $\delta^{18}O$ in the marine sediment record, and is divided into sub-stages 7a, 7b and 7c (Figure 2.4). Although there is a significant lack of terrestrial records in New Zealand after MIS 5, a pollen study by Bussell and Pillans (1997) has allowed for the interpretation of climate in New Zealand during MIS 7. MIS 7a spans the period from approximately 180 to 220ka, and thus is the only period relevant to this study (Konijnendijk et. al, 2015). MIS 7a was milder, and possibly warmer and wetter than the present day climate (Bussell & Pillans, 1997). Hardwood pollen abundance also indicates peak interglacial conditions in MIS 7a. The preceding stages of MIS 7b and 7c are described as a cool stadial with precipitation conditions similar to the present day, and a cool, dry interstadial, respectively (Bussell & Pillans, 1997).

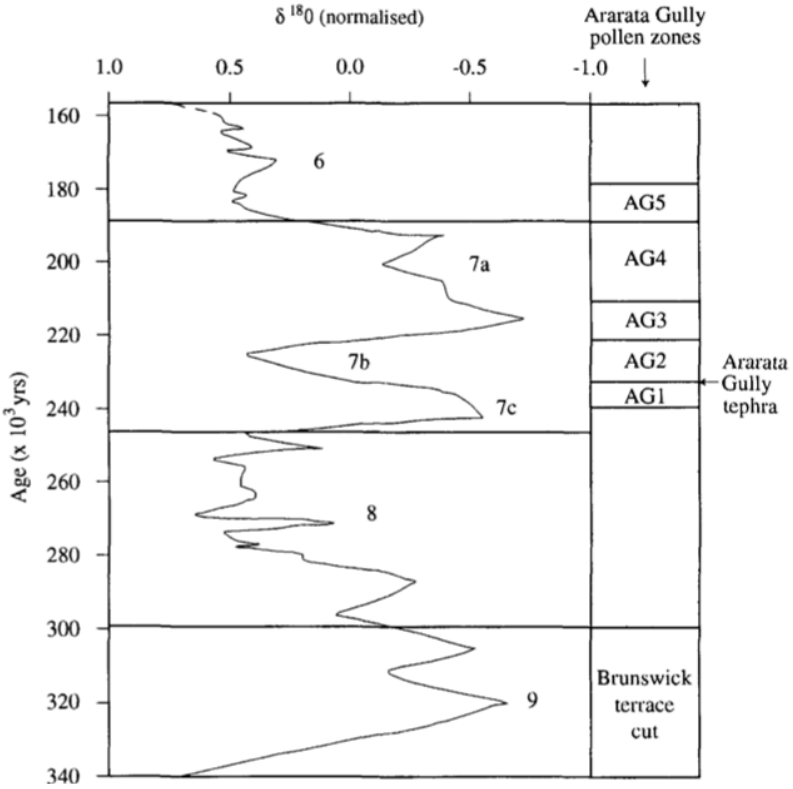

Figure 2.4 Deep-sea $\delta^{18}O$ record from 340 to 160ka and corresponding pollen boundaries in the Ararata Gully, New Zealand. Adapted from Bussell & Pillans, 1997.

MIS 6: 190ka to 129ka

A significant shift in climate at approximately 190ka marks the onset of the glacial conditions of MIS 6 (Figure 2.4). The MIS 6 glacial was similar in intensity to the Last Glacial Maximum (LGM) of MIS 2, but with wetter conditions prevailing (Palmer & Pillans, 1996; Harper & Collen, 2002). These observations are supported by the abundance of *Nothofagus* beech, which favours cool and wet conditions, in the Okarito Pakihi bog core (Ryan et. al., 2012). Gradual vegetation change towards glacial-intolerant vegetation from 140ka onwards represents a gradual increase in temperatures in the lead up to the conclusion of MIS 6, referred to as Termination II, at ~129ka.

MIS 5: 129 to 73ka

On the basis of MIS nomenclature, it is suggested that interglacial conditions dominated during MIS 5. Although warm conditions were apparent during this period, climate was significantly unstable. MIS 5 experienced several episodes of glaciation and temperatures frequently below those of the current Holocene epoch (Williams et al., 2015). MIS 5 is divided into 5 sub-stages representing the stadial and interstadial conditions of the period.

MIS 5e: 129 to 117ka

MIS 5e encompasses the *Last Interglacial Period*, which is locally named the Kaihinu Interglacial in New Zealand (Suggate, 1985, 1990; Moar & Suggate, 1996). The Kaihinu Interglacial experienced the warmest conditions and highest summer insolation values of MIS 5 at 45°S, indicating full interglacial conditions (Williams et al., 2015). Other evidence for extremely warm climate during MIS 5e includes peaks in $\delta^{18}O$ of speleothems and marine sediments, indicating low global ice volume and warm seas (Williams et al., 2015). A peak in forest pollen in the Okarito Pakihi record indicates conditions were at least as warm and humid as the present day (Ryan et. al., 2012). The Kaihinu Glacial is poorly age-constrained but is considered to be the equivalent to the Eemian Interglacial of Europe from 130 to 115ka (Lowe & Walker, 1997). Williams et al. (2015) constrained MIS5e to an 11kyr period from 128 to 117ka, and identified the peak in interglacial conditions between 128 and 122ka.

MIS 5d: 177 to 108ka

A period of cooler stadial conditions followed MIS 5e. MIS 5d is indicated by positive excursions in $\delta^{18}O$ of foraminifera *G. bulloides* in marine sediment cores, and by troughs in $\delta^{18}O$ in Antarctic ice cores, summer insolation and tree pollen percentage in the Okarito Pakihi pollen record (Williams et al., 2015; Ryan et al., 2012). Grassland vegetation dominates the palynology of MIS 5d, further indicating cold conditions (Ryan et al., 2012). MIS 5d was also cool enough to facilitate glacial advance in the Rakaia Valley from 105 to 90ka (Shulmeister et al., 2010).

MIS 5c: 108 to 98ka

Mild conditions characterise MIS 5c, an interstadial period between 108 and 98 ka (Williams et al., 2015). The warmest period of this sub-stage is indicated by summer insolation values culminating at 103ka, and a negative excursion in $\delta^{18}O$ in marine sediments around 100ka. A peak in forest pollen at 104ka provides further evidence for the maximum of warm conditions during this interval (Ryan et al., 2012).

MIS 5b: 97 to 88ka

A return to cool conditions following MIS 5c occurred between 97 and 88ka. During this stadial phase of MIS 5b, significant glacial advance and retreat events occurred on the Cascade Plateau in the Southern Alps (Sutherland et al., 2007). Cool conditions of MIS 5b are further evidenced by negative excursions in $\delta^{18}O$ of speleothems in Tasmania at 87ka and in Antarctic ice core $\delta^{18}O$ values. Low tree pollen percentages in the Okarito Pakihi core occur from 91 to 89ka, further indicating cool conditions (Ryan et al., 2012). Moraines in this region have been dated to 90ka by cosmogenic exposure aging techniques, indicating glacial extent at this time (Goede, 1994).

MIS 5a: 87 to 73ka

The succeeding interstadial period of MIS 5a is the equivalent of the Otamangakau Interstadial in New Zealand (McGlone & Topping, 1983). This period was mild but slightly cooler than the present day, and not as warm as MIS 5e. The Otamangakau Interstadial is indicated by high forest pollen percentages in the Okarito bog record and by growth peaks in local speleothems between 85 and 73ka. $\delta^{18}O$ values identify

MIS 5a as a negative excursion in marine sediments culminating at 82ka (Williams et al., 2015).

MIS 4: 73 to 61ka

Climate rapidly deteriorated following the culmination of MIS 5a, signalling the onset of MIS 4. Major glacial advances, termed the *Otira Glaciation*, occurred during this period in the Southern Alps and Fiordland. This glaciation was the most extreme of the Last Glacial Cycle in New Zealand, even larger than the global Last Glacial Maximum (Williams, 2016). In New Zealand, MIS 4 is evidenced by a sharp plunge in $\delta^{18}O$ values in speleothems at 64ka, indicating rapid cooling. $\delta^{18}O$ of *G. bulloides* in local marine sediment cores, reached values close to those of the global Last Glacial Maximum, and culminated at 67ka. The climate was cool and wet in the west coast of the South Island during MIS 4 (Ryan et al., 2012).

MIS 3: 61 to 29ka

In New Zealand, MIS 3 is divided into one interstadial and two interstadial sub-stages. The Aurora Interstadial extends from 61 to 43 ka, and is identified by a prominent flowstone sheet in the Aurora Cave on the New Zealand South Island (Williams, 1996). This period was predominantly mild and humid, but included a cold excursion from 49 to 47 ka, evidenced by glacial advance in the Southern Alps (Shulmeister et al., 2010). The subsequent stadial period was dry and cool and is evidenced by glacier advance in mountainous regions (Almond et al., 2001; Shulmeister et al., 2010). From 37 to 33 ka, cool conditions with variable precipitation dominated the region (McGlone & Topping, 1983). This period is termed the *Moerangi Interstadial*, and terminated with the first surge of LGM ice after 33.4 ka, as evidenced by the cessation of speleothem growth and various evidence for extensive ice cover (Williams, 1996).

Though MIS 2 is predominantly associated with the global LGM in most regions of the planet, conditions in New Zealand vary from this standard. Maximum glacier extent occurred at 33.0 to 26.5 ka, significantly earlier than the traditional definition of the LGM of 24 to 18 ka (Mix et al., 2001; Clark et al., 2009).

MIS2: 29 to 17ka

As discussed above, MIS 2 is typically associated with the global LGM. Though the greatest extent of glaciers occurred prior to MIS 2 in New Zealand, the coldest phase of the LGM occurred from 29 to 18 ka. This is evidenced by a sharp increase in herbfield pollen in the Okarito Pakihi core (Ryan et al., 2012). This cooling indicator occurs several thousand years prior to the same cooling trend in marine sediment records. Abrupt and rapid glaciation occurred during a 2000-year period in the Te Anau glacier in Fiordland at the onset of MIS 2 (Williams, 1996). This is hypothesized to be a result of prevailing cold and wet climate. Climate subsequently dried while remaining cold throughout the remainder of MIS 2, resulting in the rapid ablation of glaciers (Williams et al., 2015). The rapid glaciation phase evident in New Zealand records preceded glaciation in the northern hemisphere by several thousand years (Williams et al., 2015).

MIS1: 17ka to present

MIS 1 is commonly referred to as the Holocene, the current period of stable warm climate. Pollen and speleothem records identify an increase in temperature from approximately 17 ka following the global LGM (Williams et al., 2015). Speleothem precipitation further indicates warming from 16.5 ka in Nelson on the South Island (Hellstrom et al., 1998). Several phases of warming and cooling have been identified by pollen and macrofossil records from a small lake in the northwest of the South Island (Figure 2.5; Jara et al., 2015). Warming pulses occur between 13 and 10ka, and 7 and 6 ka. During the earlier warming event, temperatures reached ~1.5°C warmer than present, with reduced precipitation and cooler summers (Jara et al., 2015; McGlone et al., 2011). Cooling phases occur from 15 to 13 ka, 10 to 7 ka and 3ka to present in New Zealand (Jara et al., 2015). Cooling from 15 to 13 ka is analogous to the Antarctic Cold Reversal event identified in the EPICA Dome C core (Figure 2.5). The next cooling phase occurs during the global climatic optimum of warmer temperatures, indicating that a closer relationship existed between New Zealand and Antarctic high latitudes during the early Holocene (Jara et al., 2015). Cooling from 3 ka to present is attributed to the increased frequency of El Niño and an increased influence of low latitude climatic conditions on New Zealand since 3 ka.

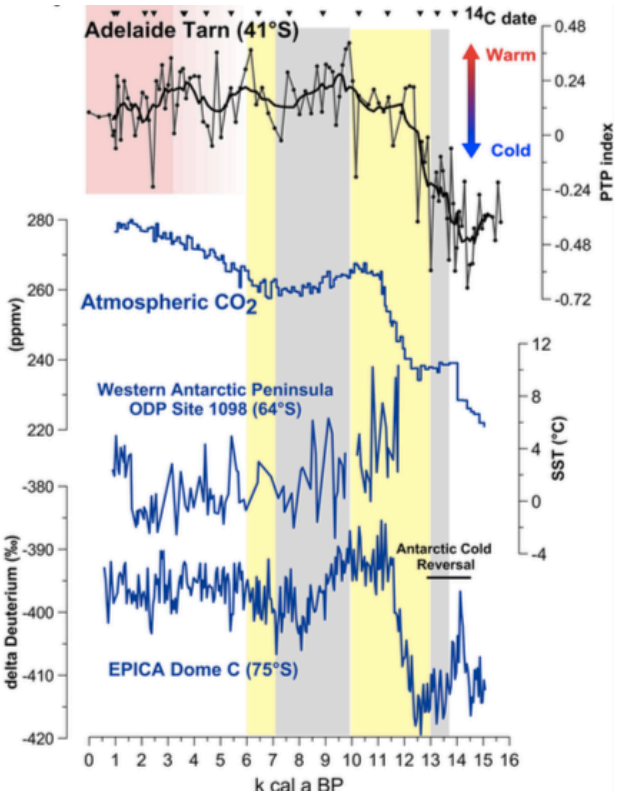

Figure 2.5 Adelaide Tarn pollen reconstruction (black curve) and associated radiocarbon dates (black triangles) compared with proxies from the Pacific, including the global atmospheric CO_2 concentration, sea surface temperature reconstructions from ODP Site 1098 and $\delta^{18}O$ reconstructions of the EPICA Dome C core. Grey and yellow rectangles indicate cooling and warming periods at Adelaide Tarn, respectively. Red rectangles indicate periods of relative increased intensity of the El Niño oscillation.

2.1.2.1 Northern hemisphere palaeoclimate

The last cold stage – 75ka to 10ka

In the Northern Hemisphere, MIS 4, 3 and 2 are often grouped together to represent the *last cold stage*, as conditions during this ~65kyr period were consistently cold (Lowe & Walker, 1997). In central Europe, the Last Cold Stage is referred to as the Würmian Glaciation, and spans the period from 75ka to 10ka. Although the last cold stage was dominated by cold climates, it is also characterized by several short-lived warmer interstadial intervals (Martinson et al., 1987). In marine sediment records, the last cold stage is identified by two isotopically "heavy" periods indicative of major increases in continental ice volume (during MIS4 and MIS2), and an intervening period of isotopically "lighter" yet variable values (during MIS3). The isotope stage boundaries of MIS4/3 and MIS3/2 are dated to 58ka and 23ka, respectively (Martinson et al., 1987). Termination 1, at the end of MIS 2, occurs at ~11ka in the northern hemisphere (Martinson et al., 1987).

Apart from the three-fold division of the last cold stage into Marine Isotope Stages, both marine sediment and ice core climate records have revealed several cooling cycles operating on shorter timescales, in the order of hundreds to thousands of years (Lowe & Walker, 1997). These excursions in isotopic signature represent *Heinrich events*, short-lived intervals of rapid cooling, were first identified by the presence of distinct layers of Ice-rafted Debris (IRD) in marine sediments of the North Atlantic by Heinrich in 1988 (Hemming, 2004; Broecker, 1994). Heinrich events are triggered by the release of armadas of icebergs from the North American Laurentide Icesheet into the Atlantic Ocean via the Hudson Strait, which causes an immense influx of cold, fresh water into the ocean. This subsequently disrupts deep-water formation and ocean circulation in the North Atlantic, causing a change towards cool conditions (Broecker, 1994). Heinrich events appear to be bounded by well-defined episodes of longer-term cooling cycles termed *Daansgaard-Oeschger* (D-O) interstadial events. Signatures of D-O events in ice cores indicate that these events begin abruptly, on the scale of decades, and terminate in a step-wise fashion up to the onset of the following Heinrich event (Figure 2.3; Johnsen et al., 1992). This millennial- and sub-millennial-scale variability is most prominent during MIS3, and punctuates MIS 2 around the time of the Last Glacial Maximum (Bonneau, 2014).

MIS 2 is the coldest period of the last cold stage, as indicated in Figure 2.1, and is dominated by the LGM, the period corresponding to the maximum extent of the global ice sheets, from 26.5ka to 19ka (Bonneau, 2014). Sea level remained relatively stable during the 7,500 years of the LGM at ~110m below present sea level (Clark et al., 2009). Dry conditions prevailed at all latitudes (Mahowald et al., 1999; Gasse 2000; Baker et al., 2001; Wu et al., 2007), resulting in undeveloped vegetation of tundra and steppe, as opposed to present day temperate forests (Velichko et al., 1997; Wu et al., 2007, Ray and Adams, 2001).

The end of the LGM towards 19-20 ka is marked by the recession of the ice caps and rapid rise in sea level of 10 to 15 m (Clark et al., 2009). Subsequently, up to 14.5 ka, the marine level increases more slowly, by less than 3.5 mm/yr (Clark et al., 2009). The subsequent period of glacial to interglacial transitions is referred to as Termination 1, and extends from 19 to 11.7 ka (Bonneau, 2014). Termination 1

includes the sharp warming and cooling events of the Bølling-Allerød from 14.7 to 12.7 ka, the Younger Dryas event, from 12.7 to 11.7 ka, respectively.

MIS1: 11.7ka to present

The Holocene is the warm period of stable climate extending from 11.7ka to the present day. The beginning of this epoch is marked by the Preboreal, a 1000-year period of rapid warming from 11.7ka to 10.7ka (Bonneau, 2014). The Preboreal is followed by a climatic optimum from 9ka to 6ka, with summer insolation values 5-8% greater than the present day, and an intensification of the monsoonal system creating wet conditions, resulting in higher temperatures and precipitation than the present day (Bonneau, 2014). Forests reached their maximum extents and elevations during this period in the Mediterranean region due to the decline in glaciated areas. 6ka marked the complete disappearance of the residual icecaps over North America and rise in sea level. The second half of the Holocene, from 6ka onwards, represents the aridification and decline in temperatures to present day climatic conditions. During this phase, Mediterranean vegetation developed (Beaudonin et al., 2007).

2.2 Sediments: from source to sink

The sedimentary system describes a defined area of space, such as a drainage basin, in which material is weathered to regolith and soils, eroded from hillslopes, transported by rivers and deposited in the marine system (Figure 2.6). In order to understand the principles behind the tools used in this study, each aspect of the fluvial sedimentary system must be investigated. This system can be classified into three idealised subsystems: the erosion, transfer and sedimentation zones (Schumm, 1977). The erosion zone ideally represents the catchment headwaters and involves the transport of sediment from hillslopes into fluvial channels. Sediment residence times in this zone are dependent upon the rates of regolith and soil production, and downslope hillslope transport. In the transfer zone, sediment is transported downstream from the catchment headwaters to the sedimentation zone, usually by rivers. Sediment residence times also depend on the duration of storage in alluvial deposits, such as floodplains, channels bars, and the valley floor.

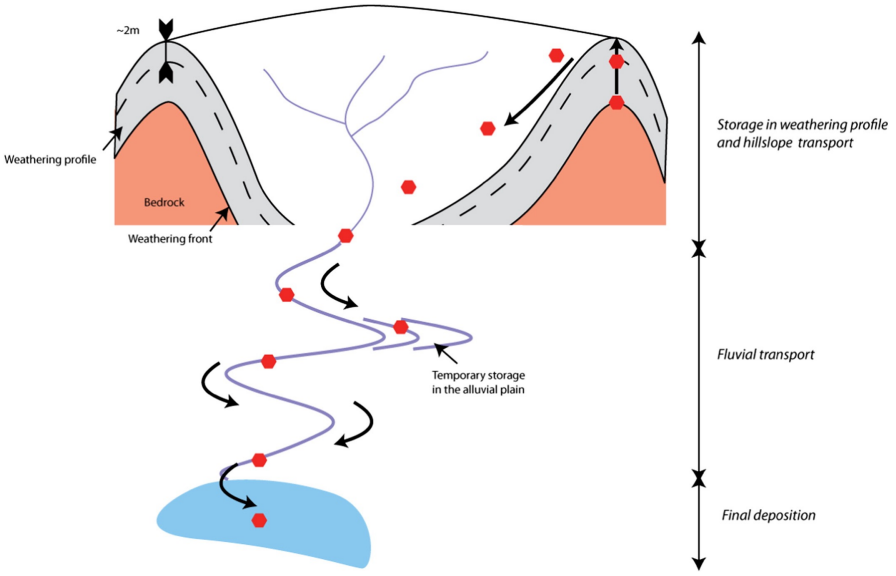

Figure 2.6 Conceptual representation of soil/sediment transport from the source to the sink in a mountainous catchment. Red polygons represent soil/sediment. Grains enter the system at the weathering front, when U isotopes begin to fractionate. Grains reside in the weathering profile until eroded, transported into fluvial systems and deposited in the marine realm. Adapted from Dosseto and Schaller, 2016.

2.2.1 Soil development in alpine regions

Soil profiles are formed by the breakdown of regolith by biological, physical and chemical weathering. Though an important tool for investigating past environments, soils in alpine regions are poorly studied (Righi et al., 1999). This is largely due to the considerable lack of soils in most alpine regions of the world. Alpine soils are often poorly developed and thin due to the high relief of alpine areas (Egli et al., 2003). The sustainability of soil resources is dependent on the rates of soil formation and erosion (Suresh et al., 2013). In alpine regions, where bedrock outcrops are often prevalent, particularly in higher elevations and in areas of high relief, it is evident that rates of erosion clearly exacerbate soil development rates, thus explaining the lack of soils often seen in alpine regions (Suresh et al., 2013).

Some studies have been undertaken in the Central European Alps to investigate soils in alpine areas. Norton and von Blackenburg (2010) studied soil formation in the Rhone Valley in the European Alps, and noted the commonality of soil mantling with few bedrock outcrops in the lower valleys. On ridge tops, soil profiles do not exceed 50cm depth, and bedrock exposure increases as soils become thinner with increasing

elevation. Soil profiles disappear almost completely above 2700m, giving way to complete bedrock exposure.

In alpine regions, soils are also influenced by the effect of denudation regimes. Denudation regimes may be "weathering-limited" or "transport-limited" (Stallard & Edmond, 1983). Weathering-limited regimes experience extensive mechanical erosion. In these regimes, the potential for extensive chemical weathering to occur is reduced, as soils are denuded quickly (Stallard & Edmond, 1983). This results in a highly selective chemical weathering process, by which only the least stable minerals will weather prior to erosion. The converse occurs in transport-limited regimes, as erosion is insignificant and residence times are long, providing situations conducive to chemical weathering.

Soil formation processes in alpine soils has also been investigated (Egli et al., 2003; Mahaney & Halvorson, 1986; Drever and Zobrist, 1992). In general, the greatest amount of mineralogical change and clay development in soils, derived from a granitic or gneissic lithology, occurs within 1000-3000 years of soil formation. A study by Drever and Zobrist (1992), indicated that elevation changes do not influence clay formation in alpine soils, but rather factors such as local relief and associated denudation regimes play a key role in clay formation.

2.2.2 Hillslope erosion

Regolith and soils produced from the bedrock are eroded from hillslopes and transported to the fluvial system in various modes. The least intensive of these modes is termed *creep*, a diffusive process that is proportional to the hillslope gradient and involves the slow downhill movement of soils (Carson & Kirkby, 1972). Creep movement rates are also dependent on soil depth, as vertical-mixing processes of bioturbation and tree-throw can enhance creep rates (Heimsath et al., 2002). Creep allows for the extended residence times of sediment on hillslopes, and is the dominating mode of transport in transport-limited regimes.

Landslides and mass wasting events dominate erosional processes in weathering-limited landscapes with steeper terrain. The rate and intensity of hillslope transport in

landslide-prone regions depends on the depth of landslide event, since deeper landslides, which involve bedrock failure, transport larger volumes of material than shallow landslides (Larsen et al., 2010). Frequent landslides on steep hillslopes thus cause fast rates, and short hillslope residence times are expected in these regions. The volume of regolith available to erode (i.e. soil thickness) also impacts the intensity of mass wasting. Therefore, regolith production rates also have an influence on erosion depth.

Glacial activity is highly abrasive to underlying landscapes (Lowe & Walker, 2002 pp. 90). Glaciers therefore have the potential to erode deeply into soil profiles as well as fresh bedrock during downslope movement. The contact plane of glaciers with the underlying landmass may be wet or dry (Lowe & Walker, 2002 pp. 90). Where the contact is wet, abraded sediments may be actively exported from under glaciers via enhanced downslope processes. Conversely, where a dry contact prevails, sediment and rock flour may be trapped under glaciers until melting enables movement. Glacial erosion provides significant volumes of sediment to depositional environments, and may overpower the sediment load of the fluvial transport system during times of high sediment export (Koppes & Montgomery, 2009),

The erosional mechanism dominating the entire catchment, a part of the catchment, or individual hillslope impacts the residence time of sediments. In-situ cosmogenic nuclides have shown that the rate of hillslope transport is dependent on slope, and hillslope residence times are inversely proportional to slope (Heimsath et al., 2002). This is similar to the relationship between slope and soil production rates. In low-relief environments, such as desert lowlands, sediment grains can remain on the hillslope for more than 10 ka due to slow transport rates (Nichols et al., 2002).

2.2.3 Sediment transfer

Sediment is predominantly delivered to the depositional setting by fluvial conduits, though wind-driven processes may also aid in sediment transport in regions conducive to aeolian transport. Storage in the alluvial plain may increase sediment residence times in the transfer zone of the fluvial system. Sediment may also be stored at the base of hillslopes as colluvium and in valley floors, point bars, channel floors, and floodplains (Dietrich et al., 1982; Reneau et al., 1990). The volume of sediment stored

in alluvial deposits commonly exceeds the sediment load of the river, increasing the likelihood of longer residence times (Trimble, 1977; Walling, 1983). Discrepancies frequently occur between sediment erosion rates and sediment yields at catchment outlets as a result of sediment storage in the transfer zone (Walling, 1983).

Sediment residence times within the fluvial system have been measured through radionuclides produced by nuclear fallout. In mountainous regions, fallout radionuclides have shown that suspended sediment is transported tens of kilometres within less than a decade once entering high gradient streams (Bonniwell et al., 1999). In contrast, in low gradient systems such as the Mississippi River, the majority of sediment does not contain fallout radionuclides, due to the increased alluvial storage capacity in large catchments (Scott et al., 1985).

2.2.4 Sediment deposition in the marine system

Sediment is delivered to the marine depositional system at the river mouth. Several modes of sediment transport are available to sediment at the outlet. These include; sediment distribution via hyperpycnal and gravity flows directly from the continental basin to the marine basin; delayed re-distribution of sediment deposited at a river mouth by high-frequency surficial failures caused by the build up of unconsolidated sediments; and low-frequency, high-volume failures caused by external forcings (Mulder et al., 1997).

A hyperpycnal plume is a current generated at a river mouth when the density of the river water exceeds the density of ambient seawater due to increased relative sediment load. Due to this, the plume plunges and develops into an auto-maintained turbidity current (Mulder et al., 1997). Hyperpycnal plumes can be produced by rivers with low-to-medium average discharge as low as 460 m^3/s (Mulder and Syvitski, 1995). The resulting sedimentary structures are termed *turbidites*. Turbidites are deposited as graded units with distinctive horizons ranging from sands in the lower horizons to very fine-grained upper strata.

The location of sediment deposition in the marine system may migrate over time as a result of variations in relative sea level and the intensity and characteristics of

sedimentary flows entering the basin. For example, Mulder et al. (1997) modelled the flow of different grain size fractions in the Var submarine canyon, and noted that typically, fine sand cannot travel more than 13 km from the river mouth, while clays may travel much farther, up to tens of kilometres away. Changes in sea level may produce discontinuous records, and it is therefore rare to obtain a completely continuous record at a given location, especially if the continental shelf is wide (Bonneau, 2014). Marine processes such as bioturbation may also alter the stratigraphic signal recorded in sedimentary cores, and complicate the interpretation of the sediments (Bonneau, 2014). Stratigraphic signals recorded by sediment cores may therefore represent changes in different variables at different times. Due to the variation in the depositional zone of sediment, records may be discontinuous, and the temporal resolution may not be fine enough to observe true variations in sediment flows. As sedimentary cores are often used to reconstruct palaeoclimatic and palaeoenvironmental conditions, it is necessary to be able to adapt sampling resolutions to the scale of climatic variations of interest (Simpson & Castelltort, 2012).

The viability of a sedimentary core from a given sedimentary system for use in palaeo-climatic and –environmental reconstruction may be enhanced by several bounding characteristics (Milliman & Syvitski, 1992; Allen, 1997; Covault et al., 2010, 2013). Firstly, periodic floods (with high transport capacity) and steep slopes allow for a quick response time to disturbances and variation occurring in the sediment source area. Secondly, where temporary storage of sediment at the river mouth is limited, there is a higher likelihood of the fluvial sedimentary load being exported directly to the sea. Finally, where a fluvial system outputs to a narrow continental shelf, sediments will be rapidly exported to the submarine basin during both high and low sea level stands.

2.3 Palaeoenvironmental Reconstruction

The purpose of this section is to briefly review the use of grain size, mineralogy and geochemistry in palaeoenvironmental reconstruction.

2.3.1 Grain Size

Grain size distribution is fundamental characteristic that can provide an indication of the origin and history of sediments, and is commonly used as an indicator of the energy of the system by which sediment is transported (Syvitski, 2007). System energy is dependent on runoff and catchment relief (Hu et al., 2012). In fluvial systems, for example, coarser grains are resultant in systems with high energy, runoff and relief, while finer grains are produced in environments with low energy, relief and runoff (Hu et al., 2012).

Several studies have utilized grain size as a palaeoenvironmental indicator. Long-term trends of grain size fluctuation can reflect interglacial to glacial changes, with finer grain sizes predominating during interstadials, and coarser grain size dominating during colder periods, as noted by Liu et al. (2005).

In glaciated catchments, increases in clay content during glacial periods may indicate increased sediment delivery from glaciers (Land et al., 2010). The silt fraction of marine sediments has also been shown to increase during glacial periods while sand decreases (Newnham et al., 1999). The interpretation of grain size of sediments is therefore dependent on the sediment type and depositional setting of the given sedimentary sequence. Other factors such as chemical weathering can also impact the resulting grain size fractions deposited (Hu et al., 2012).

2.3.2 Mineralogy

The mineralogy of sediments can play a key role in determining the source area and parent lithology of marine sediments, as the sediment will reflect the lithology from which it is derived, and therefore indicate potential changes in sediment source areas (Hu et al., 2012). Since sediment can be derived from soils rather than directly from bedrock, secondary minerals produced by chemical weathering will impact the mineralogical assemblage. The relative proportions of primary and secondary clay

minerals can therefore indicate the degree of chemical weathering that samples have been subjected to (Hu et al., 2012). Mineral phases can be identified and subsequently quantified using X-ray Diffraction (XRD).

Certain minerals form by chemical weathering under specific environmental conditions (Thiry, 2000). Soil profiles develop more rapidly and to greater depths in tropical and subtropical environments, as a result of intensified chemical weathering (Birkeland, 1984). As a result, kaolin group minerals are often abundant in well-developed soils from regions of tropical climate, while smectite-rich soil is often produced in warm regions with seasonal climate and less leaching (Adatte et al., 2002). Thus the ratios of smectite to kaolinite can be used as a weathering proxy, particularly in regions with monsoonal variation (Chamley, 1989; Wan et al., 2006; Boulay et al., 2007; Colin et al., 2010; Alizai et al., 2012). Similarly, hematite is a product of weathering under dry, hot conditions, while goethite is favoured by wetter, cooler conditions (Wang et al., 1999; Thiry, 2000). The abundance of these minerals can be utilised to develop a record of chemical weathering (Balsam and Damuth, 2000; Giosan et al., 2002).

The proportion of secondary minerals present within a sample may give an indication to the degree of weathering a sample has been exposed to, and further, provide a preliminary indication of sediment residence time in the weathering profile. A high proportion of clay minerals may indicate long residence time and slow erosion rates, as soils are exposed to chemical weathering for a longer period of time, such that primary minerals may weather to secondary clays (Hu et al., 2012). High clay content may also indicate the prevalence of humid conditions, causing the rapid weathering primary minerals to clays (Hu et al, 2012). The secondary mineral signature may therefore be influenced by different variables.

2.3.3 Chemical weathering proxies

Aside from mineralogy, chemical weathering also modifies elemental concentrations of rocks and sediments. Different elements behave differently during chemical weathering processes, particularly in terms of mobility and solubility of elements, and can therefore be used to constrain conditions of chemical weathering (Rollinson,

1993). For example, some elements such as Na, Ca and Sr are highly mobile and thus are readily leached from regolith and sediments. This results in weathering products depleted in these elements (Nesbitt and Markovics, 1997; Nesbitt et al, 1980). Other elements, such as K, Ba, Mg and Rb are readily leached off primary minerals but adhere to secondary clay mineral lattices in weathering profiles, such that they are usually enriched in weathering products following moderate chemical weathering processes (Nesbitt and Markovics, 1997; Nesbitt et al., 1980; Condie et al., 1995; Peuraniemi & Pulkkinen, 1993). In contrast, elements including Al, Fe, Ti and Zr are poorly altered during chemical weathering processes, and tend to be enriched or remain constant in weathering products comparatively to the protolith (Condie et al., 1995; Nesbitt and Markovics, 1997; Nesbitt et al., 1980; Peuraniemi and Pulkkinen, 1993). Other element abundances are sensitive to the intensity of chemical weathering. For example, K, Rb, Ti, Zr and REEs tend to be enriched in weathering products after moderate chemical weathering process, but become depleted after extreme chemical weathering processes (Condie et al., 1995; Nesbitt, 1979).

The variations of element contents in detrital sediments can be used as tracers for the intensity of chemical weathering, and therefore facilitate the reconstruction of climatic and environmental changes in the source region of the sediments via elemental ratios of mobile and immobile elements (Nesbitt and Young, 1982; Zabel et al. 2001). Elemental ratios for Al/Na, Al/K and Al/Mg have been used to assess weathering of sediment, by assuming that Al remains immobile during chemical weathering. Therefore the relative concentration of Al to mobile elements increases with intensification of chemical weathering (Limmer et al., 2012). Other studies have reliably utilized elemental ratios in terrestrially derived sediments to develop records of chemical weathering intensity (Wei et al., 2003, 2004, 2010). These chemical weathering proxies are limited to interfering effects of provenance changes, hydraulic sorting and diagenesis, as these factors can influence elemental ratios in detrital elements (Wei et al., 2010). Provenance change of the sediments may be caused by change of sediment source region and changes in delivery patterns of sediments to the marine basin (Wei et al., 2010). These factors may change the elemental ratios in sediments and obscure any chemical weathering signals. Neodymium (Nd) isotopes can be implemented to track sediment provenance changes (Viers et al., 2008). This

element is immobile and varies in isotopic composition in different lithological units. Change in sediment provenance may therefore result in the change of Nd values in sediments. Hydraulic sorting may alter elemental ratios by controlling the grain sizes of sediments, which may result in mineralogical sorting and therefore elemental ratio differences between grain size fractions (Zhang et al., 2002). Diagenesis can also change the distribution of some elements in sediments (Froelich et al., 1979).

The elements selected to reconstruct chemical weathering records have been well defined and are abundant in fine grain size fractions (Nesbitt & Young, 1982; Nesbitt & Markovics, 1997; Wei et al., 2010. Their properties are defined in Table 2.1. The selected elemental ratios used in this study are presented in Table 2.2.

Table 2-1 Properties of elements used in chemical weathering proxies.

Element	**Properties/Mobility**
Na	Mobile; readily removed (Nesbitt and Young, 1982)
Ca	Mobile; readily leached (Nesbitt and Young, 1982)
Ti	Immobile (Nesbitt and Young, 1982)
Al	Immobile; enriched in weathering products (Nesbitt and Markovics, 1997)
Ti	Immobile
K	Variable; enriched in moderately weathered weathering products, depleted following extreme weathering (Wei et al, 2010)
La	Light REE; immobile; retained in weathering products (Condie et al, 1995; Nesbitt, 1979)
Sm	Heavy REE; mobile; depleted in weathering products (Condie et al, 1995; Nesbitt, 1979)

Table 2-2 Elemental ratios and their significance.

Elemental Ratio	Significance
Na/Ti; Ca/Ti	Strong chemical weathering is evidenced by a decreased ratio (Nesbitt and Young, 1982)
Al/Ti; Al/Na	Strong chemical weathering results in higher ratios (Nesbitt and Markovics, 1997)
Al/K	Extensive chemical weathering indicated by high ratios (Wei et al, 2010)
La/Sm	Chemical weathering is indicated by higher ratios (Nesbitt, 1979)

2.3.4 Uranium isotopes

Reliable information about past erosional processes is difficult to obtain on geological time scales (Dosseto & Schaller, 2016). The advancement of uranium (U) isotopes as an erosion indicator has increased opportunities to investigate past erosional trends.

Background Theory and Conceptual Model

Uranium-238 (^{238}U) decays into a sequence of radioactive nuclides (Fig 2.7; Dosseto, 2015). U-series isotope geochemistry focuses on the top of the decay chain, in particular ^{238}U and uranium-234 (^{234}U). ^{234}U is the great-granddaughter of ^{238}U, and is formed by the decay of the short-lived, intermediate products of ^{234}Th and ^{234}Pa.

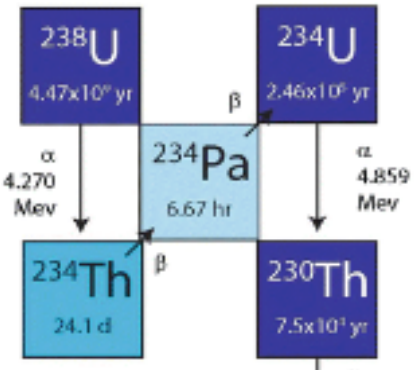

Figure 2.7 Uranium-238 decay chain. From Dosseto, 2015.

If a geological system is closed for approximately four half-lives of the daughter nuclide, the activity ratio of nuclides remains constant, resulting secular equilibrium i.e. (^{234}U) = (^{238}U); (^{234}U/^{238}U) = 1. The term *activity ratio* describes the product of the nuclide concentration and decay constant, and is denoted by parentheses in this text (Dosseto, 2015). As the half-life of ^{234}U is 245,250 ± 490 years, the system will reach secular equilibrium if undisturbed for more than 1 million years (Cheng et al., 2000). Activity ratios are also denoted by delta notation, whereby $\delta^{234}U = (((^{234}U/^{238}U) – 1) x 1000$ in parts per thousand (‰).

When bedrock is disturbed and begins to weather, mineral surfaces are exposed to an oxygenated environment, isotopic fractionation of ^{238}U and ^{234}U is initiated and the system is no longer in secular equilibrium. Due to their similar chemical properties, both U isotopes show no fractionation within igneous rocks, but exhibit fractionation at Earth's surface, with the preferential retention of ^{238}U over ^{234}U in sediments, rocks and soils, and an enrichment of ^{234}U in natural waters (Dosseto, 2015).

A leaching model was first devised by Latham and Schwarcz (1987) to account for (^{234}U/^{238}U) < 1 in weathered silicate rocks. The model assumes that (^{234}U/^{238}U) = 1 in the unweathered material. Fractionation of the two isotopes at the Earth's surface is observed as a result of the following processes:

1. Direct recoil of ^{234}Th out of the mineral grain during ^{238}U decay. ^{234}Th subsequently decays into the ^{234}U granddaughter product (Kigoshi, 1971). This method of fractionation occurs as a result of the displacement of the daughter atom ^{234}Th during decay. This displacement is referred to as *alpha recoil*, and occurs at a length between 15 and 35 nm for most minerals (Hashimoto et al., 1985). If decay occurs within the recoil length of the mineral surface, ^{234}Th, and subsequently ^{234}U, can be lost to the surrounding medium (Figure 2.8).

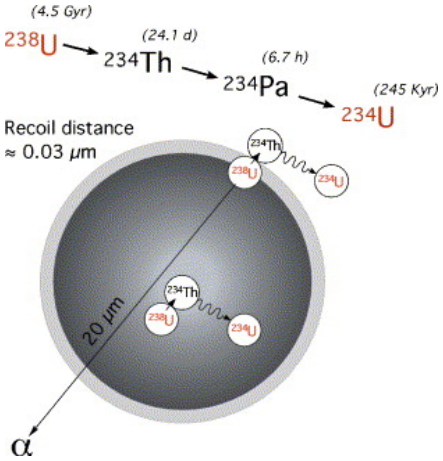

Figure 2.8 Schematic diagram of 234Th ejection from a spherical grain as a result of alpha decay of 238U, followed by subsequent decay to 234U. From DePaolo et al., 2006.

2. Preferential leaching of ^{234}U embedded in recoil tracks. When the pore space between adjacent minerals is filled with air, it becomes more possible for ^{234}Th ejected from a grain to become embedded in the recoil track of an adjacent grain and decay into ^{234}U (Sun and Furbish, 1995). ^{234}U can then be easily leached from the recoil tracks when the pore space is filled by a solution (Andersen et al., 2009; Fleischer, 1980).

3. Preferential oxidation of ^{234}U compared to ^{238}U. In minerals with a low U concentration, there is a high probability of ^{234}U to be located in the vicinity of oxygen atoms or radicals (Adloff and Roessler, 1991). ^{234}U is therefore more prone to oxidation to the mobile hexavalent (U^{6+}) state, comparatively to tetravalent, and immobile (U^{4+}) state.

These fractionation processes are triggered by the comminution of mineral grains to <63 μm at the onset of chemical weathering. Fractionation of ^{234}U becomes significant in silt- and clay-sized grains due to the large surface area-to-volume ratio (DePaolo et al., 2012; DePaolo et al., 2006; Martin et al., 2015).

Soil age increases with depth as the weathering front moves downward over time. Shallow, old regolith therefore exhibits lower ($^{234}U/^{238}U$) activity ratios due to the increased time spent leaching ^{234}U from mineral grains, comparatively to deeper regolith layers (DePaolo et al., 2006; Lee et al., 2010a; Dosseto et al., 2014). Subsequently, ($^{234}U/^{238}U$) composition of soils commonly decreases with depth in the

weathering profile (Figure 2.9). The ($^{234}U/^{238}U$) of sediment samples derived from soil-mantled hillslopes can therefore act as a proxy to erosion depth, as lower ($^{234}U/^{238}U$) values indicate erosion of upper portions of a soil profile by shallow processes such as creep, and higher ($^{234}U/^{238}U$) values indicate deep erosion of a soil profile by mass wasting processes.

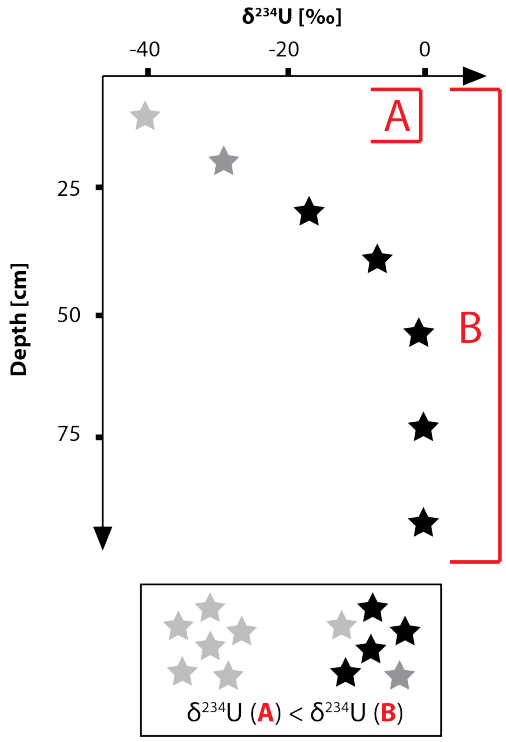

Figure 2.9 Conceptual representation of uranium isotope compositions in soil profiles in temperate climate regions. Adapted from Rothacker et al. (submitted).

Sample pre-processing

In order to use U isotopes as a geochemical approach to environmental reconstruction, detrital mineral grains must be isolated from non-detrital matter. This is because the decay process results in the development of three domains in sediments and soils with distinct ($^{234}U/^{238}U$) values exhibited in Figure 2.10 (Martin et al., 2015).

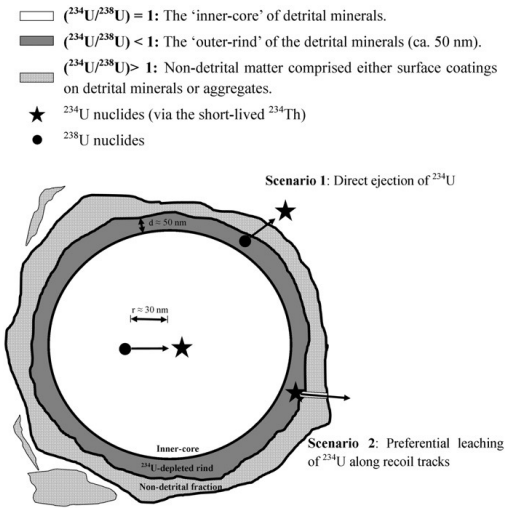

Figure 2.10 The domains present in soils and sediment in terms of their respective (234U/238U) activity ratios and the two scenarios for 234U-depletion: 1) direct ejection of 234U (via the short-lived 234Th); and 2) preferential leaching of 234U from alpha-recoil tracks which are embedded as a result of direct ejection of 234U from adjacent grains. From Martin et al., 2015.

Domain 1 includes the inner-core of detrital minerals that remains in secular equilibrium (i.e. $(^{234}U/^{238}U) = 1$). Domain 2, where $(^{234}U/^{238}U) < 1$, describes the ^{234}U-depleted outer rind of detrital minerals. Domain 3 incorporates non-detrital weathering products such as carbonates, iron oxides and organic matter. Non-detrital material is generally ^{234}U-rich, and therefore exhibits $(^{234}U/^{238}U) > 1$. This is because natural waters are enriched in ^{234}U as a result of recoil effects, and many non-detrital materials precipitate from such waters (Martin et al., 2015).

It is therefore necessary to remove non-detrital material prior to analysis to accurately measure the $(^{234}U/^{238}U)$ activity ratio recorded in Domain 2. A sequential extraction process was originally developed by Tessier et al. (1979) and further refined by Schultz et al. (1998) and Martin et al. (2015). The leaching process is designed to remove all non-detrital matter without removing the ^{234}U-depleted rind of detrital minerals, such that the lowest possible $(^{234}U/^{238}U)$ activity ratio may be measured (Figure 2.11).

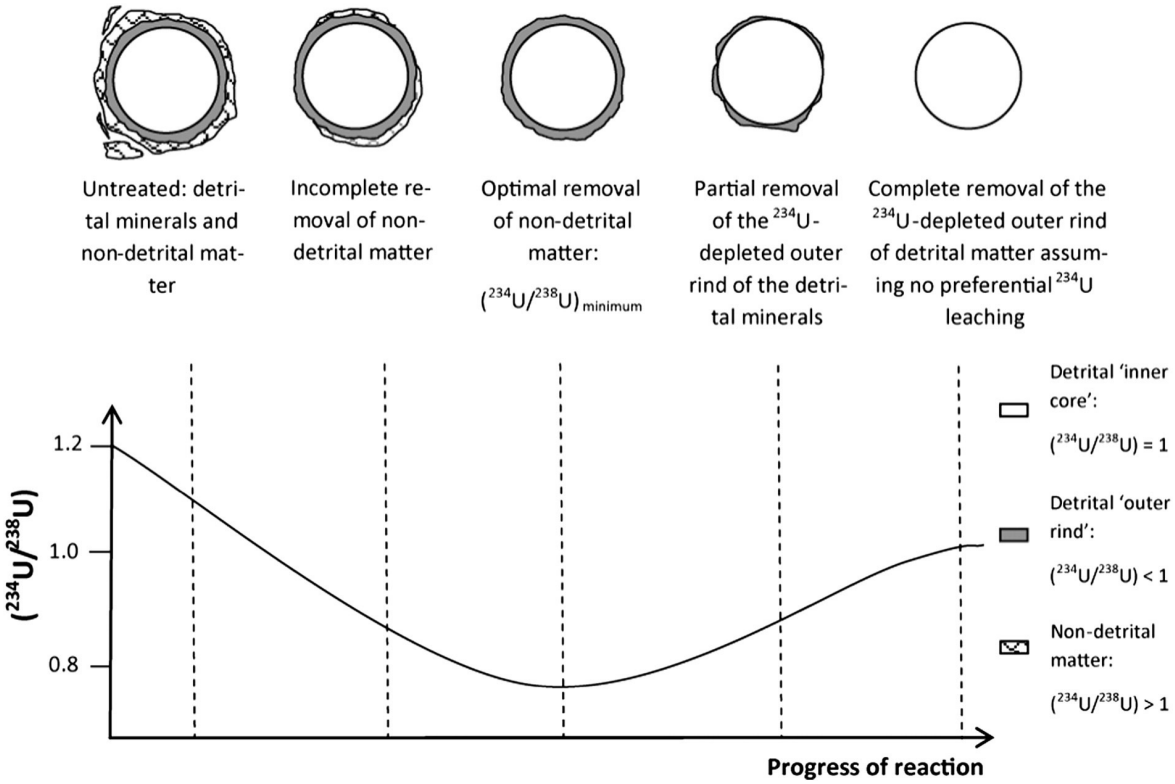

Figure 2.11 Approach for evaluating the adequacy of sample leaching (Lee, 2009; Martin et al., 2015). The optimum sample leaching protocol should result in the lowest (234U/238U) ratio in the leached residue. Because solution-derived and organic phases have (234U/238U) N1, a protocol where the removal of these phases is incomplete will result in a (234U/238U) ratio higher than with the optimum protocol. In contrast, if the protocol is too aggressive and attacks the surface of rock-derived minerals, the rind that contains the 234U depletion will be partially or completely removed, resulting in a (234U/238U) ratio in the leached residue higher than if the surface were intact.

Several fractions are extracted from the bulk sediment during sequential leaching, including exchangeable, acid-soluble, reducible, and oxidisable fractions (Martin et al., 2015). The exchangeable fraction includes elements that are weakly bound to the grain surfaces by dipole-dipole forces or weak electrostatic interactions. The abundance of U-series isotopes in the exchangeable fraction is generally low. This fraction is removed by adding a neutral salt to the sediment to disrupt these weak bonds and prevent re-sorption of U back onto the mineral grain (O'Connor & Kester, 1975).

The acid-soluble fraction is commonly referred to as the carbonate fraction. Leaching of this fraction attacks Ca- and Mg-bearing minerals such as calcite and dolomite. Significant amounts of U can be incorporated into these calcareous minerals by

surface adsorption or co-precipitation processes (Schultz et al., 1998). This fraction is usually significant in marine sediments, and is removed by acidic solutions.

The reducible fraction contains iron (Fe) and manganese (Mn) oxides, hydroxides and oxyhydroxides, and is referred to as the Fe,Mn-oxide fraction in this study. These compounds may incorporate U isotopes into their amorphous and crystalline structures in ferrihydrite and goethite, respectively (Lee & Baik, 2009). Oxides are unstable under reducing conditions, and a reducing agent is therefore implemented to selectively remove this fraction (Tessier et al., 1979).

The oxidisable fraction is primarily composed of organic matter, and is referred to as the organic fraction in this study. The organic fraction may be U-rich as a result of the strong heavy-metal binding capacity of most organic acids. The organic fraction is removed by reaction with heat and an oxidizing agent (Martin et al., 2015).

The remaining fraction following sequential extraction is the residual fraction. Theoretically this should comprise only detrital material. However, the removal of non-detrital material is often incomplete following sequential leaching (Bacon and Davidson, 2008; Gleyzes et al., 2002). As this is problematic for deriving accurate ($^{234}U/^{238}U$) activity ratios, Martin et al, (2015) developed the HF/HCl etch to remove any remaining non-detrital matter from sediment grains.

Comminution Age

($^{234}U/^{238}U$) activity ratios are also useful in determining comminution ages and residence times of sediments (Martin et al., 2015; DePaolo et al., 2006). The term *comminution age* describes the time since the parent rock was reduced to fine-grained sediment by physical and chemical weathering (Dosseto & Schaller, 2016). Thus, comminution age encompasses the entire history of regolith at the Earth's surface since its production from the parent rock, including: storage in the weathering profile, transport by rivers, with possible temporary storage in an alluvial plain, and final deposition (Figure 2.12; Dosseto & Schaller, 2016). *Residence time* describes the time sediment spends in the weathering profile and transport in the fluvial system prior to

deposition, and is calculated by subtracting deposition age from total comminution age (Figure 2.12).

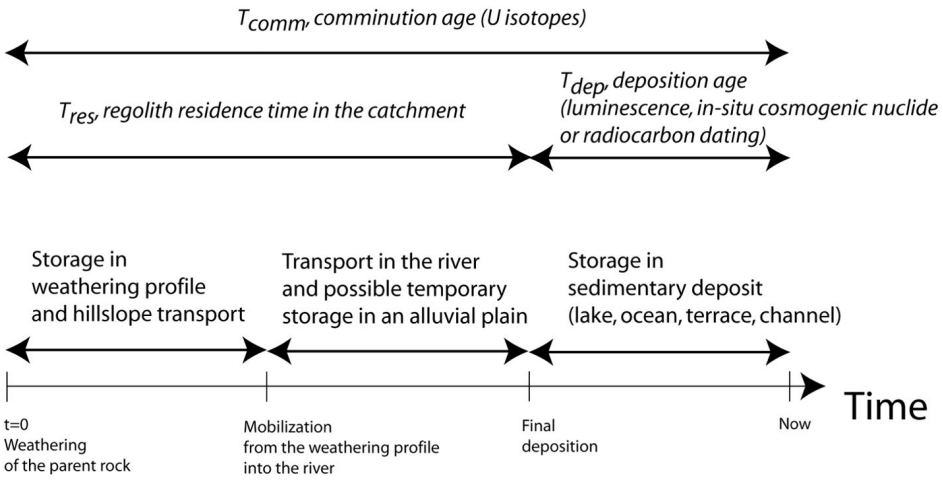

Figure 2.12 Conceptual representation of the comminution age and regolith residence time. From Dosseto & Schaller, 2016.

($^{234}U/^{238}U$) activity ratios record the time elapsed since parent material was weathered to fine-grained (typically < 63 μm) regolith (Suresh et al., 2014), due to the continual depletion of ^{234}U from mineral grains as per the processes described above. ^{234}U is therefore continuously lost from regolith during storage and hillslope transport (Dosseto et al., 2008; Suresh et al., 2014). Comminution ages of sediments can be quantified by combining the ($^{234}U/^{238}U$) activity ratio of detrital sediments with surface area measurements (DePaolo et al., 2006, 2012; Dosseto et al., 2010). DePaolo et al. (2006) suggested Equation 1 to measure comminution age.

Equation 1:

$$t_{comm} = -\frac{1}{\lambda_4}\ln\left[\frac{\left(\frac{234_U}{238_U}\right) - (1 - f_4)}{\left(\frac{234_U}{238_U}\right)_0 - (1 - f_4)}\right]$$

where:

- t_{comm} is comminution age in years
- λ_4 is the decay constant for ^{234}U in years
- f_4 is the fraction of recoiled ^{234}Th, and therefore ^{234}U
    - $(1-f_4)$ is therefore the fraction of ^{234}U remaining in the solid
- $(^{234}U/^{238}U)_0$ is the activity ratio at time = 0 (i.e. secular equilibrium; equal to 1)

Kigoshi (1971) and Luo et al., (2000) proposed Equation 2 to measure the recoil fraction (f_4) of grains.

Equation 2:

$$f_4 = \frac{1}{4} LS\rho$$

where:

- L is the recoil length in m
- S is the specific surface area of the solid in m^2/g
- ρ is the density of the solid in g/m^3

The specific surface area of the solid is generally measured through nitrogen gas sorption, as per the Brunauer–Emmett–Teller (BET) theory (Brunauer et al., 1938). However, gas adsorption generally overestimates the recoil loss fraction because it does not account for the surface roughness of mineral grains. In order to account for this, Bourdon et al. (2009) proposed to use the fractal model initially developed by Semkow (1991) presented as Equation 3.

Equation 3:

$$f_4 = \frac{1}{4}\left[\frac{2^{D-1}}{4-D}\left(\frac{a}{L}\right)^{D-2}\right] LS\rho$$

where:

- D is the fractal dimension of the surface
- a is the size of the adsorbate molecule (0.354 nm for nitrogen)

The fractal dimension (D) can be measured following BET analysis, and is a measure of surface roughness. The fractal dimension is only required if the material measured is microporous (pores < 2 nm in diameter) or mesoporous (pores between 2-50 nm in diameter)(Sing et al, 1985). Micropores and mesopores increase the measured surface area during BET analysis but do not contribute to the loss of ^{234}U in detrital matter as they are smaller than the recoil distance of ^{234}Th. Conversely, the surface area of non-porous and macroporous material (pores > 50 nm in diameter) is not overestimated when considering ^{234}Th recoil, and thus does not require a fractal correction. The shape of the adsorption-desorption isotherms can be used to assess the type of

material analysed. Type 2 isotherms are indicative of unrestricted monolayer-multilayer absorption and are characteristic of non-porous or macroporous absorbents, and therefore indicate that Equation 3 should not be implemented to calculate comminution age (Figure 2.13; Sing et al., 1985).

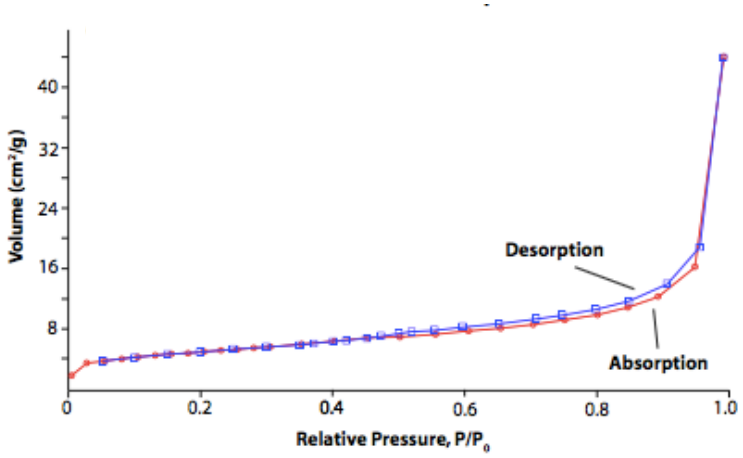

Figure 2.13 Example of a Type 2 isotherm.

3 Primary Study Site – Var River Catchment

3.1 Catchment Setting and Topography

The Var Sediment-Routing System, comprising the terrestrial Var River Catchment and marine Var Turbiditic System, extends from the upper reaches of the southern French Alps to the base of the continental slope of Corsica at 2700m water depth in the Ligurian Sea (Figure 3.1). The Var Sediment-Routing System consists of three watersheds; the larger Var watershed, and smaller Loup and Paillon watersheds to the west and east of the Var, respectively (Figure 3.1). These fluvial systems supply sediment to the submarine component of the Sediment-Routing System: the Var Turbiditic System and Var Canyon.

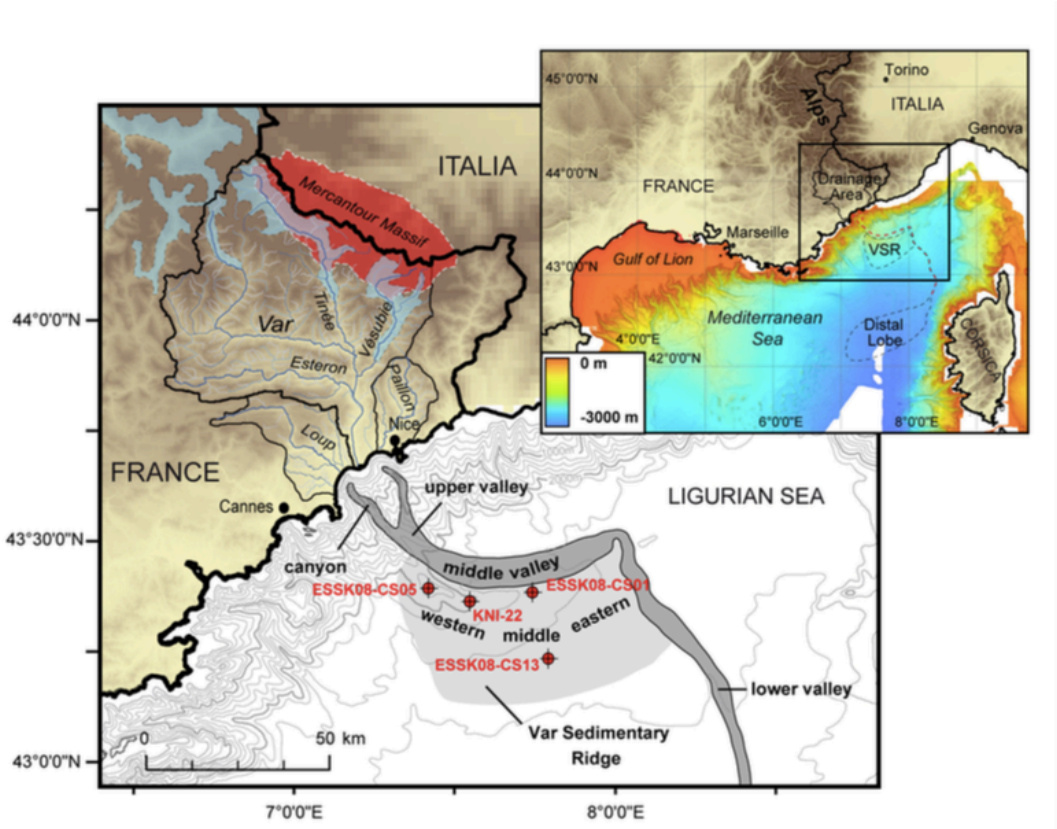

Figure 3.1 The Var Sediment-Routing System, including the Var, Loup and Paillon catchments (outlined in black) and sampling locations (shown by red text and symbols). From Bonneau et al., 2014.

The continental margin at the Var river mouth is characterized by a very narrow continental shelf and steep continental slope (2-3km maximum width, 6-15° slope gradient; Cochonat et al., 1993). These characteristics allow for the constant supply of

fluvial sediment to the Var Canyon via hyperpycnal sediment flows during both high and low stands of sea level (Bonneau, 2014). The high relief of the Var catchment results in minimal storage of sediment in alluvial plains during fluvial transport to the marine system. This allows for a negligible lag time to be assumed between erosion of sediment from hillslopes and deposition in the marine realm.

3.2 Geology

The geology of the Var River Catchment may be simply divided into carbonate lithologies in the alpine foreland and downstream areas of the basin, and igneous and metamorphic rocks in upland areas of the catchment (Bonneau, 2014). The catchment lithology also encompasses the five main lithological groups described below and depicted in Figure 3.2:

1. Palaeozoic crystalline massifs and Mercantour massif in the eastern reaches of the catchment. This group is composed of the metamorphic complexes of gneiss and migmatite and the Argentera granite, dated at 285-293Ma (Ferrara and Malaroda, 1969).

2. Permian series of schistose mudstones and sandstones outcropping at the contact with the Palaeozoic units and in the centre of the catchment, with a thickness in excess of 900m.

3. Mesozoic marl-limestones and sandstones covering the majority of the catchment.

4. Cenozoic sequence of sedimentary marl-limestones and sandstones overlying the Mesozoic unit.

5. Pliocene and Quaternary marine and fluvial deposits in the lower valley of the Var. Marine sediments were deposited during a period of higher sea level in the Pliocene, and fluvial sediments are of Quaternary age.

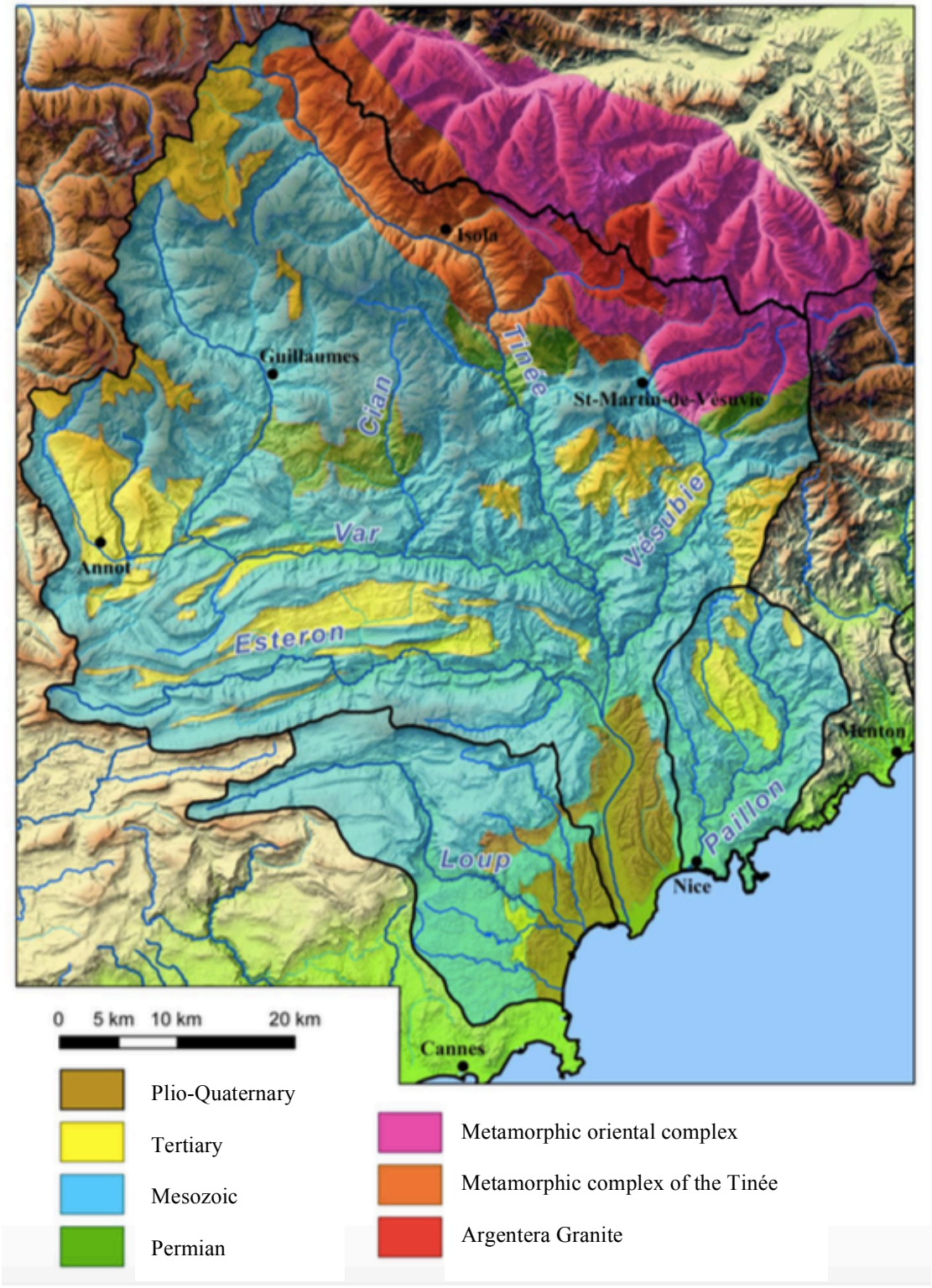

Figure 3.2 Geology of the Var River Catchment. Adapted from Bonneau, 2014.

3.3 Climate

The Var River Catchment is predisposed to Mediterranean climatic conditions. At Nice, at the Var river outlet, precipitation is heaviest during the spring and summer months, with the lowest amounts of precipitation falling during summer months (Figure 3.3; Meteo France, 2017). Nice commonly experiences temperatures of 5°C to 14°C in winter and 17°C to 28°C during summer months.

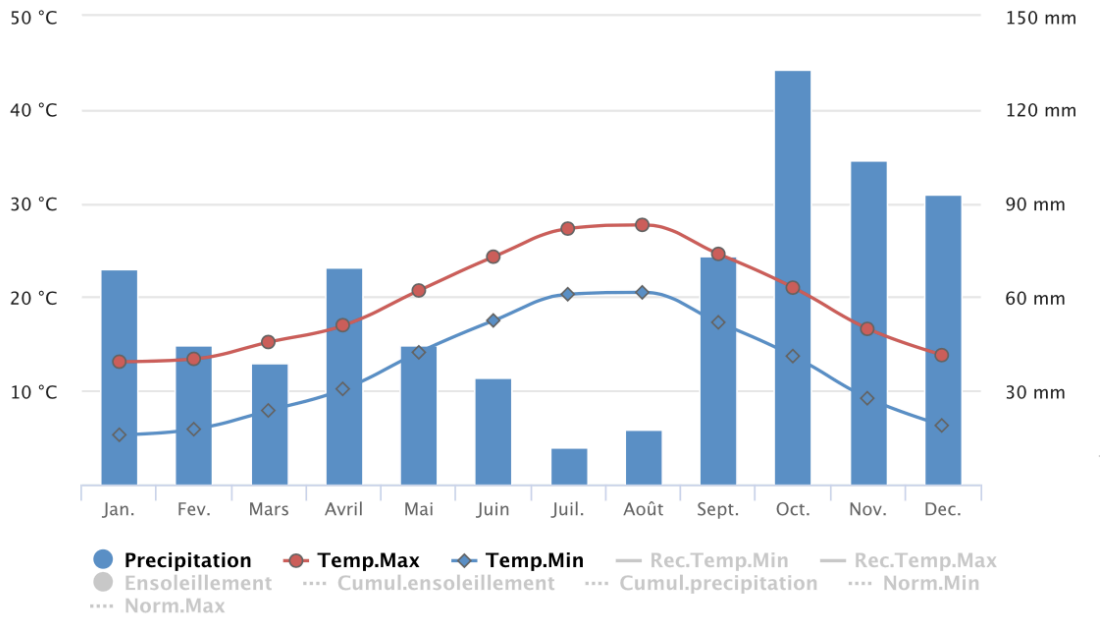

Figure 3.3 Monthly climatic conditions at Nice from 1981 to 2010 (Meteo France, 2017).

3.4 Hydrology

High sediment yields are characteristic of the Var River Catchment, with ~500 tons/km^2/yr of sediment being exported from the system annually. Mean annual discharge of the system reaches up to 70 m^3/s. Flooding of the system occurs episodically as a response to heavy rainfall periods in autumn months and snowmelt in spring months (Sage, 1976). These episodic floods may exceed the mean annual discharge in only a few hours and reach a magnitude of 1800m^3/s (Dubar and Anthony, 1995). In 1994, a high-magnitude, 200-year flood transported the amount of sediment that is normally transported in 11–14 years in a few hours (Mulder et al., 1997, 1998).

3.5 Soils

Research into the characteristics of soils within and around the Var River Catchment has been limited to date. Studies into topographically similar regions within the European Alps have noted the commonality of the presence of immature soils in alpine regions (Drever & Zobrist, 1992). In the region studied, the denudation regime is weathering-limited.(Stallard & Edmond, 1983). Soils in the Var's westerly neighbour catchment, the Rhone Valley, have been described by Norton & von Blackenburg (2010), and are likely similar to Var Catchment soils due to similarities in climate, relief and underlying geology. In the lower valley, soil mantling is common with little outcropping of bedrock occurring. On ridge tops, however, soil profiles do not exceed 50cm depth (Norton & von Blackenburg, 2010). Bedrock exposure increases as soils become thinner with increasing elevation. Soil profiles disappear almost completely above 2700m, giving way to complete bedrock exposure. Various photographs taken by Bonneau (2014) in different areas of the Var River Catchment provide an indication of the presence of soils in the study area (Figure 3.4).

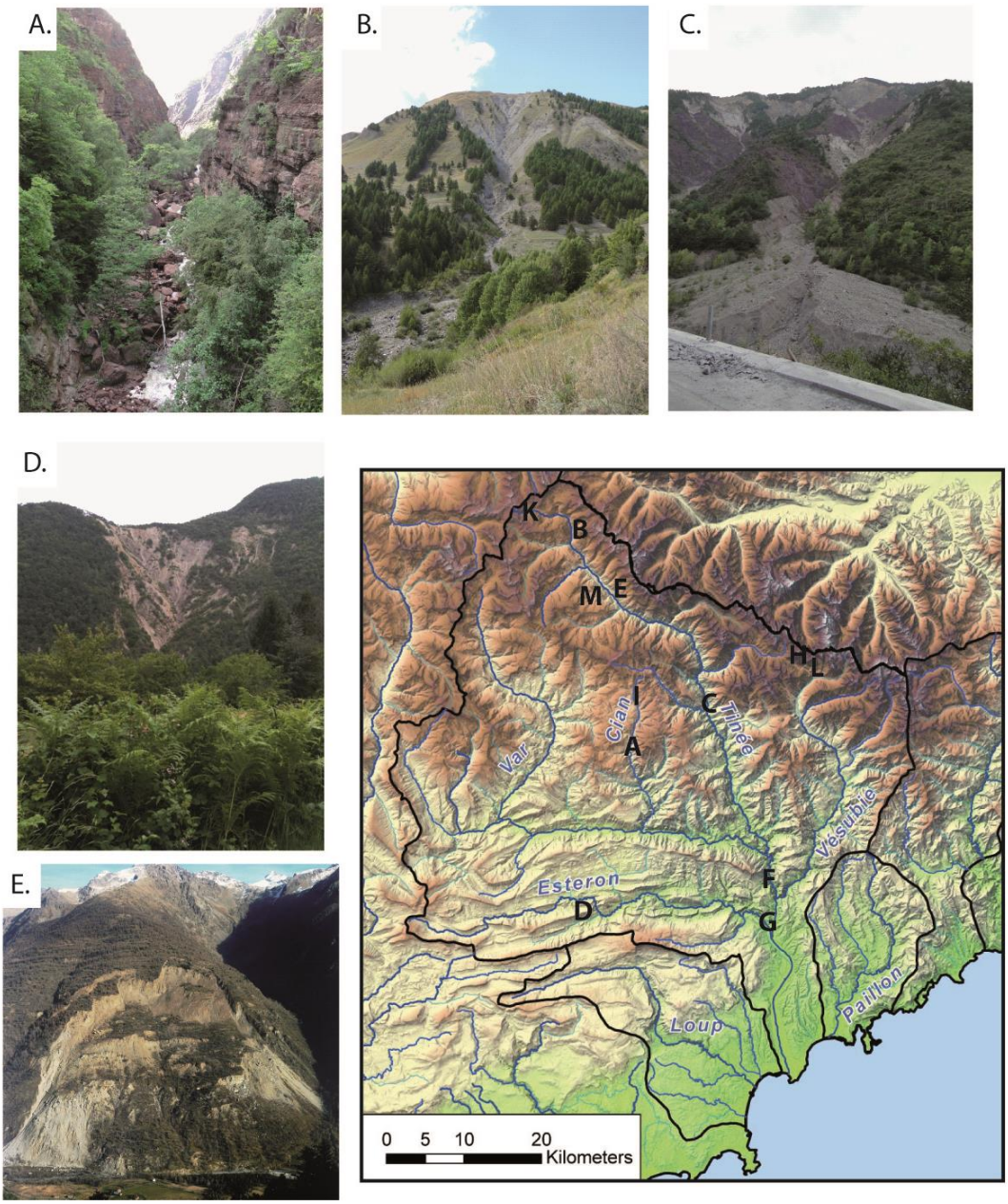

NB. Figure continued on following page.

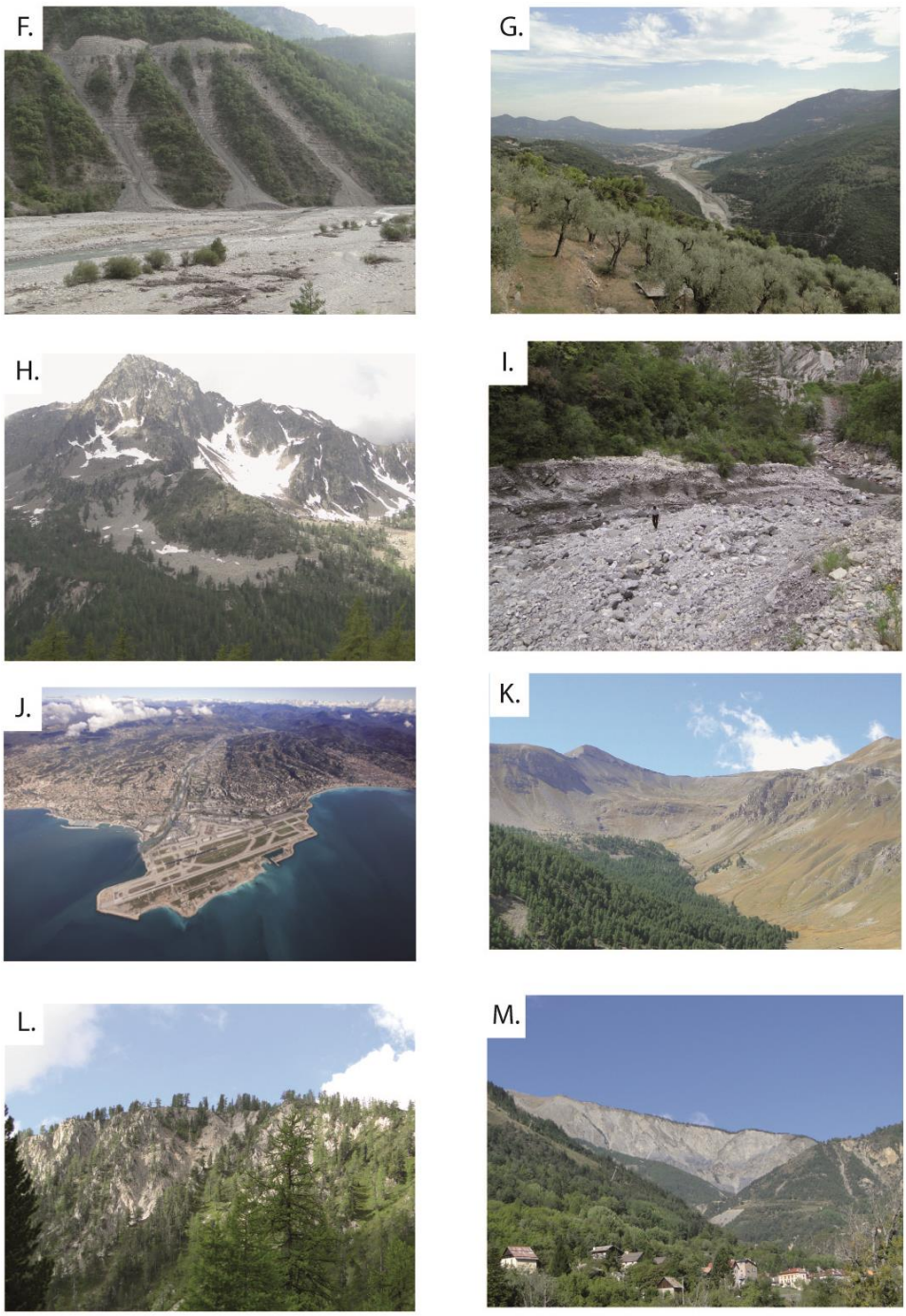

Figure 3.4 Physical context of the Var River Catchment and associated map. A. Cian gorge: B., C., and D., gullies observed in various parts of the watershed. E. Clapière landslide, the largest in Europe. F., Scree cones. G. Lower Var valley seen from the confluence of the Var and the Esteron. H., An active rocky glacier that progressively covers the vegetation; I. Torrential deposits in the Cian bed; J. Lower valley and delta of the Var; K. Glacial cirque, upper valley of the Tinea; L and M., Valley slope notched by numerous gullies. Adapted from Bonneau, 2014.

3.6 Vegetation

3.6.1 Modern-day vegetation

The present-day vegetation in Southern France forms a section of the Meso-Mediterranean belt, from sea level to 500 m, and the Supra-Mediterranean belt upwards of 500 m (Beaudonin et al., 2007). The Meso-Mediterranean Belt is dominated by sclerophyllous forests and evergreen trees. Where these forests are degraded, drought-resistant shrubs and evergreen oak forests prevail (Beaudonin et al., 2007).

The Supra-Mediterranean belt may be further divided into the temperate zone between 500 and 700 m elevation, a mountainous forest zone and the upper Alpine Belt. The temperate zone is dominated by deciduous oak mixed forests. Beech development increases from 700 to 1000 m in the mountainous forest zone. Beech is mixed with European firs in higher mountains, and conifers dominate the landscape in mountainous forests from 1450 to 2500 m altitude. In the Alpine Belt, which begins at approximately 2000 m, heath and alpine grasslands composed of various grasses, herbs and sedges are present (Beaudonin et al, 2007).

3.6.2 Palaeo-vegetation

Vegetation in southern France during the late Quaternary is highly debated, and several models for vegetation reconstruction exist (Tzedakis, 2002, 2003; Stewart, 2003).

Vegetation has been reconstructed in the neighbouring Rhone Catchment for the past 30 ka (Beaudonin et al., 2007). The pollen from cores studied display high amounts of spruce, fir and deciduous oak vegetation during MIS 3 and 2, indicating refugia of forest during the Last Glacial Maximum. Suc & Popescu (2005) reconstructed North Mediterranean climate over the past 2.7 Ma. However, the temporal and spatial resolution used in this study is not high enough to deduce vegetation characteristics in southern France for the past 70 ka.

3.7 Sediment Record/Depositional System and Modes

Two sub-marine canyons, the Var Canyon and the Paillon Canyon, incise the continental shelf at Nice. These incisions provide a conduit for the transport of fluvial sediment from the Var and Loup Rivers and the Paillon River, respectively. The two canyons merge into one valley at the base of the continental slope, which flows to a prominent levee - the Var Sedimentary Ridge – on the right-hand bank of the valley, and a distal lobe at the end of the lower submarine valley (Figure 3.5).

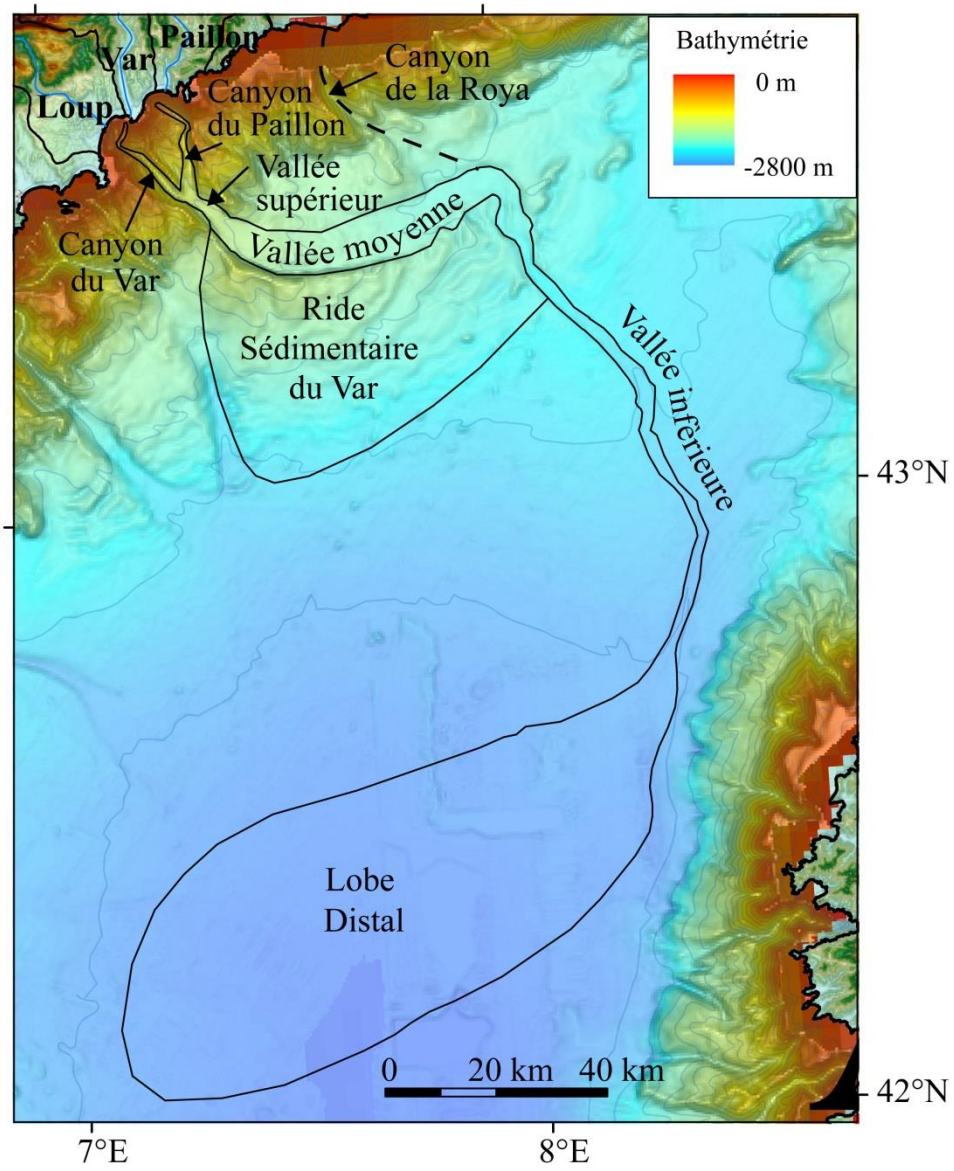

Figure 3.5 The Var Turbiditic System. Adapted from Bonneau, 2014.

Sedimentation rates on the continental slope in the Var Canyon are between one eleventh and one thirty-ninth of the rates modelled by Mulder et al. (1997). This implies that sediments are poorly trapped on the Var delta and upper continental slope during high stands of sea level (Mulder et al. 1997, 1998). Up to 63% of sediments exported at the Var River mouth were delivered to the Var Canyon through hyperpycnal currents, making them the main sediment transfer processes in the Var Turbiditic System (Mulder et al., 1997). Hyperpycnal currents must be of a sufficient magnitude to be recorded as a turbidite layer on the Var Sedimentary Ridge (VSR) (Jorry et al., 2006. Most of these events are not recorded on the VSR because of the inability of most flows to overtop the ridge wall (Mulder et al. 1998). In the middle valley, the VSR crest height reaches 300m above the main channel floor in its western part, but decreases eastward down to a few tens of meters.

A secondary sedimentary deposition process, which is significant enough to be recorded in the Var Turbiditic System, involves turbidity currents induced by the mass wasting of large portions of the continental slope (Piper and Savoye 1993; Mulder et al. 1997b, 1998, 2001a, 2001b; Migeon et al. 2012). An example of this process occurred in 1979, and was triggered by landfilling operations in the Nice airport area (Dan et al., 2007).

4 Auxiliary Study Site – Hokitika River Catchment

4.1 Tectonic Setting and Topography

The Hokitika Catchment is located on the western coast of the New Zealand South Island (Figure 4.1). The catchment covers an area of 1069km^2, and extends from the eastern limits of the Alps along the Alpine Fault to the western margin of the South Island. Sediment derived from the Hokitika Catchment is exported into the South Westland Continental Margin via the Hokitika River. Sediment is predominantly deposited via frequent sediment gravity flows into the Hokitika Canyon, a submerged meandering channel extending from ~8km seaward of the modern shoreline and reaching water depths exceeding 3500m in the Tasman Sea (Norris, 1978; Neil, 2008). The Hokitika Canyon is also open to sedimentary input from along-shore sediment transfer, although Stanton (1976) and Heath (1982) postulated this contribution to be minor. The catchment reaches elevations in excess of 1500m in the Alps, as illustrated in Figure 4.1, and is steeply sloped.

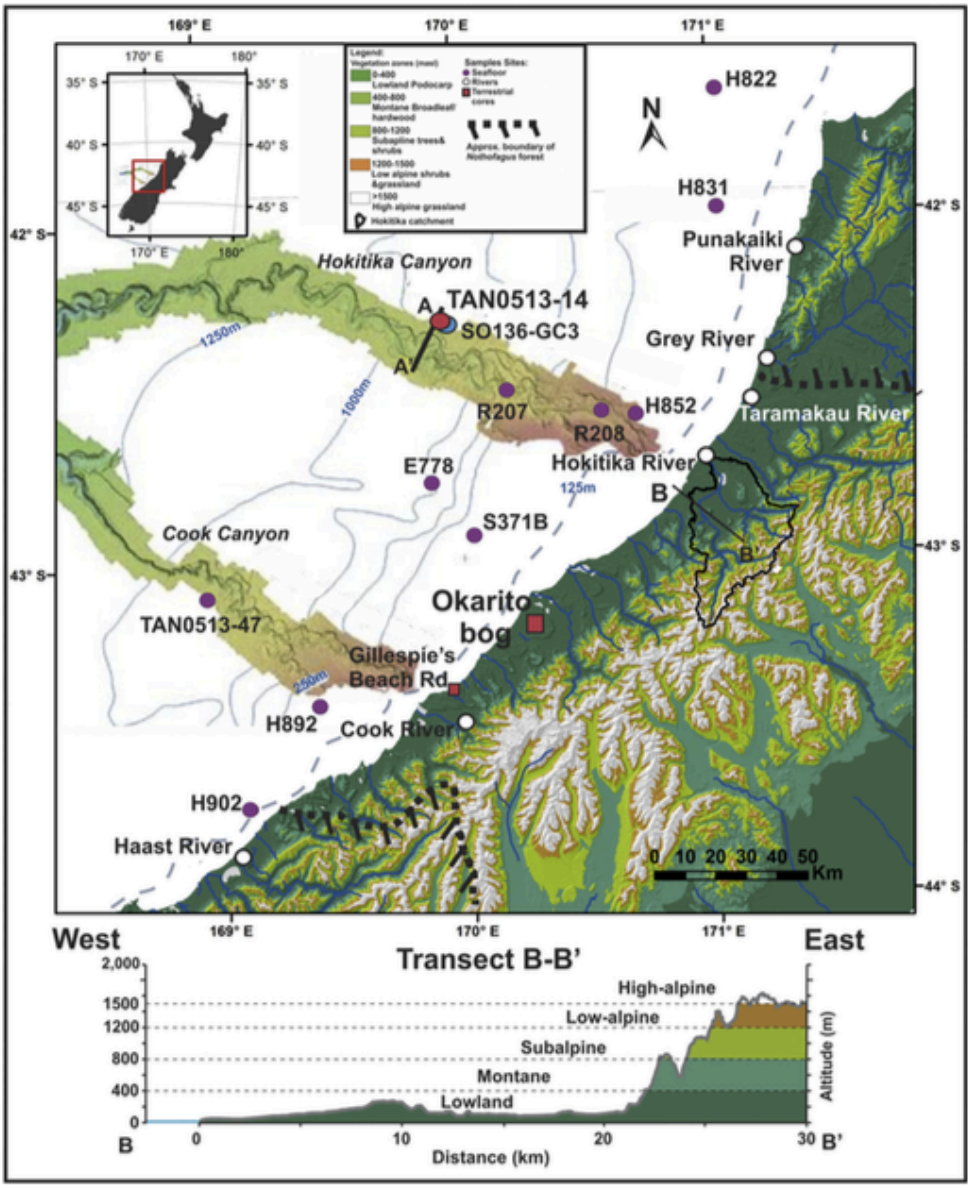

Figure 4.1Hokitika Catchment study site (outlined in black) and sampling location (TAN0513-14 red symbol), and pre-forest clearance vegetation approximated by altitudinal range on map and B-B' transect. Adapted from Ryan et al., 2012.

The high topographic relief of the site is driven by the complex tectonic activity operating along the length of the South Island of New Zealand. The oblique convergence of the Indo-Australian and Pacific plates over the past 5Ma has resulted in the uplift of the South Island (DeMets et al., 1990; Simpson et al., 1994; Chamberlain et al., 1999). Conversely to the tectonic relationships active in the North Island, in which the Pacific plate subducts under the Indo-Australian plate, in the South Island, convergence occurs by the subduction of the Indo-Australian plate under the Pacific plate, forming the Puysefur Trench (Figure 4.2). The transverse

Alpine Fault connects the two opposing trenches resulting from these contrasting tectonic regimes. Movement of this dextral reverse-slip fault has resulted in the uplift and development of the Southern Alps (Vry et al. 2008; Rattenbury et al. 2010).

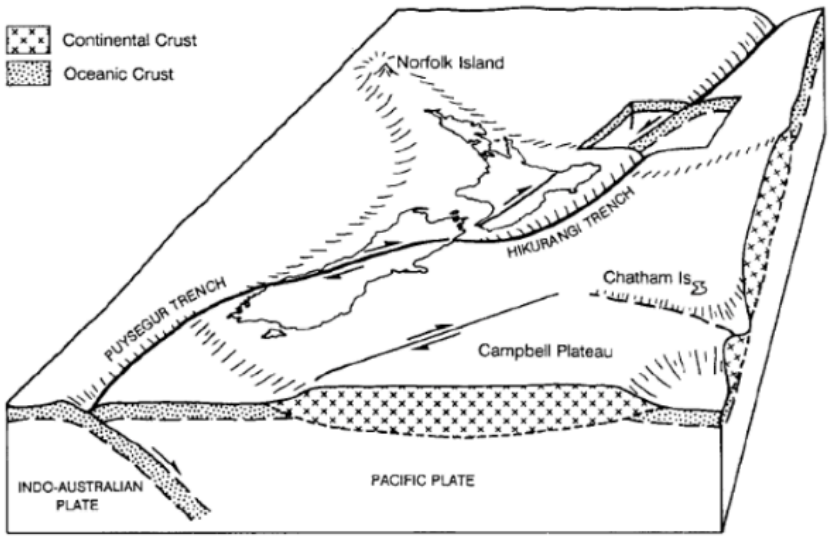

Figure 4.2 Tectonic setting of New Zealand, showing subduction zones and related faults, and the uplifted Alpine Fault (Williams, 1991).

4.2 Geology

Geology of the Hokitika Catchment is characterized by the presence of Quaternary alluvial and fluvial deposits in the lowland areas of the catchment, and Jurassic to Silurian metamorphic and igneous lithologies in upland areas (Nathan et al., 2002). The lowland deposits are most commonly composed of unconsolidated river sands and gravels, frequently accompanied by swamp deposits, screes and till. To the east of the Alpine Fault, in alpine regions, the Fraser Complex outcrops as metamorphic paragneiss and amphibolite facies. These units are also accompanied by gneissic granites, tonalites and migmatites intruded by mafic and felsic dykes (Nathan et al., 2002). The Torlesse Terrane partially outcrops to the east of the Fraser Complex as a unit of grey- and green-schists. These units also incorporate schist-derived mylonites and fault breccias (Nathan et al., 2002).

4.3 Climate

The climate of the Hokitika Catchment is dominated by high precipitation volumes triggered by moisture-laden westerly winds (Figure 4.3a). When westerly systems travel across the Tasman Sea, their moisture content increases to form low-pressure systems. These moist systems converge perpendicularly onto the west coast of the South Island. The orographic barrier of the Southern Alps leads to high precipitation rates of 5,000 mm/yr at the coast, and maximums of 12,000 mm/yr at the crest of the westernmost range (Tonkin & Basher, 1990).

The South Island experiences relatively small variations between summer and winter temperatures. Mean annual summer temperatures range between 12 and 22°C and decrease to between 1 and 10°C in winter (NIWA, 2012). The mean annual temperature ranges between 2 and 6°C in the Southern Alps (Figure 4.3b). Temperature decreases approximately 0.7°C for every 100 m of altitude, (NIWA, 2012)

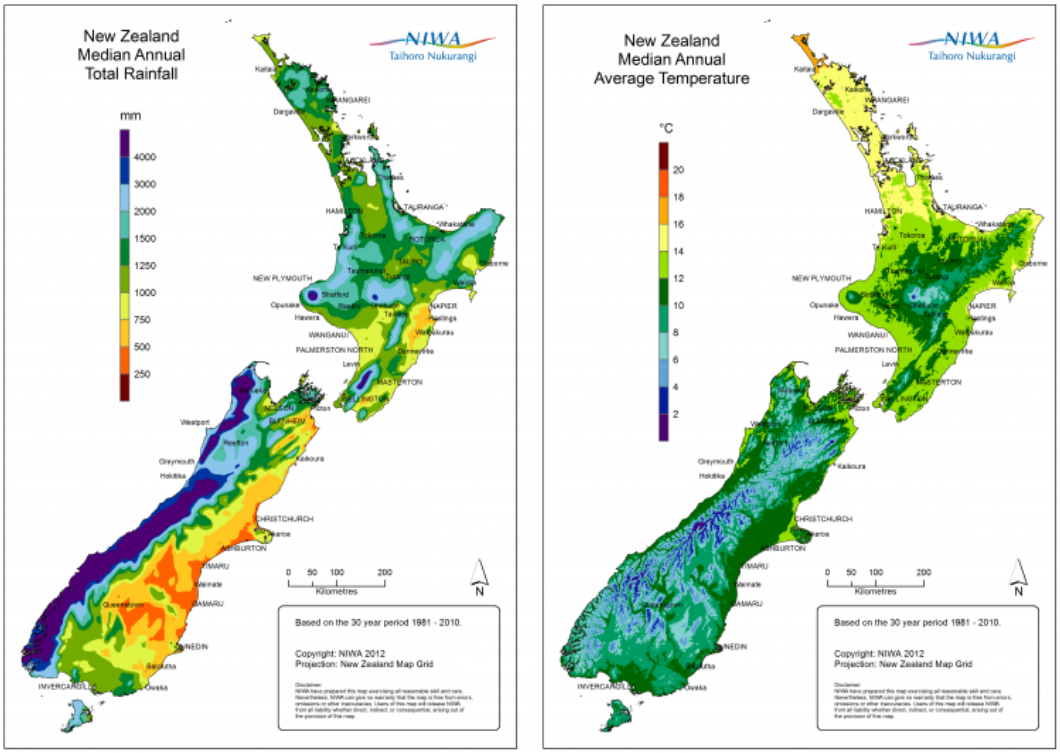

Figure 4.3 A. New Zealand Median Annual Total Rainfall for the period 1981 to 2010. B. New Zealand Median Annual Average Temperature for the period 1981 to 2010. Adapted from NIWA, 2012.

4.4 Physical Erosion

The coupling of intense rainfall and active uplift offer the potential for intense physical erosion in the Hokitika Catchment. High erosion rates and sediment yields have previously been associated with erodibility of bedrock and precipitation rates in the catchment (Hicks et al., 1996). The high precipitation rates prevailing in the Hokitika Catchment are therefore a large contributing factor to the high erosion rates of the South Island's west coast, which in turn have sculpted the dissected, steep slopes of the region (Korup 2005; Lyons et al., 2005).

4.5 Hydrology

Hydrological features of the western Southern Alps are largely attributed to the tectonic setting and prevailing climatic conditions of the region. The high relief of the Alps results in fluvial systems characterized by steep channel gradients, often incised into bedrock. This feature is advantageous for this study, as storage time of sediments within the system in alluvial plains or slow-moving rivers is minimized. Hicks and Shankar (2003) measured the annual suspended sediment output of the Hokitika River as 6.2 Mt/yr. Some of this sediment is routed into the Hokitika Canyon via hyperpycnal gravity flows (Mulder & Syvitski, 1995)

4.6 Vegetation

4.6.1 Modern-day Vegetation

The present-day ecology and distribution of vegetation in the Westland region has been comprehensively studied (Wardle, 1979; 1991; Reif & Allen, 1988; Macphail & McQueen, 1983; Vandergoes & Fitzsimons, 2003; Ryan et al., 2012). The following vegetation distribution in the Hokitika Catchment is largely controlled by elevation changes associated with temperature variations.

- From sea level to ~400 m elevation, lowland podocarp forest dominates the landscape, with prominent emergent species *Dacrydium cupressinum*, *Prumnopitys ferruginea*, and *Dacrycarpus dacrydioides* present. Tree ferns *Cyathea smithii*, *Cyathea colensoi* and *Dicksonia squarrosa* are common in the understory.

- From ~400 to 800 m, broadleaf and hardwood trees compose the majority of the montane forest present.
- From ~800 to 1200 m, in the subalpine zone, many of the species present in the montane forest remain. Vegetation also includes small tree conifers.
- The tree line occurs at approximately 1200 m, above which low-alpine open shrub and tussock grasslands predominate.
- Above 1400 m, in the high alpine zone, tall grasses and low shrubs become sparse, and shorter grasses dominate the landscape.

4.6.2 Palaeo-vegetation

The palaeo-vegetation of the Hokitika Catchment was studied through pollen analysis by Ryan et al. (2012) (Figure 4.3g,h). Results from these studies have been used to infer prevailing climatic conditions during the late Quaternary.

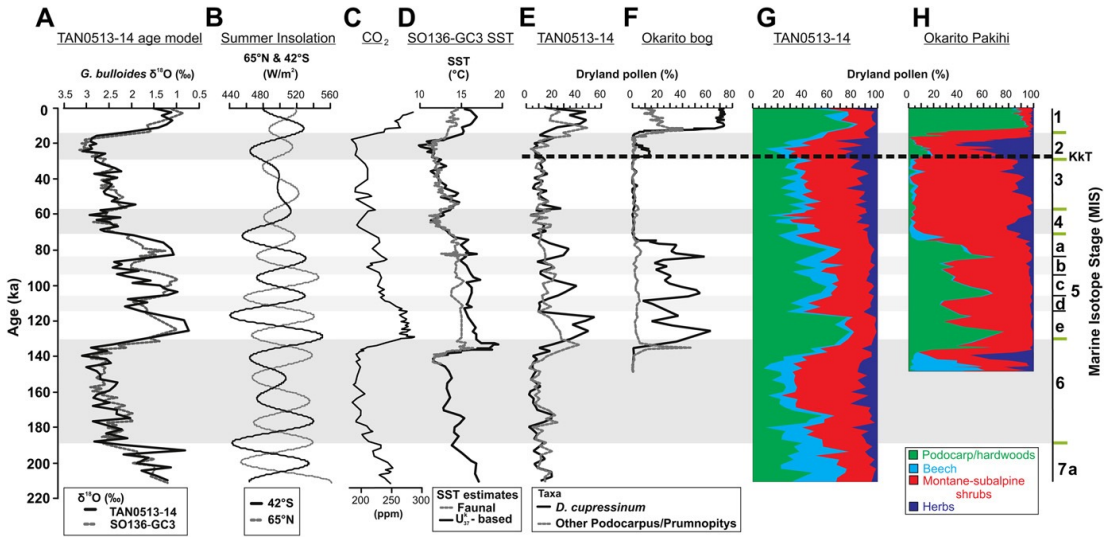

Figure 4.4 Comparison of the TAN0513-14 pollen record and other records of environmental change for the last 210 ka in New Zealand. A. $\delta^{18}O$ chronology from *G. bulloides* for TAN0513-14 and SO136GC3 B. Summer insolation at 65°N (black) and at 42°S (light grey). C. Atmospheric CO_2 from the Vostok ice core. D. SST estimates for SO136-GC3. E. & F. Dryland pollen (%) for *D. cupressinum* and all Podocarpus/Prumnopitys taxa for TAN0513-14 and the Okarito bog record; G. and H. Cumulative dryland pollen diagrams for TAN0513-14 and the Okarito bog record. MIS boundaries are shown on the far right and position of the KkT event is indicated. Adapted from Ryan et al. 2012.

In general, full interglacial periods (i.e. MIS 1 and 5e) are dominated by *D. cupressinum*, a conifer endemic to New Zealand, and smaller components of beech, asters and grasses (Figure 4.3g,h; Ryan et al., 2012). Hardwood forests reached maximum extents during these periods, causing minimum abundances of sub-alpine

and alpine vegetation. The higher levels of montane-to-subalpine pollen relative to hardwood pollen present in MIS 7 indicate a slightly cooler climate relative to the present day. Interstadial periods (MIS 3, 5a, 5c) are characterized by greater prominence of hardwood forest.

Stadial periods (MIS 4, 5b, 5d) exhibit a greater prominence of montane-to-subalpine shrubs relative to hardwoods (Ryan et al., 2012). Glacial periods (MIS 2, 6) similarly exhibit minimum abundances of hardwood pollen, and the highest abundances of grasses. Aster pollen is abundant and Fuscospora beech pollen comprises approximately 10% of dryland pollen during glacial periods. These assemblages suggest minimum forest extent and an extension of the montane-to-alpine zones, and a significantly cooler climate than other periods during MIS 2 and 6.

The Okarito Pakihi core highlights several significant excursions of climate at sub-MIS scales (Figure 4.3h). The maximum shown in beech vegetation during MIS 6 is indicative of a much significantly cool and wet climate. Peaks in hardwood pollen during MIS 5 correlate to the warmer periods of MIS 5e, 5c and 5a, similarly to MIS 1. Several smaller peaks in grass pollen abundance from MIS 2 to 4 are indicative of drier conditions (Ryan et al., 2012).

4.7 Soils

Characteristics of soils within the Hokitika Catchment are largely controlled by climatic and tectonic factors. The rapid uplift and high precipitation in the region limit the development of soil profiles, resulting in a very thin soil mantle (Tonkin & Basher, 1990). Soils have been estimated to erode from hillslopes within 2kyr of development on the western side of the Southern Alps, though soils of up to 10kyr in age have been stored on terraces and rare stable soil-mantled slopes (Tonkin & Basher, 2012). Erosion rates of soils in the region appear to be in equilibrium with local uplift rates of 1-10mm/yr (Tonkin and Basher, 2012).

4.8 The Hokitika Sedimentary Record

As previously stated, a large proportion of sediment exported from the Hokitika Catchment is deposited in the submarine Hokitika Canyon. Deposition predominantly occurs as gravity flows, and less frequently as turbidite deposits (Norris, 1978; Neil, 2008). Fluvial sediment is initially deposited on the continental slope and effectively distributed to the lower canyon during stands of high and low sea level. Seismic profiles and core stratigraphy from the Hokitika Canyon system indicate that sedimentation occurs as fine-grained levee deposits accumulated on the banks of the submarine channel at relatively uniform rates during glacial and interglacial periods (Figure 4.5; Ryan et al., 2012; Probert and Swanson, 1985).

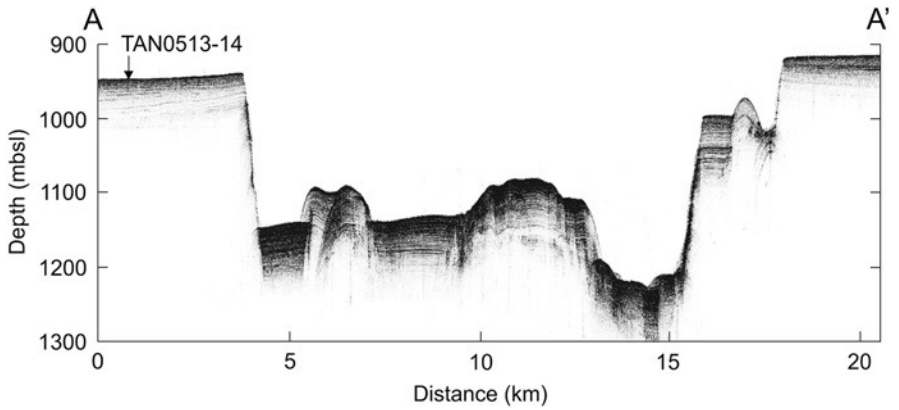

Figure 4.5 Seismic profile across the upper reaches of the Hokitika Canyon (A-A' location shown in Figure 4.1). Parallel reflectors across the northern levee (site of TAN0513-14) indicate fine-grained levee deposits. Adapted from Ryan et al., 2012.

5 Methodology

5.1 Site Selection and Sampling Technique

Field work and sample collection of Var and Hokitika sediments was carried out during the 2008 ESSDIV cruise on-board the research vessel (R/V) *Pourquoi pas?* (Institut français de recherche pour l'exploitation de la mer [IFREMER]) in the Mediterranean Sea, and during the TAN0513 cruise of the R.V. Tangaroa off the western coast of New Zealand South Island in October 2005, respectively. Var sediment samples are derived from two of the three Calypso long piston cores collected, ESSK08- CS01 and ESSK08-CS13. Core ESSK08- CS01 was collected along the levee crest and core ESSK08-CS13 was collected from the southwestern flank of the VSR (Figure 3.1). Piston core TAN0513-14 was collected from the north levee of the Hokitika submarine canyon system approximately 100km west of the New Zealand South Island (Figure 4.1). The location and characteristics of the cores are summarized in Table 5-1.

26 marine sediment samples from ESSK08-CS13 and 4 samples from ESSK08-CS01 were collected at IFREMER. Characteristics of these 30 samples are summarized in Appendix A. Samples of the same age are sampled from different horizons of a single turbidite deposits. Core age models were established through the integration of radiocarbon dating and oxygen isotope composition of planktonic *G. bulloides* forams within the cores. $\delta^{18}O$ of the forams was tied with reference Mediterranean planktonic $\delta^{18}O$ stratigraphies and on the $\delta^{18}O$ signal of GISP2 Ice Core (Bonneau et al., 2014; Cacho et al., 1999). Calculated ages of samples were provided by IFREMER and are reported to 3 significant figures in this study. Samples were received from IFREMER in Sandvik LDPE sample bags.

104 marine sediment samples spanning 33 deposition age classes from the TAN0513-14 core were received from Victoria University of Wellington. One sample from each class was selected for analysis, based on the terrigenous content of each sample and the amount of material available. The characteristics of the samples selected for analysis are summarized in Appendix A. A detailed core chronology for the TAN0513-14 core was established by measuring the $\delta^{18}O$ of *G. bulloides* at 3cm

intervals. The identification of volcanic glass shards deposited by the 25,360 ± 80 ka Kawakawa Tephra event provides additional stratigraphic control (Ryan et al., 2012).

Table 5-1 Location, bathymetry and length of studied cores.

Core	Latitude	Longitude	Water depth (m)	Length (cm)
ESSK08- CS01	43°23.24′ N	7°44.181′ E	2130	1052
ESSK08-CS13	43°14.922′ N	7°47.817′ E	2473	2450
TAN0513-14	42° 18' S	169°53'E	~950	3270

5.2 Sample Pre-processing

All samples were dried in an oven at 40°C for 18 hours. A ~10g aliquot was gently crushed to separate grains and homogenize the sample in an agate mortar. Two ~2g aliquots of each sample were separated for grain size and geochemical analyses. A separate ~2g aliquot of each Var sediment sample was finely ground in an agate mortar to be processed for mineralogical analysis. No aliquot was taken for mineralogical analysis for the Hokitika samples.

5.3 Grain Size Analysis

Grain size distribution of all samples was performed with a Malvern Mastersizer 2000 at the University of Wollongong. A ~2g aliquot of each sample was sonicated for 45 seconds to separate aggregated clasts prior to analysis. The grain size distribution for each sample was determined from the average of five consecutive measurements and reported as a percentage of sand (2000 - 63 μm), silt (63 - 4 μm) and clay (<4 μm).

5.4 Mineralogical Analysis

Mineralogical analysis was performed on Var samples via X-ray diffraction at the School of Earth and Environmental Science, University of Wollongong. The 30 sediment samples were ground to a fine powder with an agate mortar and pestle prior to analysis. Analysis was performed with a Phillips 1150 PW Braggs-Brentano diffractometer with CuKα radiation. Mineralogical phases were identified from XRD data using SiroQuant^{TM} software by matching measured diffraction peaks to reference

peaks. SiroQuant^{TM} was also used to perform quantitative analyses of the minerals in each sample. Accuracy of the analysis was determined from chi-squared values.

5.5 Isotopic Analysis for U isotopes

Sequential leaching of all samples was performed in order to remove non-detrital material from samples, so as to analyse the ($^{234}U/^{238}U$) of detrital material only. The Laboratory Procedure for U-series Isotope Sample Preparation (Dosseto, 2017), based on methods developed by Martin et al. (2015), was followed. At the completion of each of the following leaching and etching steps, samples were centrifuged at 3500rpm for 30 minutes and the supernatant was decanted. Samples were then rinsed by the addition of 18.2 MΩ water to remove any remaining reagent. Samples were centrifuged at 3500rpm for 30 minutes and the supernatant was decanted. The rinsing step was repeated once.

Wet sieving

Following sample pre-processing (Section 5.2), a ~2g aliquot of each sample was wet sieved at 63 μm using DI water. The <63 μm fraction was collected in 50mL centrifuge tubes, and centrifuged to separate the sample from any DI water collected. The overlying supernatant was discarded. The remaining sediment fraction was then dried in an oven at 50°C. Samples were gently crushed in an agate mortar and pestle to separate individual sediment grains, and stored in 50mL centrifuge tubes prior to further processing.

Sequential leaching

To leach the water-soluble fraction, 30mg of sodium citrate was added to each centrifuge tube with ≥ 16mL of 18.2 MΩ water. The sediment was suspended by shaking and placed on a mixing wheel for 1 hour.

To leach the exchangeable fraction, 30mg of sodium citrate and ≥ 16mL of 1M Suprapur $Mg(NO_3)_2$ was added to each centrifuge tube prior to being placed on the mixing wheel for 50 minutes.

To leach the carbonate fraction, 30mg of sodium citrate and ≥ 16mL 1M Suprapur CH_3COONa was added to each centrifuge tube. Each tube was agitated to resuspend the sample and placed on the mixing wheel for 5 hours.

To remove the Fe,Mn-oxide fraction, samples were heated at ~96°C for 6 hours in an oven with 30mg of sodium citrate and ≥ 40mL of 0.04M NH_2OH-HCl in 25% (v/v) CH_3COOH. The centrifuge tubes were agitated every half hour to ensure complete reaction of the reagents with the sediment.

The organic fraction was leached via a three-step process. First, ≥ 6mL Suprapur 0.02M HNO_3, ≥ 10mL Ultrapur 31% H_2O_2 and 30mg of sodium citrate were added to each sample and agitated to suspend sediment. The pH of each sample was adjusted to 2 by adding 1 drop of Suprapur 67% HNO_3 and left to react at room temperature for approximately 20 minutes. The samples were then placed in the oven and warmed slowly to 85°C and left to react for 90 minutes. Samples were then allowed to cool for 5 minutes prior to centrifugation to remove the supernatant. Samples were then slowly heated to 85°C in ≥ 6mL Ultrapur 31% H_2O_2, 30mg of sodium citrate and 1 drop of 67% HNO_3 to adjust pH to 2 for 3 hours in an oven. The centrifuge tubes were agitated every half hour to ensure complete reaction of the reagents with the sediment. Samples were again allowed to cool for 5 minutes prior to centrifugation steps to remove the reagent and rinse the samples with 18.2 MΩ water twice. Any remaining organic material was removed by adding 10mL 3.2M Suprapur $NH_4CH_3CO_2$ and 30mg of sodium citrate to the centrifuge tubes and placing on the mixing wheel for 30 minutes.

The HF/HCl etch was performed by adding 20mL of 0.3M Suprapur HF-0.1M Suprapur HCl and 30mg of sodium citrate to each centrifuge tube. Var and Hokitika samples were reacted for 6 hours on the mixing wheel. Samples were dried in ethanol in a fume hood.

Sample digestion

To prepare for mass spectrometry analysis, samples were digested in the following process. Up to 50mg of each leached sample was ground finely and transferred to a clean 30mL PFA digestion vial. Samples were reacted with 1mL Suprapur 48% HF at room temperature for 30 minutes prior to the addition of 0.5mL Suprapur 65% HNO_3. Samples were reacted on the hotplate overnight at 100°C. The following day, samples were sonicated for 10 minutes before opening the vials to check for undissolved residue. Samples were then dried to incipient dryness at 100°C. 0.5mL Suprapur 65% HNO_3 and 1.5mL Suprapur 30% HCl (aqua regia) was added to each vial and reacted on a hotplate overnight at 120°C. The following day, samples were observed for undissolved material. As most samples contained small brown-black particles, 2mL of aqua regia was added to all samples and reacted at 120°C on a hotplate for a further 3 days. Samples were dried down at 100°C and again observed for undissolved particles. 0.5mL Suprapur 31% H_2O_2 was added to each vial and reacted at 80°C overnight due to residual brown particles in some samples. Samples were dried down at 80°C the following morning.

Ion-exchange chromatography

To prepare the samples for ion-exchange chromatography, 0.5mL Suprapur 65% HNO_3 was added to each vial and dried down at 80°C on a hotplate. This step was repeated once. 2mL Suprapur 1.5M HNO_3 was then added to each vial and reacted on a hotplate at 100°C for 3 hours. The vials were sonicated for 5 minutes before being transferred to clean 15mL centrifuge tubes and centrifuged at 4000rpm for 5 minutes.

Ion exchange chromatography was performed in order to separate and elute uranium isotopes from the acidified samples. U-Th chromatography columns were prepared by loading 0.1mL pre-filter resin followed by 0.5mL TRU-resin onto 18.2 MΩ- and ethanol-rinsed columns. The resin was cleaned by loading three 2mL aliquots of Suprapur 0.5M HCl, followed by three 2mL aliquots of 0.1M HCl-0.3M HF, onto the column. Columns were pre-conditioned by loading two 2mL aliquots of Suprapur 1.5M HNO_3 onto each column. Each sample was then loaded onto its respective column in four 0.5mL aliquots. The TRU-resin trapped elements within the samples during this step. Each column was then washed with three 2mL aliquots of 1.5M

HNO_3. Neodymium and other rare-earth elements were eluted via the addition of 4.5mL of 3M Suprapur HCl onto each column. Thorium was subsequently eluted by the addition of 4.5mL of 0.5M HCl. All elutriate up to this point was collected in a plastic waste beaker. Uranium was eluted via the addition of three 2mL aliquots of 0.1M Suprapur HCl-0.3M Suprapur HF onto each column. Uranium cuts were collected in clean 15mL PFA chromatography vials and dried down on the hotplate at 80°C.

Preparation for MC-ICPMS

In preparation for MC-ICPMS analysis, 4mL Suprapur 0.3M HNO_3 was added to each 15mL vial and refluxed at 80°C for 30 minutes. The solutions were then sonicated for 10 minutes and transferred to clean ICP vials. Samples were analysed using a Neptune Multi-Collector Inductively-Coupled Plasma Mass Spectrometer in the Wollongong Isotope Geochronology Laboratory at the University of Wollongong. Samples were screened to check that the uranium concentration of samples fell within the analytical constraints of the equipment. Any necessary dilutions were performed prior to analysis. A total procedure blank and rock standard GSP-2 was also analysed for quality control and assurance. A secondary standard, U005A was also analysed throughout analysis to account for instrument drift during the analysis run.

5.6 Isotopic Analysis for method evaluation

The method used for sequential leaching of sediment samples outlined in Section 5.5 was evaluated prior to the preparation of all samples. Method evaluation was carried out by analysing the ($^{234}U/^{238}U$) activity ratio of samples after each leaching step, and at two-hourly intervals of the HF/HCl etches. Two Var samples, CS13_18 and CS13_24, and two Hokitika samples, T14-M-170 and T14-190, were analysed. A repeat aliquot of CS13_24 was analysed to assess the repeatability of results. The Following centrifugation at the completion of each step described in Section 5.5, a ~20mg aliquot of each sample was dried down in ethanol in a 15mL centrifuge tube. Aliquots were also taken after each leaching step and after 2, 4, 6 and 8hrs of the HCl-HF etch. The subsamples underwent digestion and ion exchange chromatography as per the method described in Section 5.5 prior to MC-ICPMS analysis.

5.7 Major and trace element analysis

Major and trace element analysis was performed on Var samples only. Following sequential leaching, a ~30mg aliquot of leached sample was ground finely and accurately weighed to 5 significant figures. The aliquots were digested as per the sample digestion method outlined in Section 5.5, but with Ultrapur reagents in place of Suprapur reagents in order to reduce possible contamination. The samples were dried down in 0.5mL Ultrapur 65% HNO_3 at 80°C twice prior to the addition of 4mL Ultrapur 0.3M HNO_3 to each vial and heating at 80°C for 30 minutes. The vials were then sonicated for 5 minutes before being transferred to clean 15mL centrifuge tubes and centrifuged at 4000rpm for 5 minutes.

Major and trace element concentrations were measured on a Quadrupole Inductively Coupled Plasma Mass Spectrometer (Q-ICPMS) in the Wollongong Isotope Geochronology Laboratory at the University of Wollongong. In order to constrain the concentrations of measured elements to the sensitivity parameters of the Q-ICPMS, 1:100 and 1:10,000 dilutions were performed to measure trace and major elements, respectively. A 0.04mL aliquot was extracted from each centrifuge tube and diluted to 4mL in clean ICP vials to generate the 1:100 trace element solutions. A 0.04mL aliquot was then extracted from the 1:100 trace element solutions and diluted to 4mL in clean ICP vials to generate the 1:10,000 major element solutions. Solutions were screened on the Q-ICPMS prior to analysis to check that the intensities of the elements measured fell within the sensitivity parameters of the instrument. Screening of the 1:10,000 solution indicated that the solution was too dilute to accurately measure the selected elements. The 1:100 dilutions were instead used to measure major element concentrations.

Quality control and assurance measures included the measurement of synthetic standard 71A+B (of which the concentrations of analytes is known) after every tenth sample to account for instrument drift. Blanks were also tested after every tenth sample to assess any contamination occurring during the analysis run. Major elements analysed included Na, Mg, Al, Si, K, Ca, Ti, Mn, Fe, Sr, and Ba. Trace elements analysed included B, P, Cu, Zn, Rb, Sr, Zr, Ba, La, Ce, Pr, Nd, Sm, Eu, Gd, Yb, Hf, Pb, Th and U.

5.8 Surface Area Analysis

Specific surface area measurement was performed in order to calculate the recoil fraction and comminution age of samples. The specific surface area of 8 leached and 20 sieved Var samples was measured on Quantachrome iQ equipment at the University of Wollongong. Samples selected for BET analysis was based on the availability of leached and sieved material. Samples were degassed for 9 hours at 200°C prior to analysis to remove any volatiles from the sample. Surface area measurements were determined by N_2 gas adsorption using the BET method (Martin et al., 2015).

6 Results and Discussion – Method Evaluation

This chapter presents the results of the method evaluation sequential leaching experiments. Ideally, method evaluation results should reflect the decreasing trend shown in Figure 2.11. Results for the Var sediments are presented in Figure 6.1. Results for the Hokitika sediments are presented in Figure 6.2 and 6.3. The raw data represented in these figures is presented in Appendix F.

6.1 Var Samples

The method evaluation tests for the Var sediments present several key points (Figure 6.1). The initial ($^{234}U/^{238}U$) indicates that non-detrital material was not a dominant component of the sediments, as the value is less than 1. In general, ($^{234}U/^{238}U$) declines throughout the process, with the exceptions of unexpected large negative excursions for the carbonate and Fe,Mn-oxide leach steps (Figure 6.1).

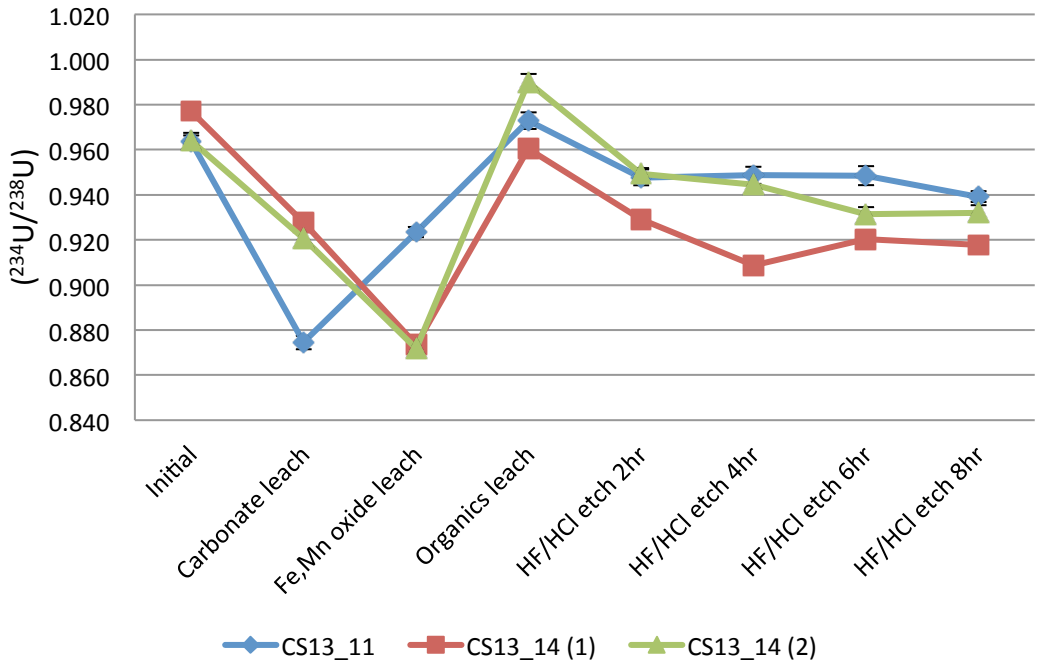

Figure 6.1 ($^{234}U/^{238}U$) evolution throughout the sequential leaching process in CS13_11 and CS13_14.

The unexpected results for the carbonate leach and Fe,Mn-oxide leach may be caused by errors that occurred when treating the respective aliquots. The ($^{234}U/^{238}U$) activity ratio after the organics leach for CS13_14 (2) is greater than the initial ($^{234}U/^{238}U$) of

the sample. This may be caused by the re-sorption of U onto mineral grains. An error in the Fe,Mn-oxide leaching step may have also contributed to the irregular trend shown, as samples were left to react with the reagent for 24 hours at room temperature following heating in the oven. This may have affected the resulting ($^{234}U/^{238}U$) activity ratio, however the chemistry behind this hypothesis has not been investigated.

The decreasing trend during the HF/HCl etch in all samples indicates removal of non-detrital material was incomplete following sequential leaching. It was therefore necessary to perform the HF/HCl etch on Var samples. The stable trend of the ($^{234}U/^{238}U$) activity ratio for CS13_11 between 2 hours and 6 hours indicates that 2 hours was sufficient to reach the average minimum ($^{234}U/^{238}U$), but further etching would not detrimentally increase the activity ratio. The lowest value after 8 hours of HF/HCl etch is assumedly caused by human error. CS13_14 (1) reached minimum ($^{234}U/^{238}U$) after 4 hours while CS13_14 (2) reached minimum ($^{234}U/^{238}U$) after 6 hours. Due to the slight variation in the length of optimal HF/HCl etching between samples, an etch time of 6 hours was chosen for the remainder of Var sediment samples.

The replicated sample CS13_14 generally follows similar trends in ($^{234}U/^{238}U$) throughout the leaching and etching process, indicating that the ($^{234}U/^{238}U$) of a given aliquot of sample may be representative of the sample as a whole. The smallest deviation between CS13_14 (1) and CS13_14 (2) is also smallest after 6 hours of etching, which contributed to selecting a 6 hour HF/HCl etch for the Var samples.

6.2 Hokitika Samples

The method evaluation results of Hokitika Catchment samples provide several interesting points to consider. Firstly, the accidental loss of samples during the process is noted. Several samples from T14-190 were lost prior to analysis. The complete dataset of ($^{234}U/^{238}U$) for T14-M-170 is presented in Figure 6.2 while Figure 6.3 presents ($^{234}U/^{238}U$) values from both samples that may be compared at the same leaching and etch step.

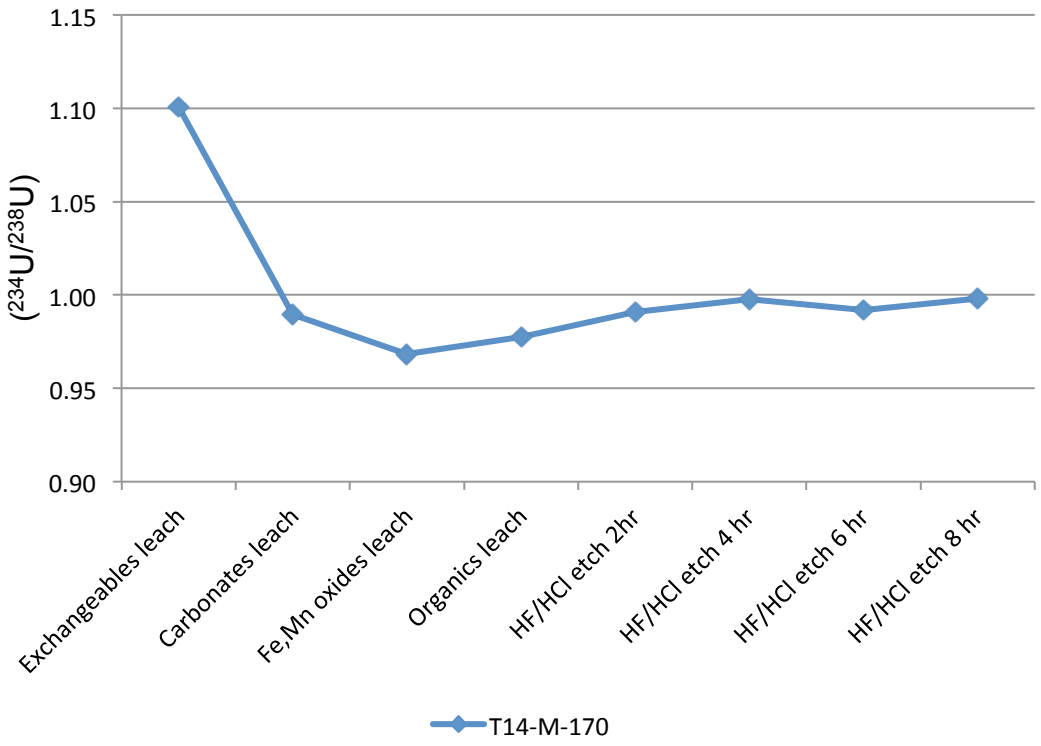

Figure 6.2 ($^{234}U/^{238}U$) evolution throughout sequential leaching process in T14_M_170.

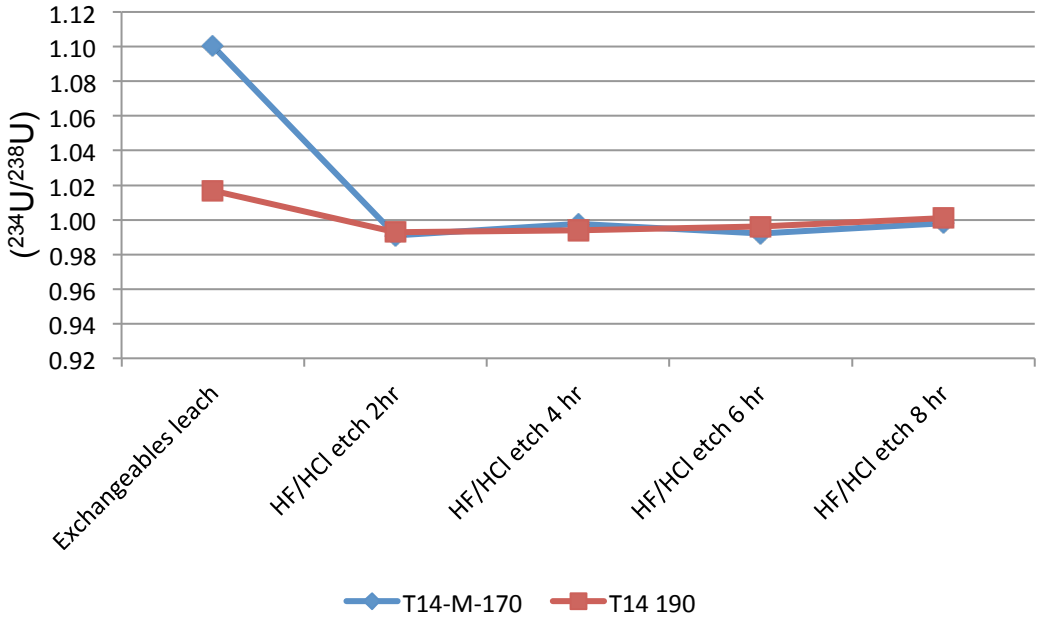

Figure 6.3 Comparison of results from T14-M-170 and T14-190.Exludes T14-170 results from solid aliquots taken after carbonate leaching, Fe/Mn oxide leaching and organic matter leaching as these did not have comparable results in T14-M-170.

The initial ($^{234}U/^{238}U$) of samples T14-M-170 and T14-190 was not measured. The ($^{234}U/^{238}U$) of the exchangeables leach step may be used as an indicator of the initial ($^{234}U/^{238}U$) of the samples, as little material is removed during this step, as discussed in Section 2.3.4. Both samples are therefore likely to have contained significant non-detrital components, as ($^{234}U/^{238}U$) is greater than 1 following exchangeable leaching. T14-M-170 reached minimum ($^{234}U/^{238}U$) following the Fe,Mn-oxides leaching step, possibly indicating that the leaching process for other Hokitika samples could have been completed at this step. The increase in ($^{234}U/^{238}U$) following this step is indicative of an over-leaching of samples, as an increase towards ($^{234}U/^{238}U$) = 1 indicates complete removal of Domain 2 of sediment grains (Figure 2.11).

Similar results are evident in both analysed samples during the HF/HCl etch, with ($^{234}U/^{238}U$) values very close to 1 at all stages. The similarity between samples shown in Figure 6.3 indicates that the Hokitika samples are similar in character and that the same process may be performed for all Hokitika samples. Figure 6.2 indicates that a HF/HCl etch does not need to be performed, and that the minimum ($^{234}U/^{238}U$) activity ratio is reached after Fe,Mn-oxide leaching in T14-M-170. However, as these results were not available prior to the leaching of the remainder of the Hokitika samples, the complete leaching and etching process was performed on all samples, with an etch time of 6 hours. This will impact the resulting ($^{234}U/^{238}U$) values of the remainder of Hokitika sediments and reduce variability in ($^{234}U/^{238}U$) values that may have been present, but removed by the overly aggressive leaching and etch steps applied.

7 Results and Discussion – Var River Catchment

This section presents grain size, mineralogy, element composition, U isotope and surface area results determined for Var samples.

7.1 Grain Size

The grain size distribution of Var sediment samples is summarized in Appendix B and is presented below in a ternary diagram of sand, silt and clay fractions in Figure 7.1. The majority of samples contain more than 50% silt, less than 40% sand and less than 25% clay. Silt content is highly variable and ranges from approximately 35 to 80%. Sand content is similar, with content ranging from approximately 5 to 60%. Clay content is much more uniform across samples, with content ranging from approximately 5 to 25% clay content.

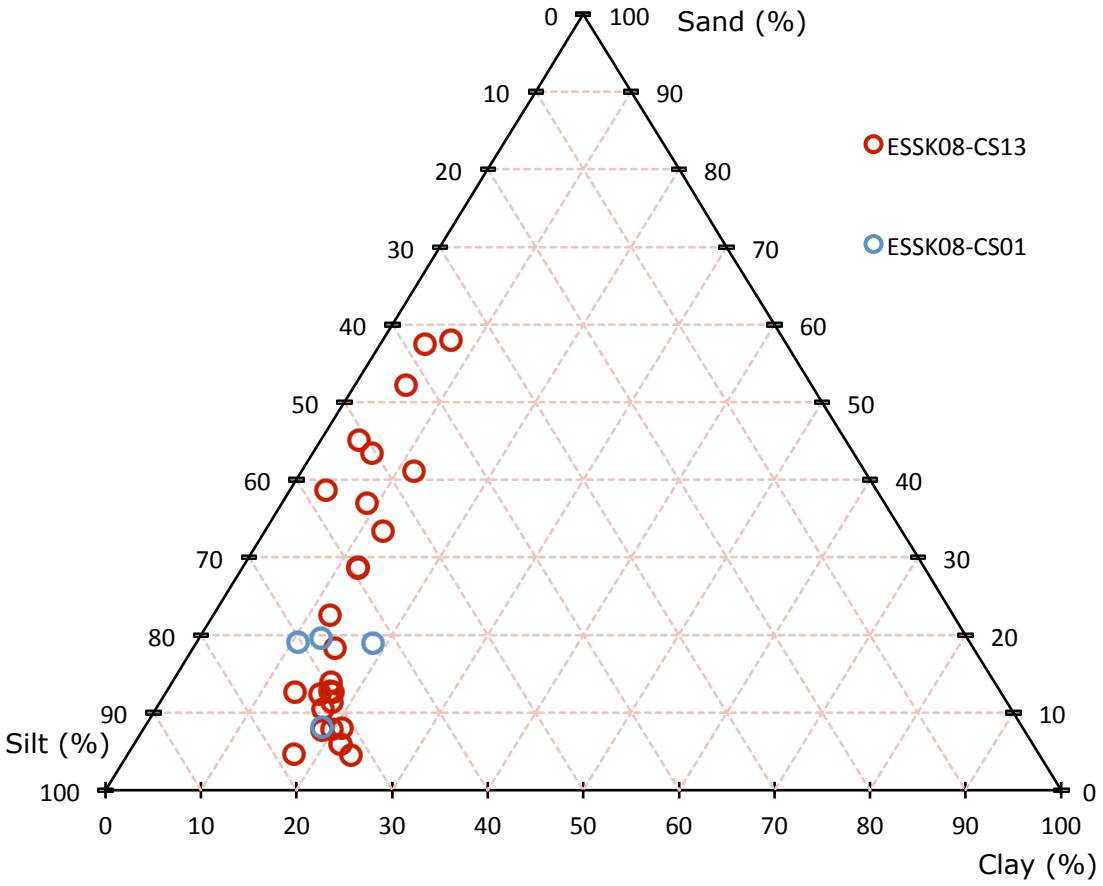

Figure 7.1 Grain size distributions of Hokitika sediments.

The relative heterogeneity demonstrated in Figure 7.1 may be reflective of the processes occurring within the Var Sediment System at the time of deposition. For example, samples with higher sand content may have been deposited from a higher energy flood than a sample with relatively lower abundances of sand particles. The distance travelled away from the Var Sedimentary Ridge may also impact upon the resulting grain size distribution of samples, particularly between the two cores. As core CS01 is located closer to the submarine valley on the VSR, it may be expected that higher sand content would predominate in CS01 samples. However, the inverse of this trend is observed, with CS01 cores containing only up to 20% sand. This may indicate that sand fractions travel farther from the submarine valley on the VSR, though due to the limited number of samples from the CS01 core, and the inability to correlate the grain size distribution of samples of the same age between cores, this observation is highly speculative.

Variation of mean grain size and the percentage content of individual grain size fractions of Var sediments during the past 70ka are presented in Figure 7.2. Assuming that the sampling process was carried out to target the same horizons within each turbidite sequence, the relationships of grain size through time may provide an indication of how the energy of the Var fluvial system has varied through time. Little variation in grain size parameters is evident during MIS3, indicating that changes occurring within the fluvial system were either negligible or not apparent at the sampling resolution used (Figure 7.2).

Mean grain size and sand content decrease from approximately 17 ka towards the Holocene (Figure 7.2a,b). This change may be indicative of a system energy decrease following the slight increase in sand content, and therefore system energy, around the time of deglaciation at 20 ka. This trend indicates that fluvial energy increased during deglaciation as rivers received increased input, and that following this pulse of increased energy, fluvial systems reduced in energy during the transition to the Holocene. A similar trend is apparent in clay content (Figure 7.2d), with clay content increasing from 17 ka, indicating a lessening of system energy.

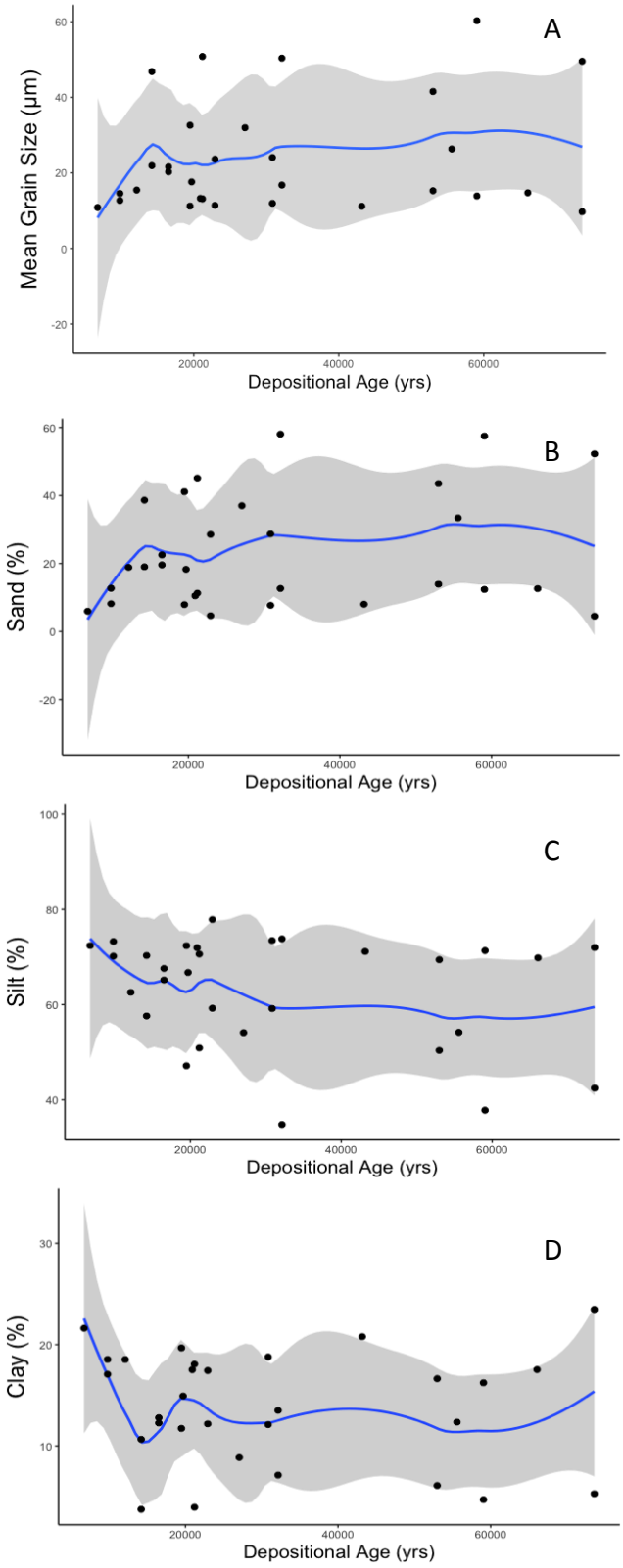

Figure 7.2 Grain size parameters of Var sediments through time. A. Mean grain size (µm). B. Sand (%). C. Silt (%). D. Clay (%). Black dots are raw data points. Blue line is a polynomial fit calculated by the 'loess' method with a span of 0.4 in RStudio. Grey area is 95% confidence interval.

The relative heterogeneity and homogeneity of samples of the same age may be indicative of the characteristics of the individual turbidite deposits from which they are sampled. The variation in grain size distribution of samples of the same age is presented in Figure 7.3. Sand content varies by more than 10% in individual turbidites, with the exception of samples at 9.8 and 14.2 ka. However, sand percentage at these depositional ages is relatively low for both samples. It is therefore likely that any homogeneity observed between samples of the same age is due to the small amount of sand present in the turbidite flow. It is postulated that heterogeneity between samples of the same age is heavily influenced by fining-upwards sorting of grains and variable intensity of individual turbidite events and deposits.

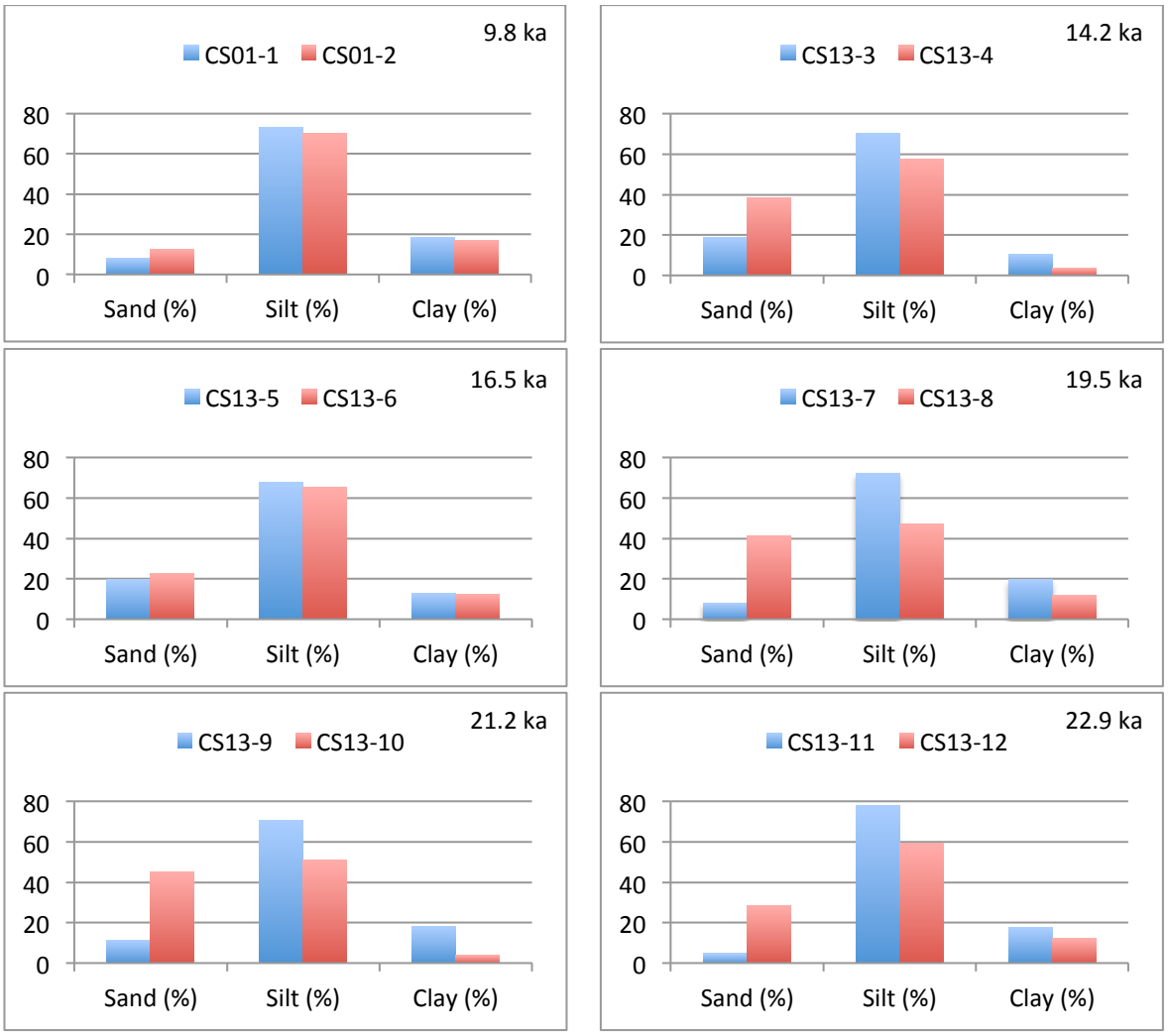

NB. Figure continued on following page.

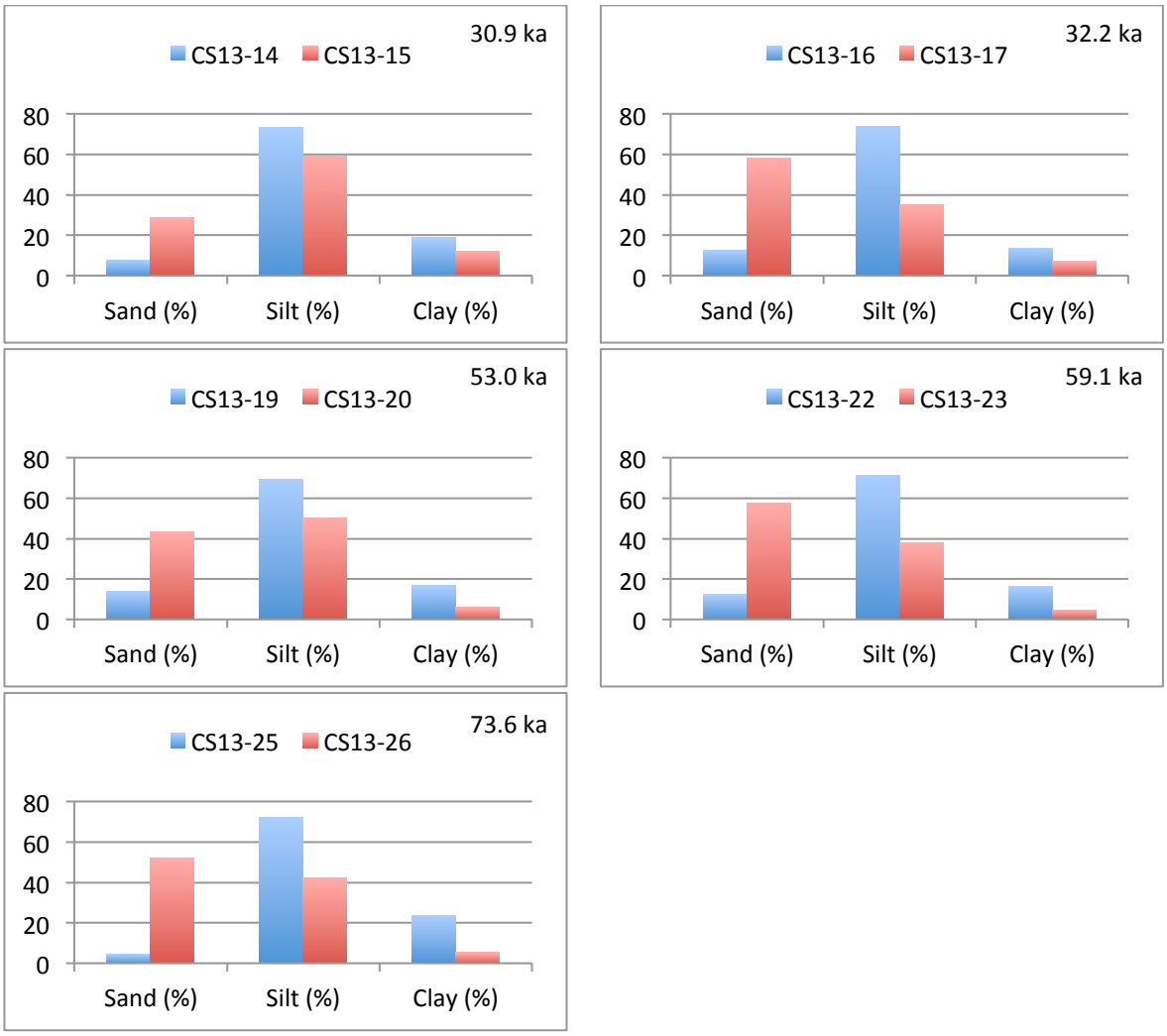

Figure 7.3 Grainsize variation between Var samples of the same deposition age.

The above grain size analysis is based on non-sieved and non-leached material. To understand how variation in grain size may influence geochemical analyses, it is necessary to investigate how the particle size distribution of sediment samples changes throughout the sieving and leaching process. Changes in grain size measured for CS13-11 are presented in Figure 7.4. Only one sample was analysed due to the limited availability of sieved and leached material. Figure 7.4 indicates that very little change in grain size occurs after sieving and leaching. However, the initially low sand content of CS13_11 may be the cause of this apparent relationship, as sand is not expected to be completely removed during the sieving process. It may therefore be possible to compare the grain size of non-sieved and non-leached samples to geochemical results of each sample. As significant reductions in sand content of samples with initially high sand content are expected, only samples with small

amounts of initial sand content (i.e. less than 10%) will be reliably compared with any U isotope data.

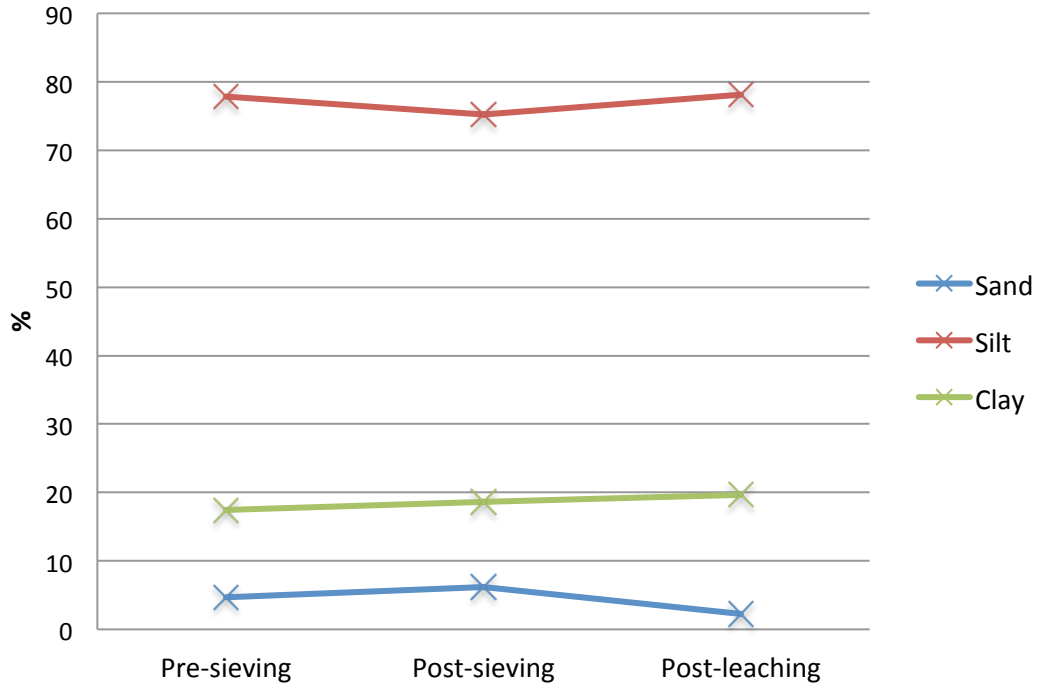

Figure 7.4 Evolution of grain size fractions following sieving and leaching in CS13_11.

7.2 Mineralogy

Variation in mineralogy of Var sediment samples is presented in Figure 7.5. Data has been normalized to 100% following the removal of halite and siderite from the data set, as halite was likely formed during the drying of the samples and siderite values were much less than 5%, and therefore unlikely to be reliable. For ease of comparison, minerals have been grouped into the categories shown in the figure.

Mineralogy is mostly consistent between samples, possibly indicating that sediments have been drained from areas with the same underlying lithology over the past 70 ka. Carbonate minerals, predominantly calcite, compose ~30-45% of all samples. Quartz content is stable across samples, commonly composing 20% of the total sample. Feldspar content, which includes labradorite, microcline and orthoclase, ranges from 10 to 20%. Finally, clay minerals, namely kaolinite, comprise the remaining 5 to 13% of the mineralogical content of Var sediments. The complete mineralogy of Var samples is tabulated in Appendix C. The low sampling resolution during MIS 3 does not allow for an in depth analysis of mineralogical variability during this period.

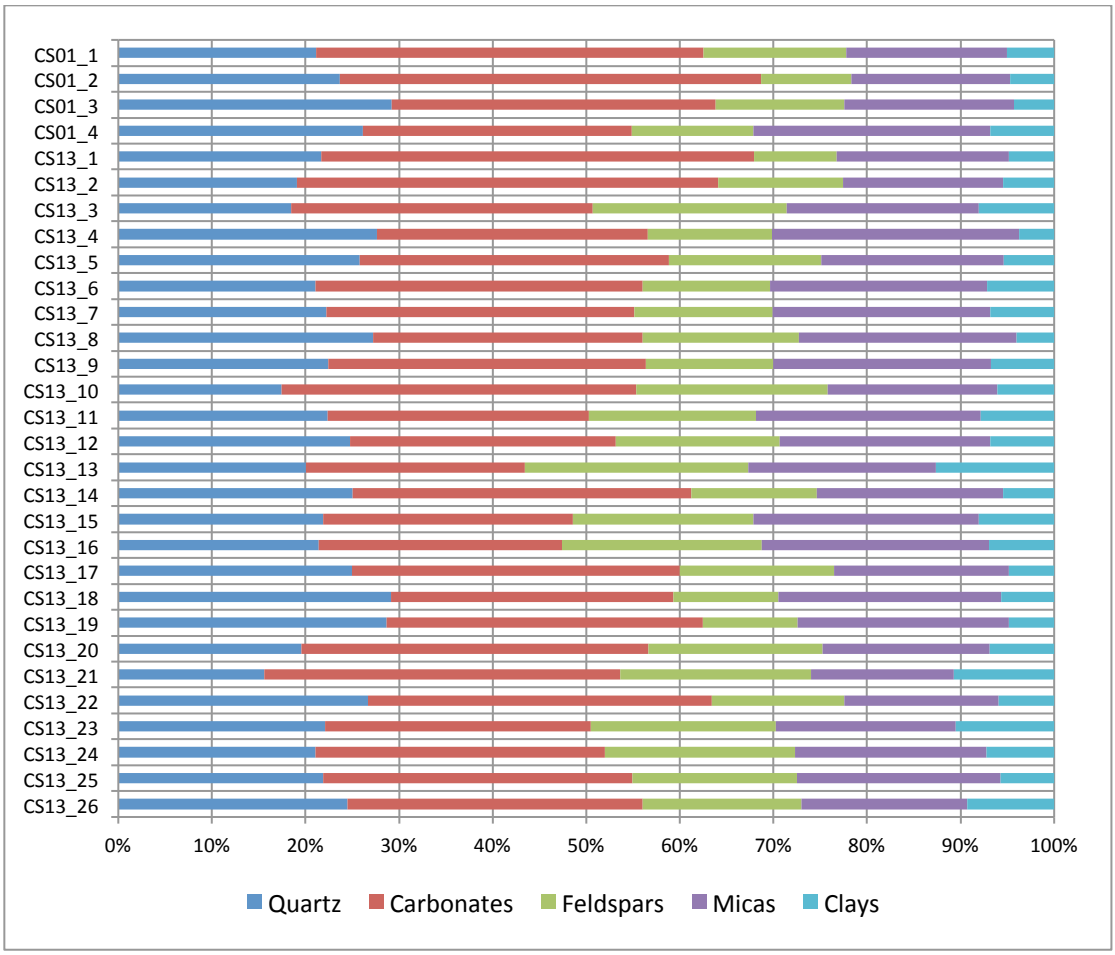

Figure 7.5 Simplified mineralogy of Var sediments.

Variations in mineralogical content of samples may be attributed to changing source areas of the fluvial system through time. Variation in percentage abundance of individual minerals through time is illustrated in Figure 7.6. A significant change in the percentage content of minerals occurs near 30 ka. Calcite content gradually increases from ~25% at 30 ka to ~45% in the early Holocene. Conversely, kaolinite and orthoclase decrease steeply in percentage content from 30 ka. Biotite content decreases more steadily than kaolinite and orthoclase into the Holocene, similarly to decreases observed in labradorite.

As discussed in Section 2.3.2, the ratio of primary minerals to secondary minerals may provide an indication of the degree of chemical weathering that occurred at a given period in time. This relationship is illustrated in Figure 7.6j. Primary minerals include quartz, muscovite, microcline, labradorite, orthoclase and biotite, and Kaolinite is the only secondary mineral present in the assemblages. A decrease in the

ratio from occurs from ~30 to 20ka, indicating a potential increase in chemical weathering during the LGM, and a return to equilibrium conditions following deglaciation (Figure 7.6j). However, as mineralogy has indicated a potential change in source area, stating that chemical weathering was altered during the same period is unfitting.

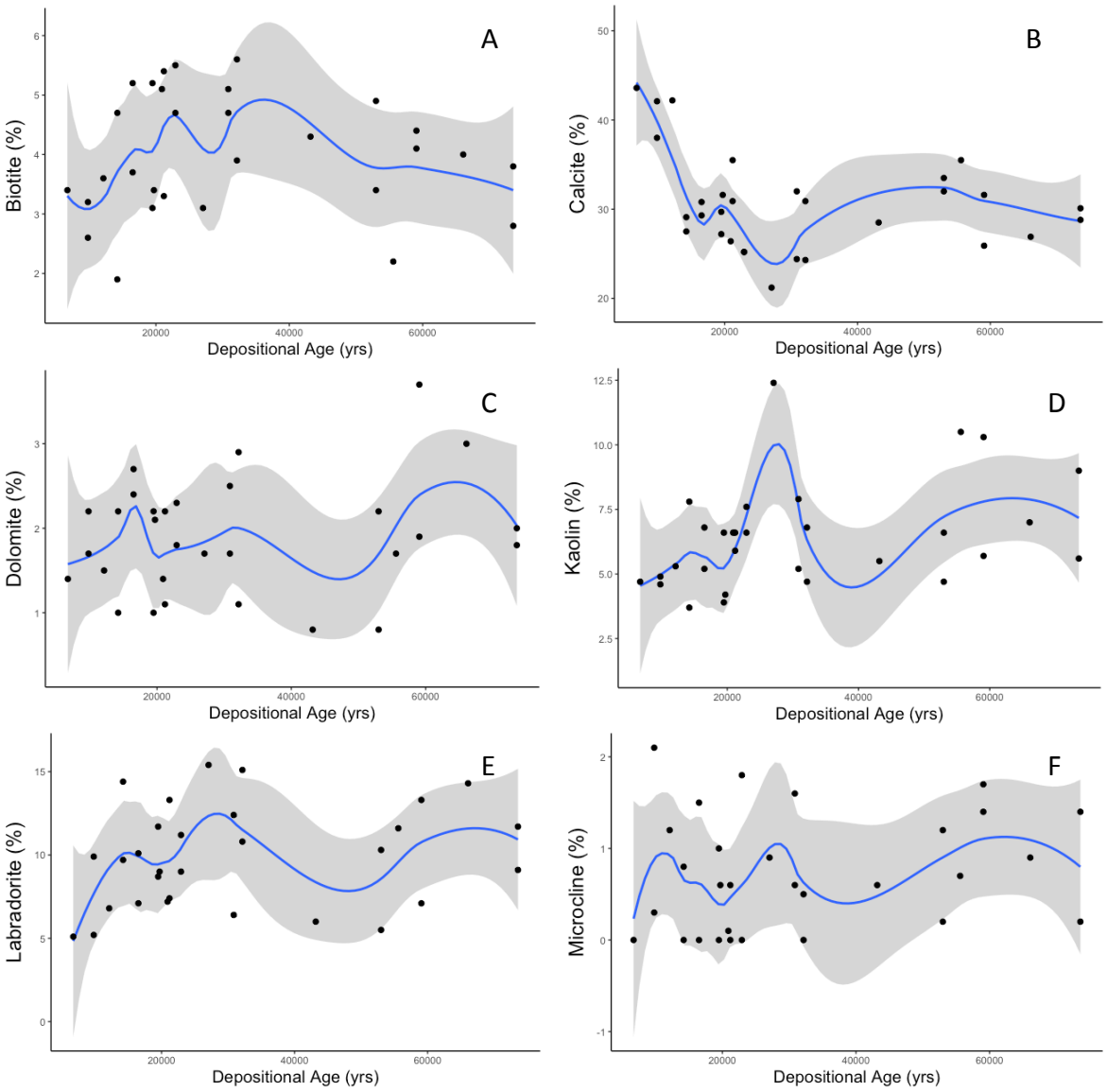

NB. Figure continued on following page.

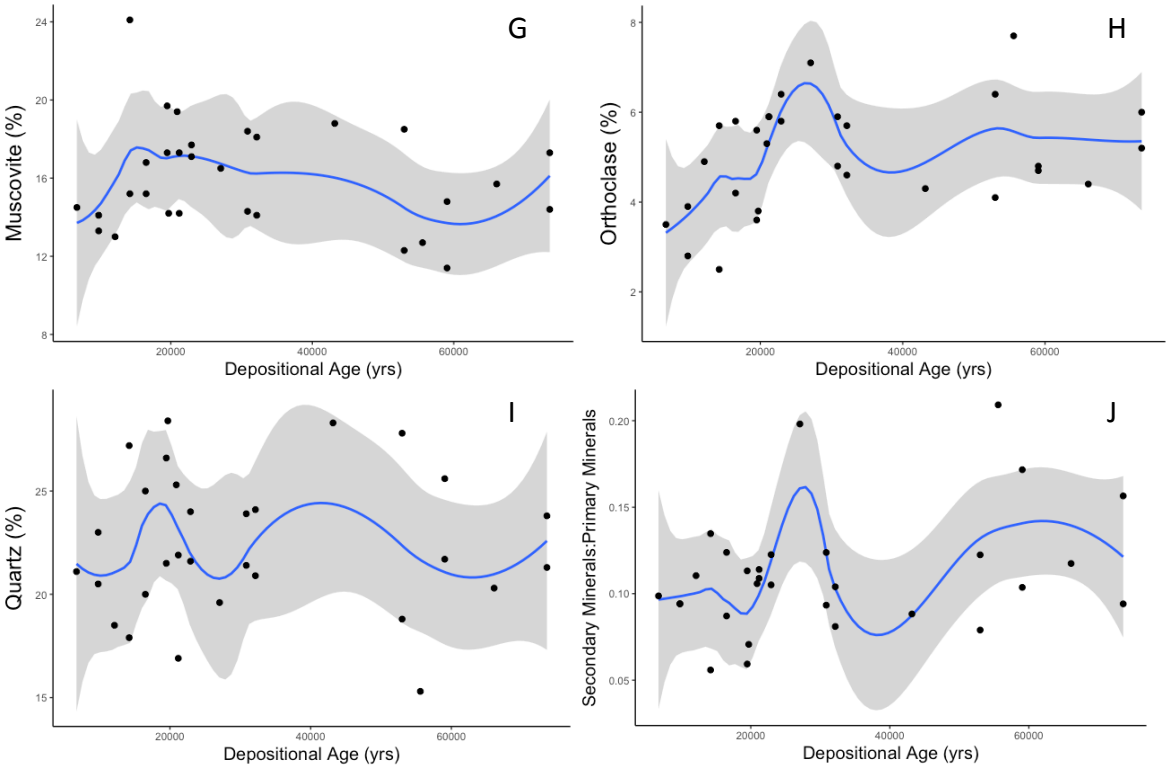

Figure 7.6 Mineral percentage content in Var sediments through time. A. Biotite. B. Calcite. C. Dolomite. D. Kaolin. E. Labradorite. F. Microcline. G. Muscovite. H. Orthoclase. I. Quartz. J. Secondary to Primary minerals. Black dots are raw data points. Blue line is a polynomial fit calculated by the 'loess' method with a span of 0.4 in RStudio. Grey area is 95% confidence interval.

7.3 Major and Trace Elements

The results of major and minor element analysis of Var samples are presented in Figure 7.7. Concentrations of major and trace elements are presented in Appendix D as wt. % and ppm, respectively.

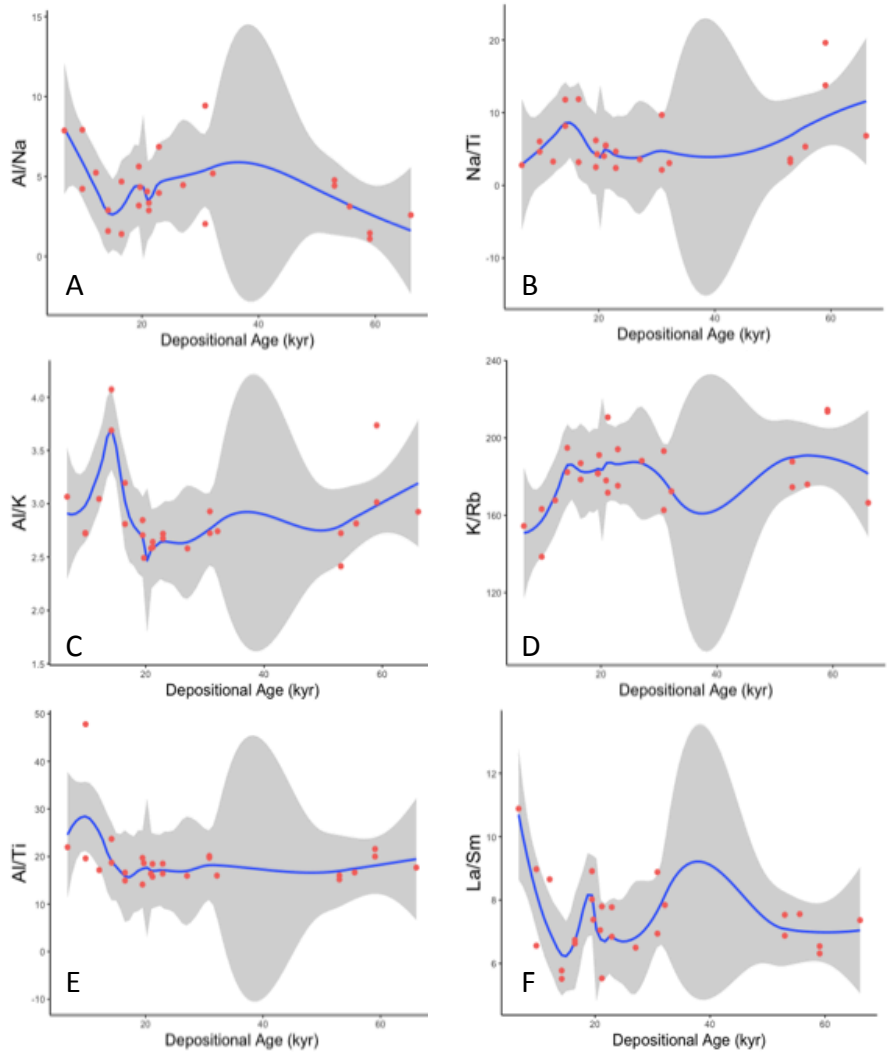

Figure 7.7 Elemental ratios in leached Var sediments. A. Al/Na. B. Na/Ti. C. Al/K. D. K/Rb. E. Al/Ti. F. La/Sm. Red dots are raw data points. Blue line is a polynomial fit calculated by the 'loess' method with a span of 0.4 in RStudio. Grey area is 95% confidence interval.

Elemental ratios presented in Table 2.2 have been implemented to infer the degree of chemical weathering active during the last 70ka. Interpretations of the chemical weathering proxies implemented are not useful for MIS 3, as the temporal resolution of data is too low to accurately interpret any apparent trends (Figure 7.7). In general, the chemical weathering proxies indicate a shift in chemical weathering towards more intense regimes at approximately 17ka, following the deglaciaton period of the LGM.

Chemical weathering subsequently increases towards the Holocene due to increased soil development and reduced disturbance of hillslopes by glacial activity.

The Al/Na, Al/Ti, Na/Ti, K/Rb and La/Sm proxies all demonstrate this trend to varying intensities (Figure 7.7). Conversely, the Al/K exhibits the inverse to the main trend by indicating a decrease in chemical weathering from 17 ka towards the Holocene. Since K is in the same periodic group as Na, and are therefore of similar behaviours, it is interesting that the two elements would behave differently during chemical weathering.

A more detailed investigation into the chemical weathering trends exhibited in Figure 7.7 is provided here. The Al/Ti ratio trend indicates a decrease in chemical weathering at approximately 11 ka, though a lack of data around this age may be the cause (Figure 7.7e). The Na/Ti proxy indicates a decrease in chemical weathering from 20 ka to 17 ka and increase in chemical weathering from 17 ka onwards (Figure 7.7b). A similar relationship is identified in the La/Sm proxy (Figure 7.7f). The decrease may be caused by weathering-limited regimes operating during the export of glacial sediment from the Var catchment during deglaciation, as discussed in the following sections (Section 7.4, 7.5). K/Rb indicates that weathering was constant from 30 to 17 ka, after which the general increase in chemical weathering is observed.

Though changes in elemental ratios are inferred as variations in chemical weathering, they may also be influenced variations in the mineralogy of sediments investigated in Section 7.2. As any significant change in mineralogy occurs around 30 ka, it is unlikely that these changes have an influence on the chemical weathering inferences made. However, as the elemental ratios contain elements present in a variety of minerals, the influence of changing mineralogy cannot be ruled out, as slight variation in several minerals at a point in time may cause a large change in the elemental ratios used.

7.4 U isotopes

Results of all U isotope analysis of Var sediments are presented as ($^{234}U/^{238}U$) activity ratio versus age in Figure 7.8. Results for the ESSK08-CS13 core only are presented in Figure 7.9. All U isotope data is tabulated in Appendix E.

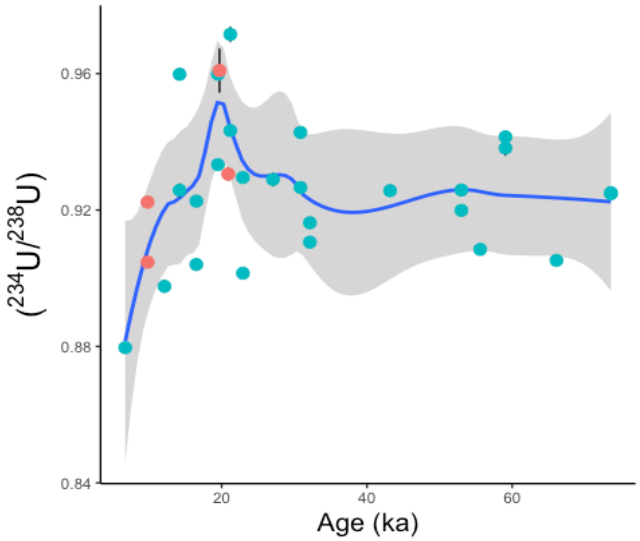

Figure 7.8 ($^{234}U/^{238}U$) in Var sediments through time in cores ESSK08-CS13 and ESSK08-CS01. Aqua dots are data points for ESSK-CS13 core. Red dots are data points for ESSK-CS01 core. Blue line is a polynomial fit calculated by the 'loess' method with a span of 0.4 in RStudio. Grey area is 95% confidence interval.

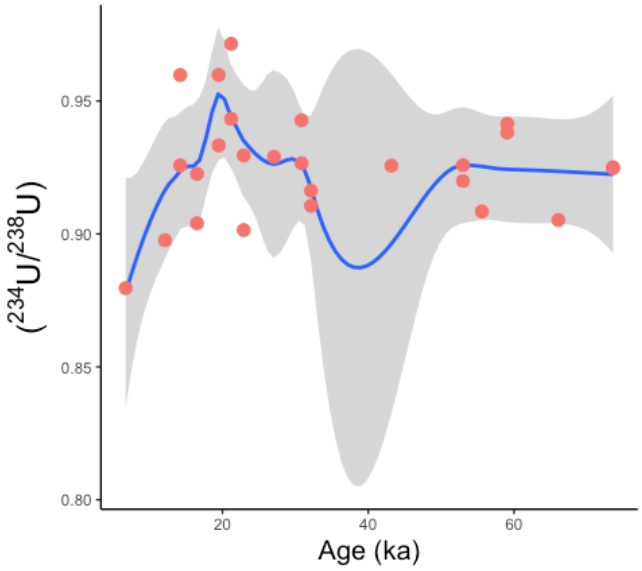

Figure 7.9 (234U/238U) in Var sediments through time in cores ESSK08-CS13. Red dots are data points for ESSK-CS13 core. Blue line is a polynomial fit calculated by the 'loess' method with a span of 0.4 in RStudio. Grey area is 95% confidence interval.

The consistent trends in ($^{234}U/^{238}U$) between Figures 7.8 and 7.9 indicate that signals are likely to be similar at the two core sites. However, the number of ESSK08-CS01 samples is small and therefore not necessarily representative of trends from the entire ESSK08-CS01 core.

The ($^{234}U/^{238}U$) trend during MIS 3 indicates negligible variability in erosion intensity in the Var Catchment (Figure 7.8). Short-lived climatic variations (D-O and Heinrich oscillations) therefore may not impact the erosional response of the catchment, however the temporal resolution of data for MIS 3 is too low to accurately infer trends during this period.

A defined positive excursion from the flat trend occurs concurrently with the onset of the LGM and subsequent deglaciation phase from 26 to 20 ka (Figures 7.8, 7.9). The increasing ($^{234}U/^{238}U$) values in this period are indicative of deepening erosion, which is likely a result of increased abrasion of soils and bedrock by glacial mechanisms. Maximum ($^{234}U/^{238}U$) values occur at the onset of deglaciation at 20 ka, and are therefore likely a result of the exposure and export of comminuted rock flour stored under the base of glaciers during the LGM. ($^{234}U/^{238}U$) subsequently decreases progressively towards the Holocene (Figures 7.8, 7.9). This trend represents erosion of mature soil profiles. As soil profiles in glaciated regions would be very poorly developed or non-existent following deglaciation, the trend observed in Figures 7.8 and 7.9 may indicate a change in the source area of sediments being contributed to the fluvial system, to an area was not glaciated during the LGM.

As only two samples are of MIS 1 age (6.7 ka and 9.8 ka), a well-informed interpretation of erosional trends in the Var River Catchment cannot be made for the Holocene. However, the two data points available are indicative of a continued decrease in erosion depth following deglaciation, as ($^{234}U/^{238}U$) continuously decreases towards 6.7 ka.

Differences in ($^{234}U/^{238}U$) of samples of the same age are presented in Figure 7.10a. Any differentiation in ($^{234}U/^{238}U$) vales between samples of the same age may be influenced by grain size distribution of samples. As discussed in Section 2.3.4, clay

sized sediment grains are ideal for U isotope analysis due to their large surface-to-volume ratio. The resulting ($^{234}U/^{238}U$) of a sample may be influenced by the grain size of samples analysed, as larger grains will lose greater amounts of ^{234}Th, and therefore ^{234}U following decay. The influence of grain size of Var sediments on the ($^{234}U/^{238}U$) activity ratio is presented in Figure 7.10b.

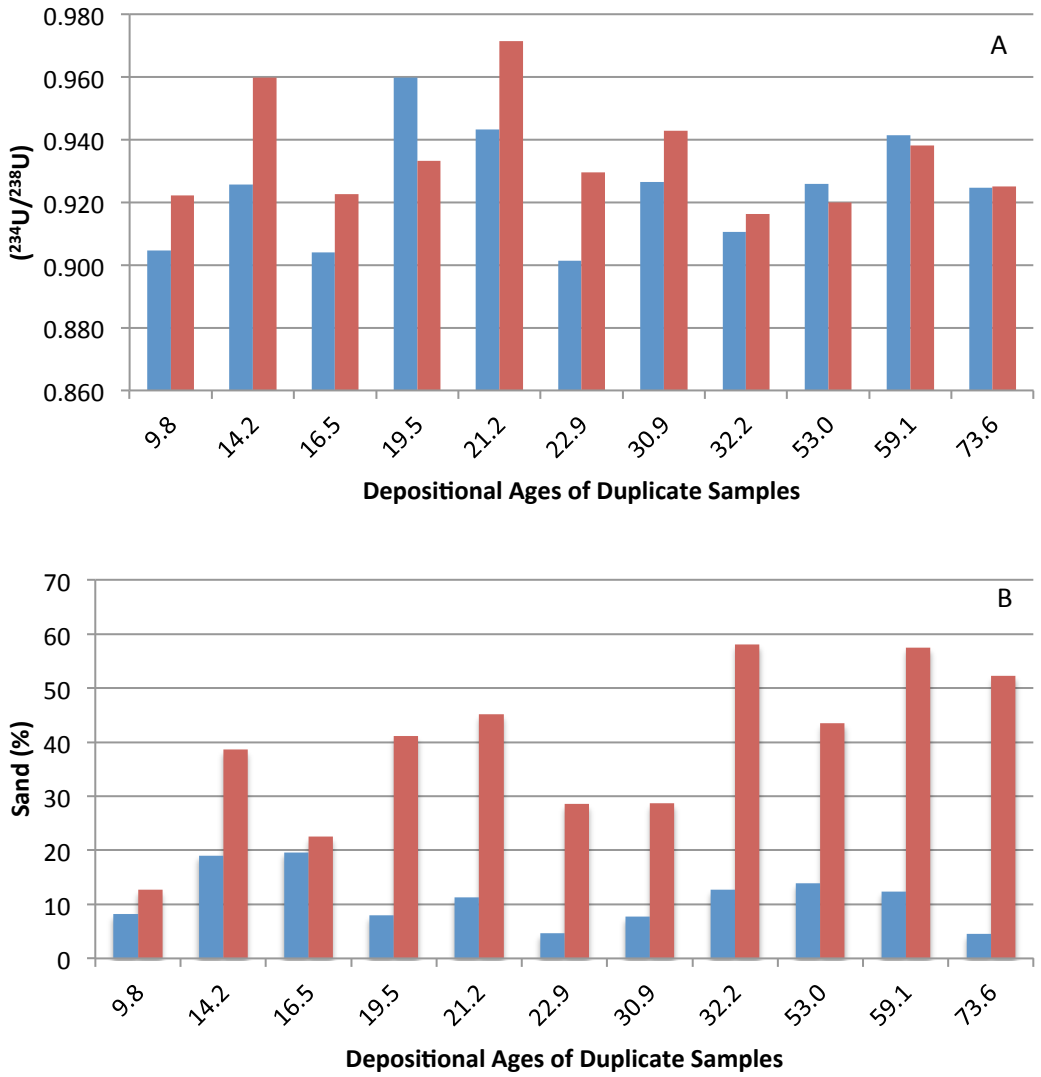

Figure 7.10. A. Differentiation in ($^{234}U/^{238}U$) activity ratios in samples of the same age. B. Differentiation in sand content in samples of the same age. Samples are represented by the same colour in both plots.

Differences in ($^{234}U/^{238}U$) greater than 0.015 are indicated in samples of 9.8, 14.2, 16.5, 19.5, 21.2, 22.9 and 30.9 ka (Figure 7.10a). The remaining four samples exhibit an insignificant difference in ($^{234}U/^{238}U$). As any sand present in samples will increase the measured ($^{234}U/^{238}U$) activity ratio, the percentage of sand in each sample is compared with the ($^{234}U/^{238}U$) in Figure 7.11b.

Since only samples with less than 10% sand may be accurately compared to the grain sizes of pre-sieved samples, as discussed in Section 7.1, only samples of 9.8 ka depositional age may be compared to the respective ($^{234}U/^{238}U$) activity ratios. In these samples, an increased ($^{234}U/^{238}U$) activity ratio is measured in the sample with increased sand content (Figure 7.11). While it has been stated that grain size data of sieved sediments is required in order to better identify any influences of grain size on the measured ($^{234}U/^{238}U$) of marine sediments, a preliminary analysis of all samples presented in Figure 11 indicate increases in ($^{234}U/^{238}U$) where samples contain greater sand content.

7.5 Surface Area Analysis

The results of specific surface area measurement of 8 leached samples and 16 sieved samples are tabulated in Table 7-1. Due to the poor availability of both leached and sieved sample at this stage of the project, making comparisons between the two sample groups is difficult.

Surface area of sieved sediments varies significantly between samples (Table 7-1). This is likely due to the influence of the grain size of samples on the surface area, as fine-grained samples will exhibit larger specific surface area values than coarser samples. Samples CS13-11, CS13-14, CS13-16 and CS13-22 were duplicated to infer reproducibility of results. Variation is as great as 1 m^2/g in sample CS13-11 and as small as 0.1 m^2/g in CS13-16, indicating that the error of the instrument may vary slightly.

Table 7-1 Specific surface area of selected leached Var sediments.

Sample	Age (ka)	Specific Surface Area (leached) (m^2/g)	Specific Surface Area (sieved) (m^2/g)
CS01_1	9.8	10.6	-
CS01_2	9.8	12.1	-
CS13_3	14.21	-	11.0
CS13_4	14.21	-	5.6
CS13_5	16.51	-	10.8
CS13_6	16.51	-	10.8
CS13_7	19.48	-	14.4
CS13_8	19.48	-	8.6
CS13_9	21.19	-	12.7
CS13_10	21.19	-	4.4
CS13_11	22.92	19.7	18.4; 19.4
CS13_12	22.92	7	12.8
CS13_13	27.06	-	7.6
CS13_14	30.85	-	15.8; 16.7
CS13_15	30.85	-	10.8
CS13_16	32.15	-	12.8; 12.7
CS13_17	32.15	-	11.0
CS13_18	43.18	-	8.6
CS13_19	53	8.3	-
CS13_20	53	5.7	-
CS13_22	59.06	-	15.6; 14.8
CS13_23	59.06	-	8.5
CS13_25	73.58	10.3	-
CS13_26	73.58	8.6	-

Sample CS13-11 experiences an increase in specific surface area between sieved and leached samples, indicating that material removed during leaching does not significantly alter the specific surface area of the sample. This inference cannot be made for all samples however, as surface area decreases significantly from 12.8 to 7 m^2/g in sample CS13-12. Further testing is necessary to accurately infer relationships between specific surface areas at different points of the sample preparation process.

Differences in specific surface area of sieved samples and percentage sand content in samples of the same age is presented in Figure 7.11. Smaller specific areas are measured in samples containing relatively greater percentages of sand, indicating that Var sediments behave as expected during surface area analyses. Further to this, the samples of 16.5 ka depositional age contain similar sand content and also exhibit extremely similar specific surface area values. However, grain size data used is based

on unsieved and unleached sediments, and may not be reliably compared with surface area measurements.

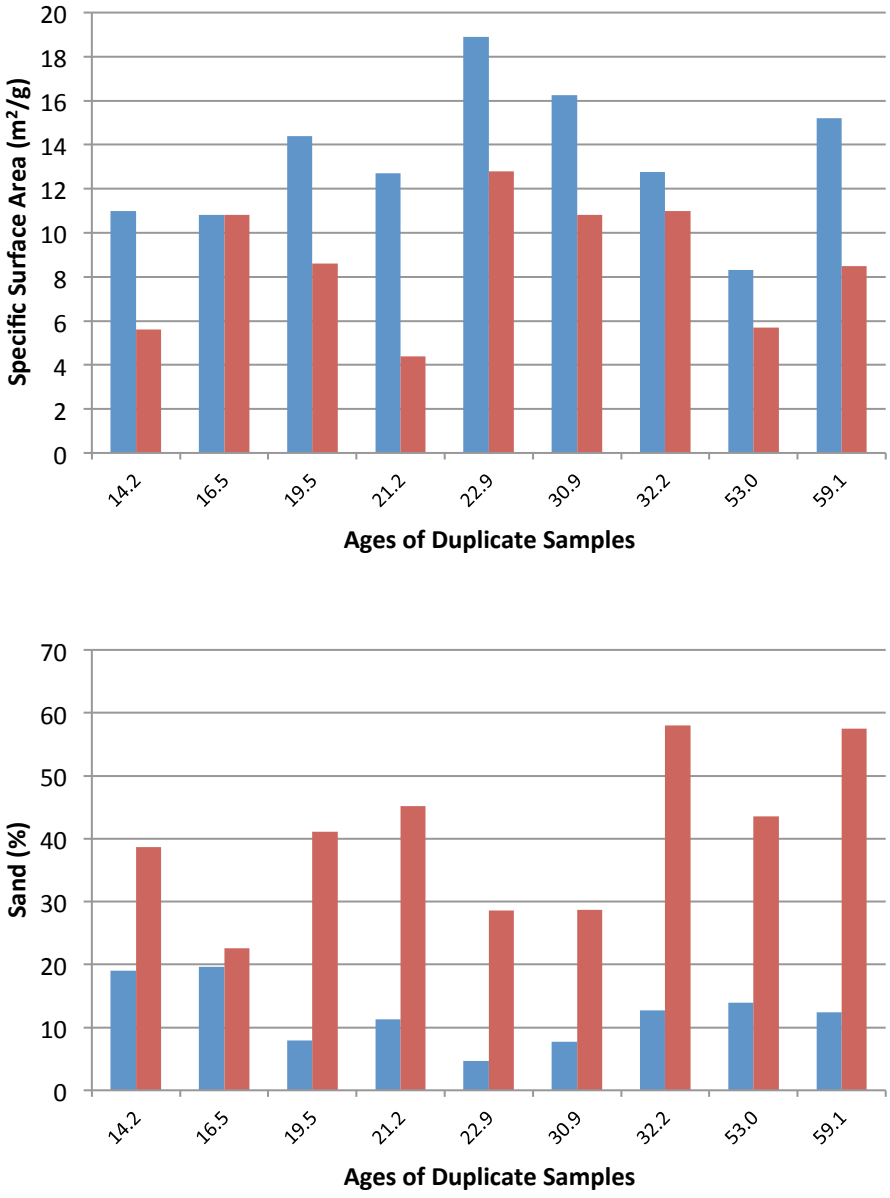

Figure 7.11 A. Differentiation in specific surface area in samples of the same age. B. Differentiation in sand content in samples of the same age. Samples are represented by the same colour in both plots.

7.6 Comminution Age

The main purpose of measuring specific surface areas of Var sediments was to derive a reliable recoil fraction length and calculate residence ages of Var sediments. Comminution ages were calculated with Equations 1 and 2 using the specific surface area measurements of leached samples shown in Table 7-1. Residence times were then calculated by subtracting the deposition age from the comminution age. An average of the eight recoil fraction lengths calculated in Equation 2 was applied to the remainder of the Var samples to derive approximate residence times for all samples. The calculated residence times are presented in Figure 7.12.

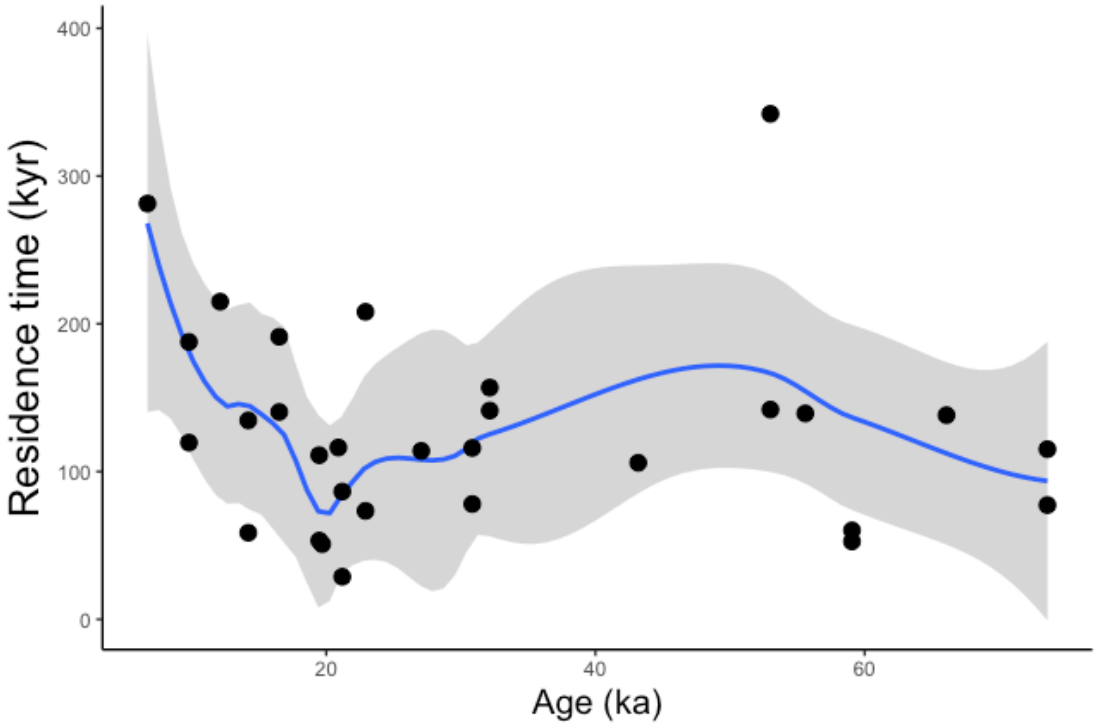

Figure 7.12 Residence time of sediments in the Var Catchment over the past 70 ka. Black dots are data points. Blue line is a polynomial fit calculated by the 'loess' method with a span of 0.4 in RStudio. Grey area is 95% confidence interval.

Residence times of approximately 100 ka are common for samples of MIS 3 age (Figure 7.12). The negligible variability observed during this period is likely due to the low sampling resolution of samples during MIS 3. The minimum residence time occurring at 20 ka coincides with the greatest erosion depths apparent in the Var during deglaciation (Figure 7.8). Residence greatly increases into the Holocene. This is unexpected, as it had been postulated that sediment would continue to be

transported quickly from hillslopes following deglaciation, despite the absence of glaciers. However, the residence times of samples younger than 20 ka suggest that sediment resided on hillslopes for a long period before being eroded during Termination 1 and the Holocene. As it is not possible for sediments with up to 300 kyr residence times to have survived the intense erosion of the LGM, it is postulated that a change in sediment source area occurred following deglaciation. As bare rock faces would be exposed in previously glaciated areas, the potential for erosion in these areas would be reduced due to the higher resistance of fresh rock to erosion processes other than glacial abrasion. This may have caused a change in the signal of erosion recorded in marine turbidite sequences, as during the LGM, the system would have been overwhelmed by glacially derived sediment.

As previously stated, the very similar specific surface area measurements of sieved and leached sample in CS13-11 may indicate that material removed during leaching may potentially not significantly alter the specific surface area of the sample. Though this relationship clearly requires further investigation, the recoil fraction of sediments has been calculated from the specific surface areas of sieved sediments. Comminution age and residence time of these sediments was subsequently calculated to produce the relationship presented in Figure 7.13.

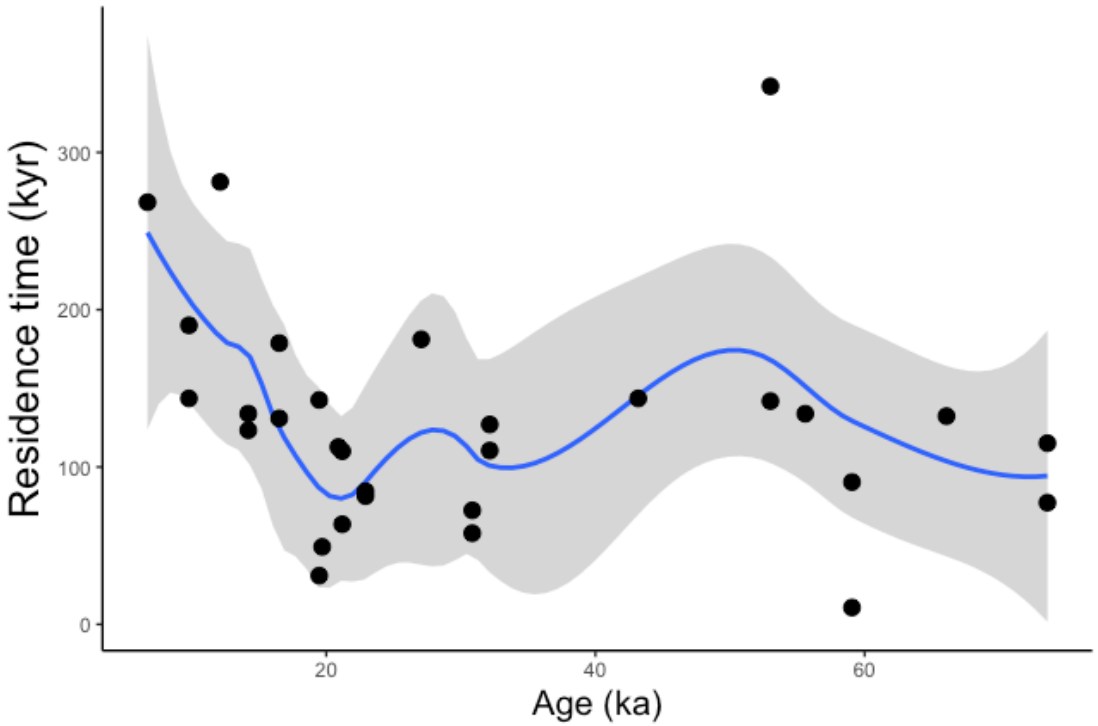

Figure 7.13 Residence time of sediments in the Var Catchment over the past 70 ka based on specific surface area measurements of sieved samples. Black dots are raw data points. Blue line is a polynomial fit calculated by the 'loess' method with a span of 0.4 in RStudio. Grey area is 95% confidence interval.

A similar history of residence times of sediments in the Var Catchment to those exhibited in Figure 7.12 is illustrated in Figure 7.13. Though there is slight variation in the trend, which indicates apparent fluctuations in residence times during mid-MIS 3 and at ~25 ka, the use of sieved sediments to calculate residence times is evidently consistent with other methods used.

8 Results and Discussion – Hokitika Catchment

This section presents grain size and U isotope results collected for Hokitika samples.

8.1 Grain Size

The grain size distribution of Hokitika samples is presented in Figure 8.1 as a ternary plot of sand, clay and silt precent. Raw grain size data is presented in Appendix B. Figure 8.1 illustrates a distinct homogeneity of Hokitika sediments, which markedly differs from Var sediment grain size distribution. All samples contain between 65 and 90% silt, and between 10 and 30% clay. The majority of samples are composed of less than 10% sand. The relative homogeneity of the Hokitika samples may be influenced by the distance of the sampling site from the river mouth, as finer grained sediments may travel farther than coarser grains in a suspended sediment delivery system.

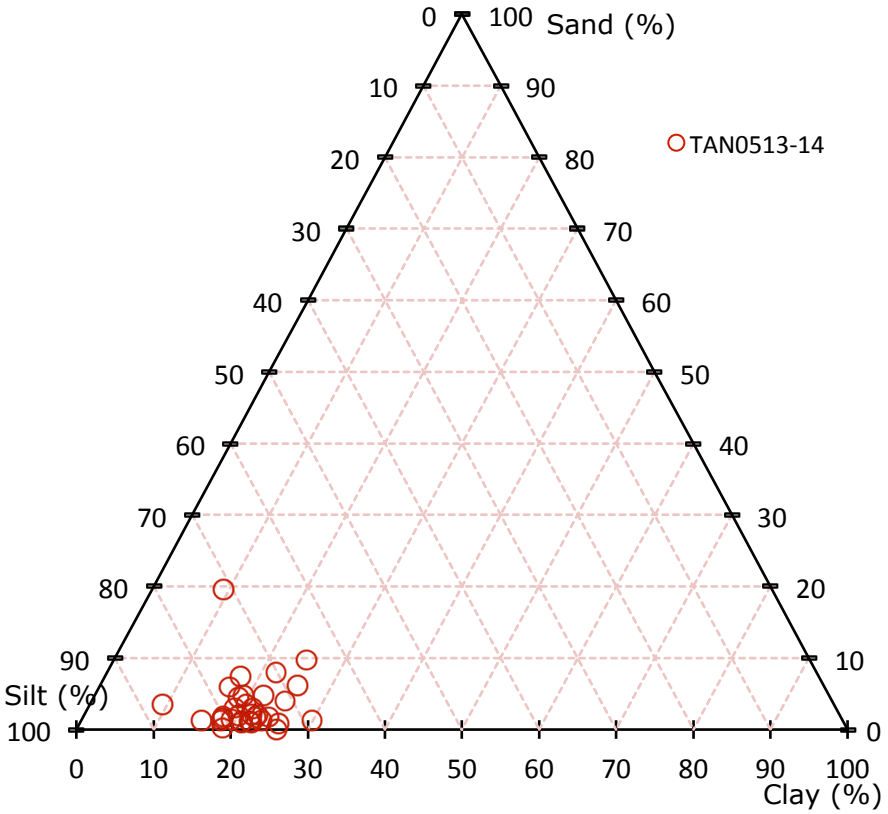

Figure 8.1 Grain size distributions of Hokitika sediments.

The relationship between mean grain size, sand, clay and silt content versus time is presented in Figure 8.2.

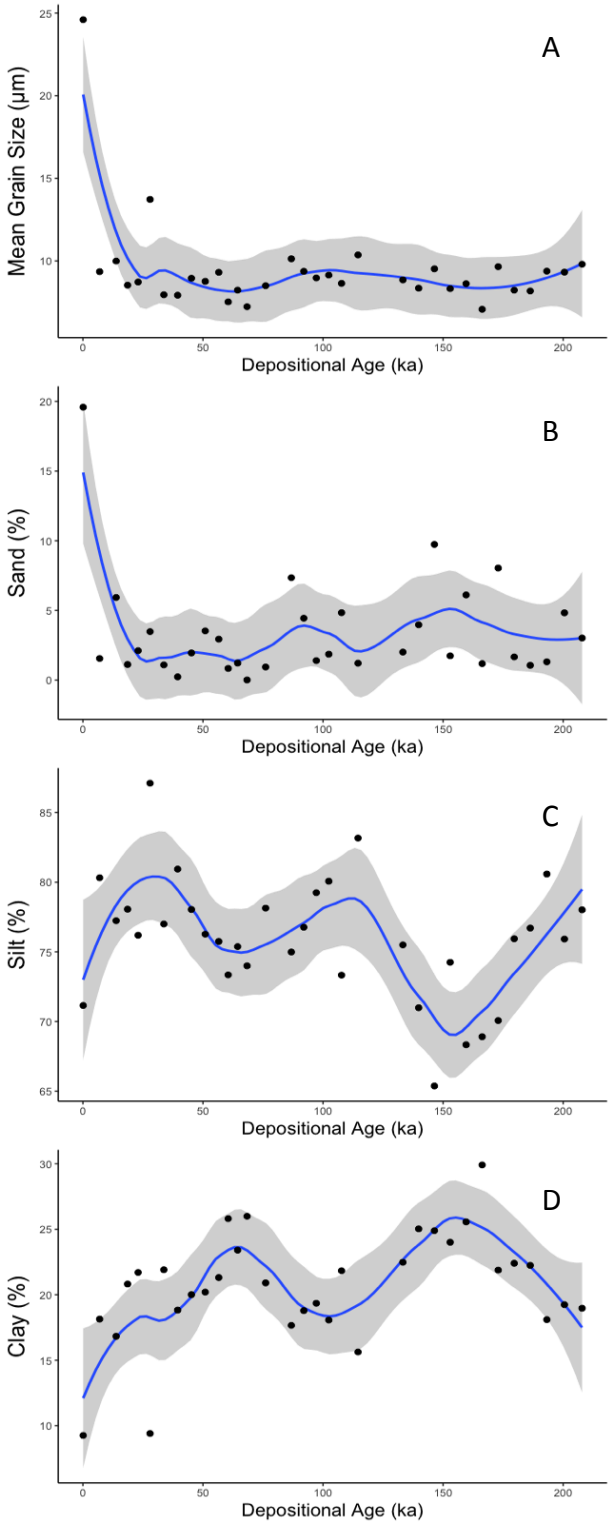

Figure 8.2 Grain size parameters of Hokitika sediments through time. A. Mean grain size (µm). B. Sand (%). C. Silt (%). D. Clay (%). Black dots are raw data points. Blue line is a polynomial fit calculated by the 'loess' method with a span of 0.4 in RStudio. Grey boxes are the 95% confidence interval.

Mean grain size does not vary greatly through time, but is slightly increased during interglacial periods MIS 7a, 5, 3 and 1, relative to glacial periods MIS 6, 4 and 2 (Figure 8.2a). This may be indicative of stronger runoff and erosion during interglacial periods, as described in Section 2.3.1. However, variability in mean grain size between interglacial and glacial periods is only ~1μm and therefore may be insignificant.

Variation in sand, silt and clay content in the Hokitika Catchment is highly variable (Figure. 8.2b,c, d). Clay content appears to be increased during glacial periods, particularly during MIS 6 and 4, relative to the interglacial periods. MIS 2 is slightly conflicting, as it forms part of the long-term decrease in clay content observed from MIS4 to MIS1, although there is a slight peak during MIS2 (Figure 8.2d). This relationship may be explained by Land et al., (2010), in which greater clay content was observed in sediments during glacial periods as a result of increases in the glacier-derived component of sediments. Both maxima and minima of sand content occur during glacial periods, indicating that sand content likely does not respond to long-term climate change in the Hokitika. Similarly, silt content does not vary with changes in climate. No trends in sand and silt variation between interglacial and glacial periods are evident.

Grain size characteristics do not appear to respond to short-term climatic fluctuation. This is exemplified by poor correlation of the MIS 5 sub-stages with variations in mean grain size, sand, clay and silt content. Overall, the homogeneity of Hokitika sediment samples shown in Figure 8.1 may indicate that grain size does not respond greatly to climatic variation, or that the intense rainfall dominating the region throughout the past 210 ka has exacerbated climatic variation in the Hokitika Catchment.

8.2 Uranium isotopes

The results from U isotope analysis of Hokitika sediments are presented in Figure 8.3. ($^{234}U/^{238}U$) values are accompanied by pollen data from the nearby terrestrial Okarito bog core (location shown in Figure 4.1; Ryan et al., 2012), which provides an indicator of palaeoclimatic conditions in the Hokitika Catchment to early MIS 6.

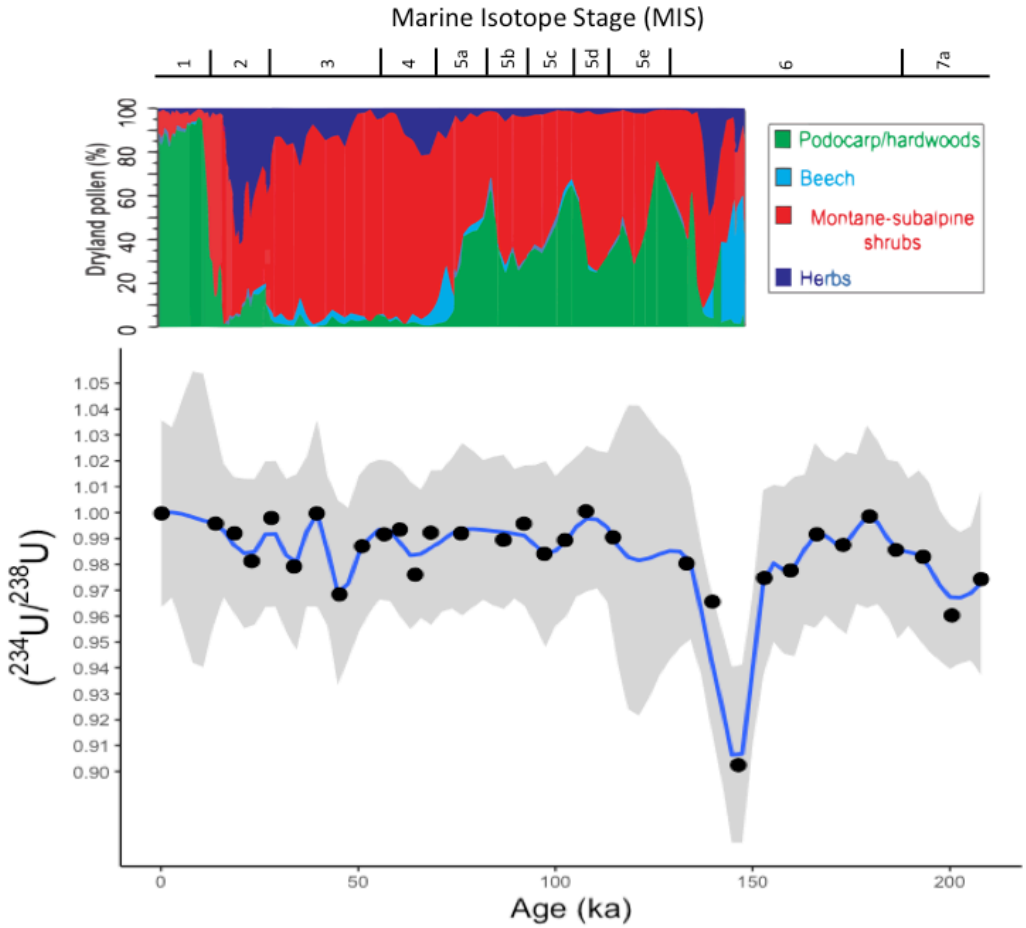

Figure 8.3 ($^{234}U/^{238}U$) of Hokitika sediments during the past 210ka and pollen record of Okarito Pakihi core (Ryan et al., 2012).

($^{234}U/^{238}U$) activity ratios are consistently equal to or approaching 1 in Hokitika sediments over the past 210ka (Figure 8.3). These high ratios may be a result of two influences. Firstly, high ($^{234}U/^{238}U$) values indicate deep and fast erosion of soils, and may therefore indicate a fast sediment erosion regime in the Hokitika Catchment, facilitated by the erosion of bedrock and thin, immature soils. The high ($^{234}U/^{238}U$) values are also influenced by the aggressive treatment steps applied to the Hokitika sediments, resulting in the leaching of Domain 2, as discussed in Section 6.2, (Figure 6.3).

Though variation is slight, ($^{234}U/^{238}U$) is generally decreased during glacial periods relative to interglacial periods in TAN0513-14 (Figure 8.3). This indicates the prevalence of slightly shallower erosion during glacial periods in the Hokitika Catchment comparatively to interglacials. This trend is likely due to the influence of greater precipitation during warm, humid interglacial periods and reduced precipitation during colder and dry glacial periods, as discussed in Section 2.2.

Figure 8.3 demonstrates slightly lower ($^{234}U/^{238}U$) values in interglacial MIS 7a relative to other interglacial periods, indicating shallower erosion during this period. This may be explained by the milder conditions of MIS 7a allowing for increased soil production and shallow erosion (Ryan et al., 2012; Bussell & Pillans, 1997).

Data from MIS 5 is not of a high enough resolution to determine if sub-stages of this MIS correlate with any discernible ($^{234}U/^{238}U$) trends. However, all ($^{234}U/^{238}U$) data recorded for MIS 5 indicate an interglacial characterised by deep intensive erosion.

As discussed in Section 2.1, maximum glacial extent occurred during MIS 4 in New Zealand. A slight decrease in ($^{234}U/^{238}U$) at 64 ka in TAN0513-14 indicates a reduction in erosion intensity during this period, which may be related to decreased precipitation on the west of the South Island at the time.

($^{234}U/^{238}U$) during MIS 3 shows a reversal in erosional trends during the middle of this period. As discussed in Section 2.1, New Zealand climate is characterised by two interstadials, separated by stadial conditions from 37 to 33 ka. The peak in ($^{234}U/^{238}U$) near 35 ka indicates increased erosion depth during this stadial, furthering the observation of deeper erosion occurring during glacial periods in the Hokitika Catchment.

During MIS 2, ($^{234}U/^{238}U$) values are variable. As discussed in Section 2.1, precipitation decreased while cool temperatures stayed constant as the LGM progressed. This may be reflected in a significant decrease of ($^{234}U/^{238}U$) at 23 ka

comparatively to 28 ka. The increase in ($^{234}U/^{238}U$) at 19 ka may indicate the transition towards interglacial conditions as erosion increased.

MIS 1 exhibits high ($^{234}U/^{238}U$) values, indicative of deep and fast erosion, throughout the current interglacial. Sample T14_M_10 (deposited at 6.86ka) was not included in analysis due to a high standard error from the sample being too dilute for precise MC-ICP-MS analysis. This limits the interpretation of U isotope data during the Holocene and prevents comparison between erosion and shifting climate teleconnections.

U isotope values also correlate with pollen data of the Okarito Bog record (Figure 8.3). The four minima evident in the ($^{234}U/^{238}U$) record from MIS 4 to MIS 2 correlate with periods of increased herb vegetation in the catchment. As herbs thrive in cold and dry conditions, decreased erosion during these intervals may be resultant of reduced precipitation and water availability. A large peak in *Nothofagus* beech vegetation during MIS 6 correlates with the lowest ($^{234}U/^{238}U$) value in the Hokitika record (Figure 8.3). Significant amounts of *Nothofagus* pollen indicate a proliferation of cool and wet conditions. It is therefore unexpected that a period of both wet and cold conditions would result in a shallowly eroded landscape with more developed soils than both adjoining interglacial and glacial periods.

9 Synthesis

The purpose of this chapter is to consolidate and synthesise the interpretations of the results and discussion in previous chapters.

9.1 Landscape Change in the Var River Catchment

Many proxies were implemented on Var River Catchment sediments with the aim of developing a history of erosion and chemical weathering for the past 70 ka. The sample resolution for MIS 3 is too broad to identify any potential erosional or weathering response to short-term variability in this period. The majority of proxies implemented in this study exhibit a key change in the Var system at the time of deglaciation in the northern hemisphere.

U isotope results implicate a shift to fast and deep erosion during deglaciation, which may be a result of receding glaciers exposing rock flour which had been ground and stored under glaciers during the LGM. The subsequent decline in U isotope values implies a slowing and shallowing of erosion in the catchment. As glaciated areas will be reduced to bare rock faces following deglaciation, it is inferred that this trend indicates erosion is predominantly occurring on soil-mantled slopes in a different part of the catchment that was not glaciated during the LGM.

The relationship indicated by residence times and catchment-wide erosion implies that sediments did not spend a long period of time in the catchment during the phase of deglaciation, which is fitting with the deep erosion depths observed. Similarly, residence times increase with the shallowing in erosion into the Holocene, indicating a long hillslope storage time of sediments during this period of shallow erosion. As soils must be older to develop U isotope ratios as low as 0.8, material must reside in the weathering profile for a greater amount of time. This sediment must not be derived from a glaciated region of the catchment, as residence times are too old and U isotope ratios too low to have survived the intense glaciation and subsequent deep erosion of the LGM.

Figure 9.1 illustrates the conceptual model of erosion change in the Var River Catchment. It is postulated that, following the erosion of sediment from glaciated

areas at 20 ka, erosion of a different part of the catchment headwaters predominated. As residence times of up to 300 ka are observed in Holocene sediments in the Var, it is proposed that sediment may be derived from transport-limited lowland hillslopes, as it has been shown that residence times of ~200 kyrs can occur as a result of very long hillslope transport in long, shallow slopes in other catchments (Suresh et al., 2014). This switch in the signal dominating the Var sedimentary record does not imply that low land areas were not being eroded at 20 ka, but rather that the U isotope signal was obscured by the large volumes of glacial sediment being provided to the depositional system during this period.

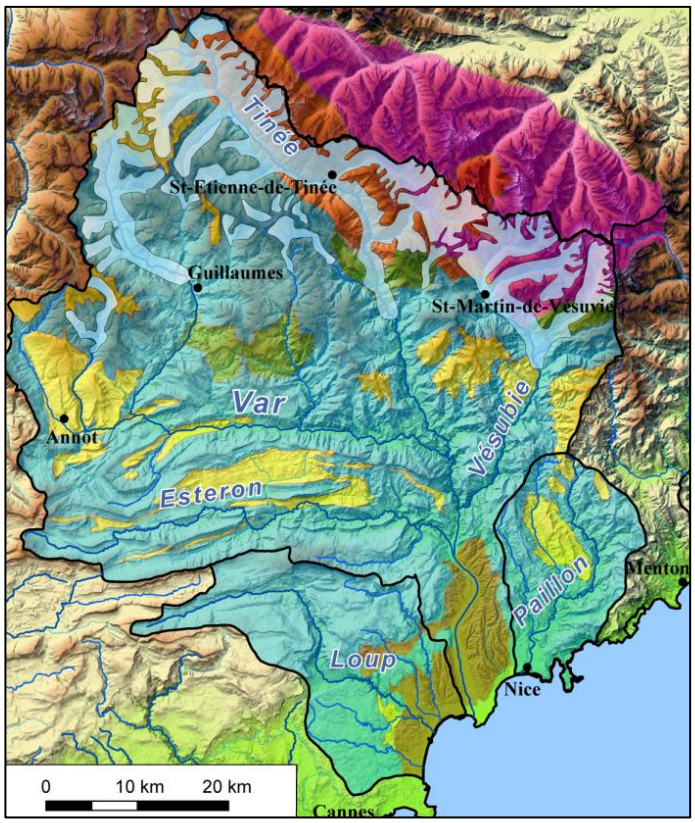

Figure 9.1 Glacial cover in the Var Basin during the LGM, indicated by pale blue areas. Pink, orange, red, blue, green and yellow areas represent different lithologies described in Figure 3.2. Adapted from Bonneau, 2014.

Records of chemical weathering and sediment provenance correlate with the inferred change in erosional processes near Termination 1. Mineralogical changes primarily involve primary minerals, and may therefore indicate changes in sediment provenance, in fitting with the aforementioned changes in sediment source area. Geology of the Var River Catchment is not known in enough detail to make an

educated hypothesis of source area change. Inferred increases in chemical weathering from elemental ratios observed may also be influenced by changes in mineralogy. However, as the distribution of elements across the minerals present in Var sediments is similar in many minerals, a no definitive conclusion can be made. It is likely that the signal does indicate an increase in chemical weathering, as well-developed soils will have been subjected to greater degrees of weathering relative to sediments exported directly after the LGM.

Decreases in average grain size and sand content from approximately 17 ka may be indicative of an energy and transport capacity decrease following the slight increase in sand content during deglaciation at 20ka. This trend indicates that fluvial energy increased during Termination 1, as glacial recession increased discharge. Following this pulse of increased energy, fluvial systems reduced in energy leading into the Holocene.

9.2 Landscape Change in the Hokitika Catchment

Fewer proxies were studied for the Hokitika Catchment and therefore the interpretation is incomplete in terms of chemical weathering. In general, broad-scale variations are observed, and any responses to short-term climatic fluctuation, such as in MIS 5, are not readily observed.

Erosion has been consistently deep throughout the last 210 ka, as exhibited by the continuously high U isotope values near or equal to 1 (Figure 8.3). Though variability in erosion is very small, U isotopes indicate that glacial periods experience slightly reduced intensity and depth of erosion relative to interglacial periods. This is likely due to the influence of greater precipitation during warm, humid interglacial periods and reduced precipitation during colder glacial periods in the Hokitika Catchment. Correlation of erosion intensity with specific periods indicated by the local Okarito pollen record indicates that erosion responds to local climatic conditions. The shallowing of erosion indicated by U isotopes during the wet and cool conditions of MIS 6 is unexpected and requires further investigation to consolidate, as very intense erosion in the period was expected caused by intense precipitation or glacial abrasion.

Grain size varies on a long time-scales relating to marine isotope stages in the Hokitika. Clay content is the most variable grain size fraction, and generally appears to be increased during glacial periods, particularly MIS6 and MIS4, relative to the interglacial periods. The relationships observed in clay content variation might by caused by the increased delivery of glacially abraded detrital matter during glacial periods in New Zealand, which has been previously observed (Land et al., 2010).

9.3 Landscape Change in the late Quaternary

The study of these two antipodal catchments allows for inferences to made regarding landscape change throughout the late Quaternary. A key conflict in erosional responses is observed between the two catchments, as the Hokitika undergoes the deepest periods of erosion during warm periods, conversely to the Var, which experiences the greatest depths of erosion during MIS 2. This inverse relationship indicates that catchments do not respond to climatic variability in the same manner, and is likely due to local precipitation factors. Rainfall conditions are enhanced during interglacial periods on the west coast of the New Zealand South Island, which is generally always wet. Conversely, the Var does not experience such intense rainfall conditions, and therefore responds differently to the Hokitika Catchment.

A comparison of the same event between the two orogens studied may further our understanding of landscape responses to significant climatic events. For example, the response of erosion to the climatic conditions of the global LGM in both catchments indicates a deep erosional response in both catchments. However, as the Hokitika frequently experiences very deep erosion, this is not distinctly different from neighbouring intervals of time, conversely to the Var. Different sampling intervals limit the comparisons that can be made between the two orogens, as does the slight variation in timing of the LGM in both hemispheres.

9.4 Implications for potential erosional responses to anthropogenic climate change

By studying palaeoenvironments, inferences may be made as to the potential landscape responses to anthropogenic climate change. MIS 5e has previously been used as an analogue for present-day warming, as a fast warming of 2°C occurred in

this stage. As the Var record does not extend past 70 ka, potential responses of future climate change may only be made for the Hokitika Catchment. The U isotope ratio during MIS 5e is slightly lower than the surrounding data, indicating a slight shallowing in erosion, though erosion is deep overall. MIS 5e does not indicate any significant change in erosion in the Hokitika Catchment.

The development of U isotope palaeo-erosion archive, particularly for MIS 5, would improve understandings of potential implications for soil availability during anthropogenic climate change. However, the current method is very time-consuming, thus limiting the amount of data that can be obtained. As the local conditions acting on a catchment can impact significantly on erosional trends, a large data set would be required in order to develop models of potential erosion for larger regions. The continued development of palaeo-erosion records may eventually allow for the inclusion of relevant data into environmental change models to inform on issues relevant to modern day society, such as agriculture and crop production.

10 Conclusions and Further Research

In this study, the grain size, mineralogy, elemental concentrations, surface area and U-isotope signature of marine sediments were quantified in order to develop records of palaeo-erosion and chemical weathering in two antipodal catchments for the late Quaternary. Key conclusions of this study are summarised below:

- In the Var River Catchment, a change in soil erosion was triggered during deglaciation at 20 ka. The U isotope record indicates that erosion was very deep during deglaciation as a result of the export of glacially abraded sediments produced and stored in glaciers during the LGM. An apparent shallowing of erosion following 20 ka is indicative of a change in source area of eroded sediment to a more stable area of the catchment. Residence times further showed that periods of deep erosion are correlated with short residence times, and vice versa.
- Chemical weathering trends in the Var River Catchment indicate increased chemical weathering from the LGM towards the Holocene, further indicating the shift towards erosion of well-developed soils during the transition to the Holocene. Variation in mineralogy may influence these apparent trends and more investigation is required.
- In the Hokitika Catchment, erosion is consistently deep during the past 210 ka due to prevailing high precipitation rates operating in the area constantly eroding immature soils. As glacial periods are slightly drier in New Zealand, a slight lessening in erosion is observed during these periods.

Further research into the erosional and weathering history of the Var and Hokitika catchments should involve:

- Determination of comminution ages and mineralogical and elemental abundances for Hokitika sediments.
- Increasing the resolution of data during MIS 3 for Var sediments and throughout MIS 5 for Hokitika sediments, in order to determine any variability in erosion responses to short-lived climatic variations.
- Investigation of hillslopes in the Var River Catchment to assess the accuracy of calculated residence times of up to 300 kyr.

- Investigations of the ($^{234}U/^{238}U$) activity ratio with depth in soil profiles in the Var and Hokitika Catchments.
- Implementation of Nd isotopes to accurately assess sediment provenance changes in the Var River Catchment

11 References

Acosta, VT, Schildgen, TF, Clarke, BA, Scherler, D, Bookhagen, B, Wittmann, H, von Blanckenburg, F & Strecker, MR 2015, 'Effect of vegetation cover on millennial scale landscape denudation rates in East Africa', *Lithosphere*, vol. 7, no. 4, pp. 408-420.

Adatte, T, Keller, G & Stinnesbeck, W 2002, 'Late Cretaceous to early Paleocene climate and sea-level fluctuations: the Tunisian record', *Palaeogeography, Palaeoclimatology, Palaeoecology*, vol. 178, pp. 165–196.

Adloff, JP & Roessler, K 1991, 'Recoil and transmutation effects in the migration behaviour of actinides', *Radiochimica Acta*, vol. 52, no. 53, pp. 269–274.

Alizai, A, Hillier, S, Clift, PD, Giosan, L, Hurst, A, Van Laningham, S & Macklin, M 2012, 'Clay mineral variations in Holocene terrestrial sediments from the Indus Basin', *Quaternary Research*, vol. 77, no. 3, pp. 368–381.

Allen, PA 1997, 'Earth surface processes', Blackwell Science ed. Oxford: Blackwell Science.

Almond, PC, Moar, NT & Lian, OB 2001, 'Reinterpretation of the glacial chronology of south Westland', *New Zealand Journal of Geology and Geophysics*, vol. 44, pp. 1-15.

Andersen, MB, Erel, Y & Bourdon, B 2009, 'Experimental evidence for 234U–238U fractionation during granite weathering with implications for 234U/238U in natural waters', *Geochimica et Cosmochimica Acta*, vol. 73, no. 14, pp. 4124–4141.

Bacon, JR & Davidson, CM 2008, 'Is there a future for sequential chemical extraction?', *Analyst*, vol. 133, pp. 25-46.

Baker, PA, Seltzer, GO, Fritz, SC, Dunbar, RB, Grove, MJ, Tapia, PM, Cross, SL, Rowe, HD & Broda, JP 2001, 'The history of South American tropical precipitation for the past 25,000 years', *Science*, vol. 291, pp.640-643.

Ballance, PF & Williams, PW 1992, 'The geomorphology of Auckland and Northland', Soons, JM & Selby MJ (eds.), *Landforms of New Zealand (second ed.)*, Longman Paul, Auckland, pp. 210-232.

Balsam, WL & Damuth, JE 2000, 'Further investigations of shipboard vs. shore-based spectral data: implications for interpreting Leg 164 sediment composition', Paull, CK, Matsumoto, R, Wallace, PJ, Dillon, WP (eds), *Proceedings of the Ocean Drilling Program, Scientific Results. Ocean Drilling Program, College Station*, TX, pp. 313–324.

Barker, S, Diz, P, Vautravers, MJ, Pike, J, Knorr, G, Hall, IR & Broecker WS 2009, 'Interhemispheric Atlantic seesaw response during the last deglaciation', Nature, vol. 457, pp. 1097-1102.

Barrows, TT, Juggins, S, De Deckker, P, Calvo, E & Pelejero, C 2007, 'Long term sea surface temperature and climate change in the Australian New Zealand region', *Paleoceanography*, vol. 22, pp. 1-17.

Beaudouin, C, Jouet, G, Suc, JP, Berné, S & Escarguel, G, 2007, 'Vegetation dynamics in southern France during the last 30kyBP in the light of marine palynology', *Quaternary Science Reviews*, vol. 26, no. 7, pp.1037-1054.

Birkeland, PW 1984, 'Soils and geomorphology', Oxford University Press, Oxford.

Blum, MD & Valastro, S 1989, 'Response of the Pedernales River of central Texas to late Holocene climatic change', *Ann. Assoc. Am. Geogr.*, vol. 79, no. 3, pp. 435–456.

Blunier, T & Brook, EJ 2001, 'Timing of millennial-scale climate change in Antarctica and Greenland during the last glacial period', *Science*, vol. 291, pp. 109-112.

Bonneau, L 2014, 'Impact des oscillations climatiques rapides du dernier cycle glaciaire sur l'erosion et les transferts sedimentaires dans le sud des Alpes, (SE France)', PhD thesis, L'Universite Pierre et Marie Curie.

Bonneau, L, Jorry, SJ, Toucanne, S, Silva Jacinto, R & Emmanuel, L 2014, 'Millennial-scale response of a western Mediterranean river to late Quaternary climate changes: a view from the deep sea', *The Journal of Geology*, vol. 122, no. 6, pp. 687-703.

Bonniwell, EC, Matisoff, G & Whiting, PJ 1999, 'Determining the times and distances of particle transit in a mountain stream using fallout radionuclides', *Geomorphology*, vol. 27, pp. 75-92.

Bookhagen, B, Thiede, RC & Strecker, MR 2005, 'Late Quaternary intensified monsoon phases control landscape evolution in the northwest Himalaya', *Geology*, vol. 33, no. 2, pp. 149-152.

Boulay, S, Colin, C, Trentesaux, A, Clain, S, Liu, Z & Lauer-Leredde, C 2007 'Sedimentary responses to the Pleistocene climatic variations recorded in the South China Sea', *Quaternary Research*, vol. 68, no. 1, pp. 162-172.

Bourdon, B, Bureau, S, Andersen, MB, Pili, E & Hubert, A 2009, 'Weathering rates from top to bottom in a carbonate environment', *Chemical Geology*, vol. 258, no.3–4, pp. 275–287.

Broecker, WS 1994, 'Massive iceberg discharges as triggers for global climate change', *Nature*, vol. 372, pp. 421-424.

Brown, ET, Stallard, RF, Larsen, MC, Raisbeck, GM & Yiou, F 1995, 'Denudation rates determined from the accumulation of in situ-produced 10 Be in the Luquillo Experimental Forest, Puerto Rico' *Earth and Planetary Science Letters*, vol. 129, pp. 193-202.

Brunauer, S, Emmett, PH & Teller, E 1938, 'Adsorption of gases in multimolecular layers', *Journal of the American Chemical Society*, vol. 60, no. 2, pp. 309–319.

Bussell, MR and Pillans, B, 1997, 'Vegetational and climatic history during oxygen isotope stage 7 and early stage 6, Taranaki, New Zealand', *Journal of the Royal Society of New Zealand*, vol. 27, no.4, pp.419-438.

Cacho, I, Grimalt, JO, Pelejero, C, Canals, M, Sierro, FJ, Flores, JA & Shackleton, N 1999, 'Dansgaard-Oeschger and Heinrich event imprints in Alboran Sea paleotemperatures', *Paleoceanography*, vol. 14, pp. 698–705.

Carson, MA & Kirkby, MJ 1972, 'Hillslope form and process', Cambridge University Press, New York.

Chabaux, F, Granet, M, Pelt, E, France-Lanord, C & Galy, V 2006, '238U–234U–230Th disequilibria and timescale of sedimentary transfers in rivers: clues from the Gangetic plain rivers', *Journal of Geochemical Exploration*, vol. 88, no. 1–3, pp. 373–375.

Chamberlain, CP, Poage, MA, Craw, D & Reynolds, RC 1999, 'Topographic development of the Southern Alps recorded by the isotopic composition of authigenic clay minerals, South Island, New Zealand', *Chemical Geology*, vol. 155, pp. 279-294.

Chamley, H 1989, 'Clay Sedimentology', Springer-Verlag, Berlin.

Cheng, H, Edwards, RL, Hoff, J, Gallup, CD, Richards, DA & Asmerom, Y 2000, 'The half-lives of uranium-234 and thorium-230', *Chemical Geology*, vol. 169, pp. 17-33.

Clark, PU, Dyke, AS, Shakun, JD, Carlson, AE, Clark, J, Wohlfarth, B, Mitrvica, JX, Hostetler, SW & McCabe, AM 2009, 'The Last Glacial Maximum', *Science*, vol. 325, pp. 710-714.

Cochonat, P, Bourillet, JF, Savoye, B & Dodd, L 1993, 'Geotechnical Characteristics and Instability of Submarine Slope Sediments, the Nice Slope (N-W Mediterranean Sea', *Marine Georesources and Geotechnology*, vol. 11, pp. 131-151.

Colin, C, Siani, G, Sicre, MA & Liu, Z 2010, 'Impact of the East Asian monsoon rainfall changes on the erosion of the Mekong River basin over the past 25,000 yr', *Marine Geology*, vol. 271, no. 1–2, pp. 84–92.

Condie, KC, Dengate, J & Cullers, RL 1995, 'Behavior of rare earth elements in a paleoweathering profile on granodiorite in the Front Range, Colorado, USA', *Geochimica et Cosmochimica Acta*, vol. 59, no. 2, pp.279-294.

Covault, JA, Romans, BW, Fildani, A, McGann, M, & Graham, SA 2010, 'Rapid climatic signal propagation from source to sink in a southern California sediment-routing system. *Journal of Geology*, vol. 118, pp. 247– 259.

Dan, G, Sultan, N & Savoye, B 2007, 'The 1979 Nice harbour catastrophe revisited: Trigger mechanism inferred from geotechnical measurements and numerical modelling', *Marine Geology*, vol. 245, pp. 40-64.

DeMets, C, Gordon, RG, Argus, DJ & Stein S 1990, 'Current plate motions', *Geophysical Journal International*, vol. 101, pp. 425-478.

DePaolo, DJ, Lee, VE, Christensen, JN & Maher, K 2012, 'Uranium comminution ages: sediment transport and deposition time scales', Comptes Rendus Geoscience, vol. 344, no. 11–12, pp. 678–687.

DePaolo, DJ, Lee, VE, Christensen, JN & Maher, K 2012, 'Uranium comminution ages: Sediment transport and deposition time scales', *Comptes Rendus Geoscience*, vol. 344, pp. 678-687.

DePaolo, DJ, Maher, K, Christensen, JN & McManus, J 2006, 'Sediment transport time measured with U-series isotopes: Results from ODP North Atlantic drift site 984', *Earth and Planetary Science Letters*, vol. 248, pp. 394-410.

DePaolo, DJ, Maher, K, Christensen, JN & McManus, J 2006, 'Sediment transport time measured with U-series isotopes: results from ODP North Atlantic drift site 984'. *Earth and Planetary Science Letters*, vol. 248, no. 1–2, pp. 394–410.

Dietrich, WE, Reiss, R, Hsu, ML & Montgomery, DR 1995, 'A process-based model for colluvial soil depth and shallow landsliding using digital elevation data', *Hydrological processes*, vol. 9, pp. 383-400.

Dosseto, A & Schaller, M 2016, 'The erosion response to Quaternary climate change quantified using uranium isotopes and in situ-produced cosmogenic nuclides', *Earth-Science Reviews*, vol. 155, pp.60-81.

Dosseto, A 2014, 'Chemical Weathering (U-Series)', Rink, WJ & Thompson, J (eds), *Encyclopedia of Scientific Dating Methods*. Springer Netherlands, pp. 1-28.

Dosseto, A 2015, 'Chemical weathering (U-series)', *Encyclopedia of Scientific Dating Methods*, pp.152-169.

Dosseto, A, Bourdon, B & Turner, SP 2008, 'Uranium-series isotopes in river materials: Insights into the timescales of erosion and sediment transport', *Earth and Planetary Science Letters*, vol. 265, pp. 1-17.

Dosseto, A, Bourdon, B, Gaillardet, J, Allègre, CJ & Filizola, N 2006, 'Timescale and conditions of chemical weathering under tropical climate: study of the Amazon basin with U-series', *Geochimica et Cosmochimica Acta*, vol. 70, no. 1, pp. 71–89.

Dosseto, A, Buss, HL & Chabaux, F 2014, 'Age and weathering rate of sediments in small catchments: The role of hillslope erosion', *Geochimica et Cosmochimica Acta*, vol. 132, pp. 238-258.

Dosseto, A, Hesse, PP, Maher, K, Fryirs, K & Turner, S 2010, 'Climatic and vegetation control on sediment dynamics during the last glacial cycle', *Geology*, vol. 38, pp. 395-398.

Drever, JI & Zobrist, J 1992, 'Chemical weathering of silicate rocks as a function of elevation in the southern Swiss Alps', *Geochimica et Cosmochimica Acta*, vol. 56, no. 8, pp. 3209-3216.

Dubar, M & Anthony, EJ 1995, 'Holocene Environmental Change and River-Mouth Sedimentation in the Baie des Anges, French Riviera', *Quaternary Research*, vol. 43, pp. 329-343.

Dühnforth, M, Anderson, RS, Ward, D & Stock, GM 2010, 'Bedrock fracture control of glacial erosion processes and rates', *Geology*, vol. 38, no. 5, pp. 423-426.

Egli, M, Mirabella, A & Fitze, P 2003, 'Formation rates of smectites derived from two Holocene chronosequences in the Swiss Alps', *Geoderma*, vol. 117, no. 1, pp.81-98.

EPICA Community Members 2006, 'One-to-one coupling of glacial climate variability in Greenland and Antarctica', *Nature*, vol. 444, pp. 195-198.

Ferrara, G & Malaroda, M 1969, 'Radiometric age of granitic rocks from the Argentera massif (Maritime Alps)', *Bollettino della Società geologica italiana*, vol. 88, pp. 311-320.

Fleischer, RL 1980, 'Isotopic disequilibrium of uranium: Alpha-recoil damage and preferential solution effects', *Science*, vol. 207, pp. 979-981.

Follacci, JP 2000. 'Seize ans de surveillance du glissement de la Clapiere (Alpes-Maritimes), *Bulletin des laboratoires des Ponts et Chaussées*, pp. 9-25.

Froelich, P, Klinkhammer, GP, Bender, ML, Luedtke, NA, Heath, GR, Cullen, D, Dauphin, P, Hammond, D, Hartman, B & Maynard, V 1979, 'Early oxidation of organic matter in pelagic sediments of the eastern equatorial Atlantic: suboxic diagenesis', *Geochimica et Cosmochimica Acta*, vol. 43, no. 7, pp. 1075-1090.

Gasse, F, 2000, 'Hydrological changes in the African tropics since the Last Glacial Maximum', *Quaternary Science Reviews*, vol, 19, no. 1, pp.189-211.

Giosan, L, Flood, RD, Grutzner, J & Mudie, P 2002, 'Paleoceanographic significance of sediment color on western North Atlantic drifts: II. Late Pliocene–Pleistocene sedimentation', *Marine Geology*, vol. 189, no. 1–2, pp. 43–61.

Gleyzes, C, Tellier, S & Astruc, M 2002, 'Fractionation studies of trace elements in contaminated soils and sediments: a review of sequential extraction procedures', *Trends in Analytical Chemistry*, vol. 21, pp. 451-467.

Goede, A 1994, 'Continuous early Last Glacial palaeoenvironmental record from a Tasmanian speleothem based on stable isotope and minor element variations', *Quaternary Science Reviews*, vol. 13, pp. 283-291.

Granet, M, Chabaux, F, Stille, P, Dosseto, A, France-Lanord, C & Blaes, E 2010, 'U-series disequilibria in suspended river sediments and implication for sediment transfer time in alluvial plains: the case of the Himalayan rivers', *Geochimica et Cosmochimica Acta*, vol. 74, pp. 2851–2865.

Granet, M, Chabaux, F, Stille, P, France-Lanord, C & Pelt, E 2007, 'Time-scales of sedimentary transfer and weathering processes from U-series nuclides: clues from the

Himalayan rivers', *Earth and Planetary Science Letters*, vol. 261, no.3–4, pp. 389–406.

Harper, MA, & Collen, JD 2002, 'Glaciations, interglaciations and reworked microfossils in Poukawa Basin, New Zealand', *Global Planetary Change*, vol. 33, pp. 243-256.

Hashimoto, T, Aoyagi, Y, Kudo, H & Sotobayashi, T 1985, 'Range calculation of alpha-recoil atoms in some minerals using LSS-theory', *Journal of radioanalytical and nuclear chemistry*, vol. 90, no. 2, pp.415-438.

Heath, R 1982, 'What drives the mean circulation on the New Zealand west coast continental shelf?', *New Zealand Journal of Marine and Freshwater Research*, vol. 16, pp. 215-226.

Heimsath, AM, Chappell, J, Spooner, NA & Questiaux, DG 2002, 'Creeping soil', *Geology*, vol. 30, no. 2, pp.111-114.

Heinrich, H 1988, 'Origin and consequences of cyclic ice rafting in the northeast Atlantic Ocean during the past 130,000 years', *Quaternary Research*, vol. 29, no. 2, pp. 142-152.

Hellstrom J, McCulloch M & Stone J 1998, 'A detailed 31,000-year record of climate and vegetation change, from the isotope geochemistry of two New Zealand speleothems', *Quaternary Research*, vol. 50, pp.167–178.

Hemming, SR 2004, 'Heinrich events: massive late Pleistocene detritus layers of the North Atlantic and their global climate imprint', *Reviews of Geophysics*, vol. 42, no. 1.

Hicks, D & Shankar, U 2003, 'Sediment from New Zealand rivers', *NIWA Misc. Chart 236*.

Hicks, DM, Hill J & Shankar, U 1996, 'Variation of suspended sediment yields around New Zealand: The relative importance of rainfall and geology', *IAHS-AISH Publication*, vol, 236, pp. 149-156.

Hu, D, Böning, P, Köhler, CM, Hillier, S, Pressling, N, Wan, S, Brumsack, HJ & Clift, PD 2012, 'Deep sea records of the continental weathering and erosion response to East Asian monsoon intensification since 14ka in the South China Sea', *Chemical Geology*, vol. 326, pp. 1-18.

Huybers, P & Eisenman, I 2006, 'Integrated summer insolation calculations', *IGBP PAGES/World Data Center for Paleoclimatology Data Contribution Series*, *79*.

Imbrie, J, Berger, A & Shackleton, NJ 1993, 'Role of orbital forcing: a two-million-year perspective', *Global Changes in the Perspective of the Past*, pp.263-277.

Imbrie, J, Boyle, EA, Clemens, SC, Duffy, A, Howard, WR, Kukla, G, Kutzbach, J, Martinson, DG, McIntyre, A, Mix, AC, Molfino, B, Morley, JJ, Peterson, LC, Pisias, NG, Prell, WL, Raymo, ME, Shackleton, NJ & Toggweiler, JR 1992, 'On the structure and origin of major glaciation cycles 1. Linear responses to Milankovitch forcing', *Paleoceanography*, vol. 7, pp. 701-738.

Johnsen, SJ, Clausen, HB, Dansgaard, W, Fuhrer, K, Gundestrup, N, Hammer, CU, Iversen, P, Jouzel, J, Stauffer, B & Steffensen JP 1992, 'Irregular glacial interstadials recorded in a new Greenland ice core', *Nature*, vol. 359, pp. 311-313.

Johnsson, MJ & Basu, A eds, 1993, *Processes controlling the composition of clastic sediments* (Vol. 284). Geological Society of America.

Johnsson, MJ 1990, 'Tectonic versus chemical-weathering controls on the composition of fluvial sands in tropical environments', *Sedimentology*, vol. 37, no. 4, pp. 713-726.

Kigoshi, K 1971, ‘Alpha-recoil thorium-234: Dissolution into water and the uranium-234/uranium-238 disequilibrium in nature’, *Science*, vol. 173, pp. 47-48.

Kigoshi, K 1971, ‘Alpha-recoil thorium-234: Dissolution into water and the uranium-234/uranium-238 disequilibrium in nature’, *Science*, vol. 173, pp. 47-48.

Knox, JC 1972, ‘Valley alluviation In Southwestern Wisconsin’, *Ann. Assoc. Am. Geogr.*, vol. 62, no. 3, pp. 401–410.

Konijnendijk, TYM, Ziegler, M & Lourens, LJ 2015, ‘On the timing and forcing mechanisms of late Pleistocene glacial terminations: Insights from a new high-resolution benthic stable oxygen isotope record of the eastern Mediterranean’, *Quaternary Science Reviews*, vol. 129, pp. 308-320.

Korup, O 2005, ‘Geomorphic imprint of landslides on alpine river systems, southwest New Zealand’, *Earth Surface Processes and Landforms*, vol. 30, no. 7, pp. 783‐800.

Land, M, Wust, RA, Robert, C & Carter, RM 2010, ‘Plio-Pleistocene paleoclimate in the Southwest Pacific as reflected in clay mineralogy and particle size at ODP Site 1119, SE New Zealand’, *Marine Geology*, vol. 274, no. 1, pp.165-176.

Langbein, WB & Schumm, SA 1958, ‘Yield of sediment in relation to mean annual precipitation’, *Eos*, Transactions American Geophysical Union, vol. 39, no. 6, pp. 1076–1084.

Larsen, IJ, Montgomery, DR & Korup, O 2010, ‘Landslide erosion controlled by hillslope material’, *Nature Geoscience*, vol. 3, pp. 247-251.

Laskar, J, Robutel, P, Joutel, F, Gastineau, M, Correia, A & Levrard, B 2004, ‘A long- term numerical solution for the insolation quantities of the Earth’, *Astronomy & Astrophysics*, vol. 428, pp. 261-285.

Latham, A & Schwarcz, H 1987, 'On the possibility of determining rates of removal of uranium from crystalline igneous rocks using U-series disequilibria—1: a U-leach model, and its applicability to whole-rock data', *Applied Geochemistry*, vol. 2, pp. 55-65.

Lee, SY & Baik, MH 2009, 'Uranium and other trace elements' distribution in Korean granite: implications for the influence of iron oxides on uranium migration', *Environmental geochemistry and health*, vol. 31, pp. 413-420.

Lee, V, DePaolo, DJ & Christensen, JN 2010. 'Uranium-series comminution ages of continental sediments: case study of a Pleistocene alluvial fan', *Earth and Planetary Science Letters*, vol. 296, no. 3–4, pp. 244–254.

Limmer, DR, Böning, P, Giosan, L, Ponton, C, Köhler, CM, Cooper, MJ, Tabrez AR & Clift PD 2012, 'Geochemical record of Holocene to Recent sedimentation on the Western Indus continental shelf, Arabian Sea', *Geochemistry, Geophysics & Geosystems*, vol. 13.

Lisiecki, L & Raymo, M 2005, 'A Pliocene Pleistocene stack of 57 globally distributed benthic d18O records', *Paleoceanography*, vol. 20.

Liu, Z, Colin, C, Trentesaux, A, Siani, G, Frank, N, Blamart, D & Farid, S, 2005. 'Late Quaternary climatic control on erosion and weathering in the eastern Tibetan Plateau and the Mekong Basin', *Quaternary Research*, vol. 63, no. 3, pp.316-328.

Lowe, JJ & Walker, MJ 1997, Reconstructing quaternary environments. 2nd ed. Addison Wesley Longman Limited, Essex.

Luo, S, Ku, TL, Roback, R, Murrell, M & McLing, TL 2000, 'In-situ radionuclide transport and preferential groundwater flows at INEEL (Idaho): decay-series disequilibrium studies', *Geochimica et Cosmochimica Acta*, vol. 64, no. 5, pp. 867–881.

Lyons, WB, Carey, AE, Hicks DM & Nezat, CA 2005, 'Chemical weathering in high sediment-yielding watersheds, New Zealand', *Journal of Geophysical Research*, vol. 110, no. F1, F01008.

Macphail, MK & McQueen, DR 1983, 'The value of New Zealand pollen and spores as indicators of Cenozoic vegetation and climates', *Tuatara*, vol. 26, pp. 37-59.

Mahaney, WC & Halvorson, DL 1986, 'Rates of mineral weathering in the wind river mountains, western Wyoming', *Rates of Chemical Weathering of Rocks and Minerals*, pp. 147–167.

Mahowald, N, Kohfeld, K, Hansson, M, Balkanski, Y, Harrison, SP, Prentice, IC, Schulz, M & Rodhe, H 1999, 'Dust sources and deposition during the last glacial maximum and current climate: A comparison of model results with paleodata from ice cores and marine sediments', *Journal of Geophysical Research: Atmospheres*, vol. 104, pp.15895-15916.

Martin, AN, Dosseto, A & Kinsley, LPJ 2015, 'Evaluating the removal of non-detrital matter from soils and sediment using uranium isotopes', *Chemical Geology*, vol. 396, pp. 124–133.

Martinson, DG, Pisias, NG, Hays, JD, Imbrie, J, Moore Jr., TC & Shackleton, NJ 1987, 'Age dating and the orbital theory of the ice ages: development of a high-resolution 0 to 300,000 year chronostratigraphy', *Quaternary Research*, vol. 27, pp. 1-29.

McCaskill, M 1956, 'The goldrush population of Westland', *New Zealand Geographer*, vol. 12, no. 1, pp. 32-50.

McGlone, MS & Topping, WW 1983 'Late Quaternary vegetation, Tongariro region, central North Island, New Zealand', *New Zealand Journal of Botany*, vol. 21, pp. 53-76.

Meteo France, 2017. Donnees Climatiques de la station de Nice, Meteo France, viewed 10/09/17, <http://www.meteofrance.com/climat/france/nice/06088001/normales>

Milliman, JD & Syvitski, JPM 1992, 'Geomorphic/ tectonic control of sediment discharge to the ocean: the importance of small mountainous rivers', *Journal of Geology*, vol. 100, pp. 525–544.

Mix, AC, Bard, E & Schneider, R 2001, 'Environmental processes of the ice age: land, oceans, glaciers (EPILOG)', *Quaternary Science Reviews*, vol. 20, pp. 627-657.

Moar, NT & Suggate RP 1996, 'Vegetation history from the Kaihinu (Last) Interglacial to the present, West Coast, South Island, New Zealand', *Quaternary Science Reviews*, vol. 15, pp. 521-547.

Mulder, T & Syvitski, JPM 1995, 'Turbidity currents generated at river mouths during exceptional discharges to the world oceans', *Journal of Geology*, vol. 103, pp. 285-299.

Mulder, T, Migeon, S, Savoye, B & Faugères, JC 2001, 'Inversely graded turbidite sequences in the deep Mediterranean: a record of deposits from flood-generated turbidity currents?', *Geo-Marine Letters*, vol. 21, pp. 86-93.

Mulder, T, Migeon, S, Savoye, B & Jouanneau, JM 2001, 'Twentieth century floods recorded in the deep Mediterranean sediments', *Geology*, vol. 29, pp. 1011-1014.

Mulder, T, Savoye, B, Piper, DJW & Syvitski, JPM 1998, 'The Var submarine sedimentary system: understanding Holocene sediment delivery processes and their importance to the geological record', *Geological Society, London, Special Publications*, vol. 129, pp. 145-166.

Mulder, T, Savoye, B, Syvitski, JPM & Parize, O 1997, 'Des courants de turbidité hyperpycnaux dans la tête du canyon du Var? Données hydrologiques et observations de terrain', *Oceanologica Acta*, vol. 20, pp. 607–626.

Nathan, S, Rattenbury, MS & Suggate, RP 2002, 'Geology of the Greymouth area: scale 1:250,000 geological map, *Institute of Geological & Nuclear Sciences*.

Neil, HL, 2008, 'Sediment conduits to the deep Tasman: two contrasting large canyons-channel complexes from the West Coast, South Island, New Zealand', *Geol. Society NZ, NZ Geophysical Society, NZ Geochemical & Mineralogical Society Joint Annual Conference Miscellaneous Publication 234*.

Nesbitt, HW & Markovics, G 1980, 'Chemical processes affecting alkalis and alkaline earths during continental weathering', *Geochimica et Cosmochimica Acta*, vol. 44, no. 11, pp.1659-1666.

Nesbitt, HW & Markovics, G 1997, 'Weathering of granodioritic crust, long-term storage of elements in weathering profiles, and petrogenesis of siliciclastic sediments', *Geochimica et Cosmochimica Acta*, vol. 61, pp. 1653–1670.

Nesbitt, HW & Young, GM 1982, 'Early Proterozoic climate and plate motions inferred from major element chemistry of lutites', *Nature*, vol. 299, pp. 715–717.

Nesbitt, HW 1979, 'Mobility and fractionation of rare earth elements during weathering of a granodiorite', *Nature*, vol. 270, pp. 206–210.

Nesbitt, HW, Fedo, CM & Young, GM 1997, 'Quartz and feldspar stability, steady and non steady state weathering, and petrogenesis of siliciclastic sands and muds', *Journal of Geology*, vol. 105, no. 2, pp. 173-192.

Newnham, R.M., Lowe, D.J. and Williams, P.W., 1999. Quaternary environmental change in New Zealand: a review. *Progress in Physical Geography*, vol. 23, no. 4, pp.567-610.

Nichols, KK, Bierman, PR, Hooke, RL, Clapp, EM & Caffee, M 2002, 'Quantifying sediment transport on desert piedmonts using 10Be and 26Al', *Geomorphology*, vol. 45, pp. 105-125.

NIWA 2012, 'National and Regional Climate Maps', viewed 10 July 2017, <https://www.niwa.co.nz/climate/national-and-regional-climate-maps/national>.

Norris, RM 1978, 'Late Cenozoic Geology of the West Coast Shelf between Karamea and the Waiho River, South Island, New Zealand', *New Zealand Oceanographic Institute*, vol. 81.

Norton, KP & Von Blanckenburg, F 2010, 'Silicate weathering of soil-mantled slopes in an active Alpine landscape', *Geochimica et Cosmochimica Acta*, vol. 74, no. 18, pp. 5243-5258.

O'Connor, TP & Kester, DR 1975, 'Adsorption of copper and cobalt from fresh and marine systems', *Geochimica et Cosmochimica Acta*, vol. 39, pp. 1531-1543.

Palmer, AS & Pillans, BJ 1996, 'Record of Climatic Fluctuations from ca. 500ka loess deposits and paleosols near Wanganui, New Zealand', *Quaternary International*, vol. 34-36, pp. 155-162.

Pavich, MJ, Brown, L, Harden, J, Klein, J & Middleton, R 1986, '10Be distribution in soils from Merced River terraces, California', *Geochimica et Cosmochimica Acta*, vol. 50, pp. 1727- 1735.

Pelejero, C, Calvo, E, Barrows, TT, Logan, GA & DeDeckker, P 2006, 'South Tasman Sea alkenone palaeothermometry over the last four glacial/interglacial cycles', *Marine Geology*, vol. 230, pp. 73-86.

Pelejero, C, Calvo, E, Logan, GA & De Deckker, P 2003, 'Marine isotopic stage 5e in the Southwest Pacific: similarities with Antarctica and ENSO inferences', *Geophysical Research Letters*, vol. 30.

Petit, JR, Jouzel, J, Raynaud, D, Barkov, NI, Barnola, JM, Basile, I, Bender, M, Chappellaz, J, Davis, M, Delaygue, G, Delmotte, M, Kotlyakov, VM, Legrand, M, Lipenkov, VY, Lorius, C, Pepin, L, Ritz, C, Saltzmann, E & Stievenard, M 1999, 'Climate and atmospheric history of the past 420,000 years from the Vostok ice core, Antarctica', *Nature*, vol. 399, pp. 429-436.

Peuraniemi, V & Pulkkinen, P 1993, 'Preglacial weathering crust in Ostrobothnia, western Finland, with special reference to the Raudaskyla occurrence', *Chemical Geology*, vol. 107, pp. 313–316.

Philip H 1987, 'Plio-Quaternary evolution of the stress field in Mediterranean zones of subduction and collision', *Annales Geophysicae*, vol. 3, pp. 301–320.

Piper, DJW & Savoye, B 1993, 'Processes of late Quaternary turbidity current flow and deposition on the Var deep-sea fan, north-west Mediterranean Sea', *Sedimentology*, vol. 40, pp. 557-582.

Probert, PK & Swanson, KM 1985, 'Sediment texture of the continental shelf and upper slope off the west coast of the South Island, New Zealand', *New Zealand Journal of Marine and Freshwater Resources*, vol. 19, pp. 563-573.

Ray, N & Adams, J 2001, 'A GIS-based vegetation map of the world at the last glacial maximum (25,000-15,000 BP)', *Internet archaeology*, vol. 11.

Reif, A & Allen, R 1988, 'Plant communities of the steepland conifer-broadleaved hardwood forests of central Westland, South Island, New Zealand', *Phytocoenologia*. vol. 16, pp. 145-224.

Reneau, SL, Dietrich, WE, Donahue, DJ, Jull, AT & Rubin, M 1990, 'Late Quaternary history of colluvial deposition and erosion in hollows, central California Coast Ranges', *Geological Society of America Bulletin*, vol. 102, pp. 969-982.

Riebe, CS, Kirchner, JW & Finkel, RC 2003, 'Long-term rates of chemical weathering and physical erosion from cosmogenic nuclides and geochemical mass balance', *Geochimica et Cosmochimica Acta*, vol. 67, pp. 4411-4427.

Righi, D, Huber, K & Keller, C 1999, 'Clay formation and podzol development from postglacial moraines in Switzerland', *Clay Minerals*, vol. 34, no. 2, pp. 319-332.

Rollinson, HR 1993, 'Using geochemical data: evaluation, presentation, interpretation', Harlow, Essex, England.

Rothacker L (2017), 'Human impact overprints natural controls on soil systems in the Iron Age' (submitted).

Ryan, MT, Dunbar, GB, Vandergoes, MJ, Neil, HL, Hannah, MJ, Newnham, RM, Bostock, H & Alloway, BV 2012, 'Vegetation and climate in Southern Hemisphere mid-latitudes since 210 ka: new insights from marine and terrestrial pollen records from New Zealand', *Quaternary Science Reviews*, vol. 48, pp. 80-98.

Sage, L 1976, 'La sédimentation à l'embouchure d'un fleuve côtier méditerranéen: le Var', *Université de Nice*.

Savage, KM & Potter, PE 1991, 'Petrology of Modern Sands of the Rios Guaviare and Inirida, Southern Colombia: Tropical Climate and Sand Composition', *Journal of Geology*, vol. 99, no. 2, pp. 289-298.

Schultz, MK, Burnett, WC & Inn, KGW 1998, 'Evaluation of a sequential extraction method for determining actinide fractionation in soils and sediments', *Journal of Environmental Radioactivity*, vol. 40, pp. 155-174.

Schumm, SA 1977, 'The fluvial system', Wiley Inter-Science Pub, New York, N.Y.

Scott, M, Rotter, R & Salter, P 1985, 'Transport of fallout plutonium to the ocean by the Mississippi River', *Earth and Planetary Science Letters*, vol. 75, pp. 321-326.

Semkow, TM 1991, 'Fractal model of radon emanation from solids', *Physical Review Letters*, vol. 66, no. 23, pp. 3012–3015.

Shulmeister, J, Fink, D, Hyatt, OM, Thackray, JD & Rother, H 2010, 'Cosmogenic 10Be and 26Al exposure ages of moraines in the Rakaia Valley, New Zealand and the nature of the last termination in New Zealand glacial systems', *Earth and Planetary Science Letters*, vol. 297, pp. 558-566.

Simpson, G & Castelltort, S 2012, 'Model shows that rivers transmit high-frequency climate cycles to the sedimentary record', *Geology*, vol. 40, pp. 1131–1134.

Simpson, GDH, Cooper, AF & Norris RJ 1994, 'Late Quaternary evolution of the Alpine Fault Zone at Paringa, South Westland, New Zealand', *New Zealand Journal of Geology and Geophysics,* vol. 37, pp. 49-58.

Sing, KS 1985, 'Reporting physisorption data for gas/solid systems with special reference to the determination of surface area and porosity (Recommendations 1984)', *Pure and Applied Chemistry*, vol. 57, pp. 603-619.

Stallard, RF & Edmond, JM 1983, 'Geochemistry of the Amazon: 2. The influence of the geology and weathering environment on the dissolved load', *Journal of Geophysical Research*, vol. 88, pp. 9671-9688.

Stanton, BR 1976, 'Circulation and hydrology off the west coast of the South Island, New Zealand', *New Zealand Journal of Marine and Freshwater Research*, vol. 10, pp. 445-467.

Stewart, JR 2003, Comment on 'Buffered Tree Population Changes in a Quaternary Refugium: Evolutionary Implications', *Science*, vol. 299, 825a.

Suc, JP & Popescu, SM, 2005, 'Pollen records and climatic cycles in the North Mediterranean region since 2.7 Ma', *Geological Society, London, Special Publications*, vol. 247, no. 1, pp.147-158.

Suggate RP 1990, 'Late Pliocene and Quaternary glaciations of New Zealand', *Quaternary Science Reviews*, vol. 9, pp. 175-197.

Suggate, RP 1985, 'The Last Glacial/interglacial Sequence of North Westland, New Zealand', *New Zealand Geological Survey Record 7*, DSIR, p. 22.

Sun, H & Furbish, DJ 1995, 'Moisture content effect on radon emanation in porous media', *Journal of Contaminant Hydrology*, vol. 18, no. 3, pp. 239–255.

Suresh, P, Dosseto, A, Hesse, P & Handley, H 2014, 'Very long hillslope transport timescales determined from uranium-series isotopes in river sediments from a large, tectonically stable catchment', *Geochimica et Cosmochimica Acta*, vol. 142, pp. 442-457.

Sutherland, R, Kim, K, Zondervan, A & McSaveney, M 2007, 'Orbital forcing of mid-latitude Southern Hemisphere glaciation since 100 ka inferred from cosmogenic nuclide ages of moraine boulders from the Cascade Plateau, southwest New Zealand', *Geological Society of America Bulletin*, vol. 119 no. 3-4, pp. 443-451.

Syvitski, J.P. ed., 2007, 'Principles, methods and application of particle size analysis', Cambridge University Press.

Tessier, A, Campbell, PGC & Bisson, M 1979, 'Sequential extraction procedure for the speciation of particulate trace metals', *Analytical Chemistry*, vol. 51, pp. 844-851.

Thiry, M 2000, 'Palaeoclimatic interpretation of clay minerals in marine deposits; an outlook from the continental origin', *Earth Science Reviews*, vol. 49, no. 1–4, pp. 201–221.

Tonkin, PJ & Basher LR 1990, 'Soil - stratigraphic techniques in the study of soil and landform evolution across the Southern Alps, New Zealand', *Geomorphology*, vol. 3, no. 3–4, pp. 547-575.

Tzedakis, PC, Lawson, IT, Frogley, MR, Hewitt, GM & Preece, RC 2002, "Buffered Tree Population Changes in a Quaternary Refugium: Evolutionary Implications", *Science*, vol. 297, pp. 2044-2047.

Tzedakis, PC, Lawson, IT, Frogley, MR, Hewitt, GM & Preece, RC 2003, Comment on "Buffered Tree Population Changes in a Quaternary Refugium: Evolutionary Implications", *Science*, vol. 299, 825b.

Vandergoes, MJ & Fitzsimons, SJ 2003, 'The Last Glacial-Interglacial transition (LGIT) in south Westland, New Zealand: paleoecological insight into mid- latitude Southern Hemisphere climate change', *Quaternary Science Reviews*, vol. 22, pp. 1461-1476.

Velichko, AA, Andreev, AA & Klimanov, VA 1997, 'Climate and vegetation dynamics in the tundra and forest zone during the Late Glacial and Holocene', *Quaternary International*, vol. 41, pp.71-96.

Viers, J, Roddaz, M, Filizola, N, Guyot, JL, Sondag, F, Brunet, P, Zouiten, C, Boucayrand, C, Martin, F & Boaventura, GR 2008, 'Seasonal and provenance controls on Nd–Sr isotopic compositions of Amazon rivers suspended sediments and implications for Nd and Sr fluxes exported to the Atlantic Ocean' *Earth and Planetary Science Letters*, vol. 274, no. 3–4, pp. 511-523.

Vry, JK, Powell, R & Williams, J 2008, 'Establishing the P–T path for Alpine Schist, Southern Alps near Hokitika, New Zealand', *Journal of Metamorphic Geology*, vol. 26, no. 1, pp.81-97.

Walling, DE 1983, 'The sediment delivery problem', *Journal of Hydrology*, vol. 65, pp. 209-237.

Wan, S, Li, A, Clift, P & Jiang, H 2006, 'Development of the East Asian summer monsoon: evidence from the sediment record in the South China Sea since 8.5 Ma', *Palaeogeography, Palaeoclimatology, Palaeoecology*, vol. 241, no. 1, pp. 139–159.

Wang, L, Sarnthein, M, Erlenkeuser, H, Grimalt, J, Grootes, P, Heilig, S, Ivanova, E, Kienast, M, Pelejero, C & Pflaumann, U 1999, 'East Asian monsoon climate during the Late Pleistocene: high-resolution sediment records from the South China Sea', *Marine Geology*, vol. 156, no. 1, pp.245-284.

Wardle, P 1979, 'Plants and landscape in Westland National Park', *National Parks Scientific Series 3*.

Wardle, P 1991, 'Vegetation of New Zealand', Cambridge University Press, Cambridge, England.

Wei, G, Li, XH, Liu, Y, Shao, L & Liang, X 2006, 'Geochemical record of chemical weathering and monsoon climate change since the early Miocene in the South China Sea', *Paleoceanography*, vol. 21.

Wei, G, Liu, Y, Li, X, Shao, L & Liang, X 2003, 'Climatic impact on Al, K, Sc and Ti in marine sediments: evidence from ODP Site 1144, South China Sea', *Geochemical Journal,* vol. 37, no. 5, pp.593-602.

Wei, G, Liu, Y, Li, XH, Shao, L & Fang, D 2004, 'Major and trace element variations of the sediments at ODP Site 1144, South China Sea, during the last 230 ka and their paleoclimate implications', *Palaeogeography, Palaeoclimatology, Palaeoecology*, vol. 212, no.3, pp.331-342.

Williams, PW 1996, 'A 230 ka record of glacial and interglacial events from Aurora Cave, Fiordland, New Zealand', *New Zealand Journal of Geology and Geophysics*, vol. 39, pp. 225-241.

Williams, PW, McGlone, M, Neil & H, Zhao, JX 2015, 'A review of New Zealand palaeoclimate from the Last Interglacial to the global Last Glacial Maximum', *Quaternary Science Reviews*, vol. 110, pp. 92-106.

Windom, HL 1976, 'Lithogenous materials in marine sediments', Riley, JP & Chester, R (eds), *Chemical Oceanography*, Elsevier, New York.

Woodham, AH, 1981, 'Development of a West Coast dairy farm in a high rainfall area', In *Proceedings of the New Zealand Grassland Association*, Conference.

Wu, H, Guiot, J, Brewer, S & Guo, Z 2007, 'Climatic changes in Eurasia and Africa at the last glacial maximum and mid-Holocene: reconstruction from pollen data using inverse vegetation modelling', *Climate Dynamics*, vol. 29, no. 2-3, pp.211-229.

Zabel, M, Schneider, RR, Wagner, T, Adegbie, AT, de Vries, U & Kolonic, S 2001, 'Late Quaternary climate changes in Central Africa as inferred from terrigenous input to the Niger Fan', *Quaternary Research*, vol. 56, no. 2, pp.207-217.

Zhang, C, Wang, L, Li, G, Dong, S, Yang, J & Wang, X 2002, 'Grain size effect on multi‐ element concentrations in sediments from the intertidal flats of Bohai Bay, China', *Applied Geochemistry*, vol. 17, no. (1), pp. 59‐68.

12 Appendices

Appendix A: Sample Ages and Characteristics

Var Data

Core	Sample	Depth (cm)	Age (yrs)	Description
ESSK08-CS01	CS01_1	350-352	9800	clay
	CS01_2	352-355	9800	silt
	CS01_3	803-807	19700	clay+silt
	CS01_4	948-949	20900	clay
ESSK08-CS13	CS13_1	92-93	6720	clay+silt
	CS13_2	268-269	12120	clay+silt
	CS13_3	336-338	14210	clay
	CS13_4	339-342	14210	silt
	CS13_5	438-440	16510	clay
	CS13_6	440-442	16510	silt
	CS13_7	603-605	19480	clay
	CS13_8	610-615	19480	silt
	CS13_9	722-723	21190	clay
	CS13_10	723-724	21190	silt
	CS13_11	816-818	22920	clay
	CS13_12	818-820	22920	silt
	CS13_13	949-951	27060	silt
	CS13_14	1048-1050	30850	clay
	CS13_15	1050-1053	30850	silt
	CS13_16	1085-1086	32150	clay
	CS13_17	1090-1091	32150	silt
	CS13_18	1358-1362	43180	silt+clay
	CS13_19	1561-1562	53000	clay
	CS13_20	1562-1565	53000	silt
	CS13_21	1633-1636	55590	silt+clay
	CS13_22	1741-1743	59060	clay
	CS13_23	1742-1748	59060	silt
	CS13_24	1975-1976	66080	clay
	CS13_25	2168-2188	73580	clay
	CS13_26	2188-2190	73580	silt

Hokitika Data

Core	Sample	Depth (cm)	Age (kyr)	Description
TAN0513-14	T14_M_01	0	0.1	Mud
	T14_M_10	10	6.96	Mud
	T14_M_20	20	13.83	Mud
	T14_M_30	30	18.6	Mud
	T14_M_40	40	22.98	Mud
	T14c_50	50	27.96	--
	T14_M_60	60	33.7	Mud
	T14_M_70	70	39.45	Mud
	T14_L2_M_80	80	45.19	Mud
	T14_M_90	90	50.94	Mud
	T14_M_100	100	56.57	Mud
	T14_110	110	60.5	--
	T14_M_120	120	64.43	Mud
	T14_M_130	130	68.36	Mud
	T14_M_140	140	76.09	Mud
	T14_L1_M_150	150	86.8	Mud
	T14_M_160	160	91.99	Mud
	T14_M_170	170	97.19	Mud
	T14_L2_M_180	180	102.39	Mud
	T14_190	190	107.71	--
	T14_200	200	114.57	--
	T14_210	210	133.25	--
	T14_220	220	139.82	--
	T14_L1_230	230	146.38	--
	T14_240	240	152.95	--
	T14_250	250	159.59	--
	T14_260	260	166.27	--
	T14_M_270	270	172.95	Mud
	T14_280	280	179.63	--
	T14_L2_290	290	186.3	--
	T14_L2_300	300	193.2	--
	T14_L2_310	310	200.54	--
	T14_NL_320	320	207.89	--

Appendix B: Grain Size Data

Var Data

Sample Name	Sand (wt. %)	Silt (wt. %)	Clay (wt. %)	Mean Grain Size (μm)	Standard Deviation	Skewness	Kurtosis
CS01-1	8.19	73.27	18.55	12.66	1.68	-0.02	0.78
CS01-2	12.73	70.19	17.08	14.53	1.8	0	0.81
CS01-3	18.3	66.76	14.93	17.59	1.98	0	0.91
CS01-4	10.51	71.95	17.53	13.23	1.73	-0.06	0.82
CS13-1	5.98	72.41	21.62	10.82	1.65	-0.09	0.81
CS13-2	18.87	62.6	18.54	15.44	2.18	-0.2	0.93
CS13-3	19.03	70.32	10.66	21.89	1.74	0.24	0.9
CS13-4	38.62	57.63	3.75	46.79	1.29	0.3	1.4
CS13-5	19.6	67.61	12.79	20.25	1.8	0.24	0.77
CS13-6	22.54	65.19	12.27	21.58	1.84	0.23	0.78
CS13-7	7.93	72.39	19.68	11.19	1.66	-0.13	0.89
CS13-8	41.09	47.17	11.74	32.57	2.3	0.16	0.72
CS13-9	11.29	70.62	18.08	13.1	1.77	-0.09	0.83
CS13-10	45.14	50.9	3.95	50.79	1.45	0.28	1.37
CS13-11	4.66	77.89	17.45	11.38	1.51	-0.04	0.84
CS13-12	28.54	59.26	12.19	23.62	1.99	0.17	0.77
CS13-13	36.99	54.15	8.86	31.92	1.98	0.29	0.88
CS13-14	7.73	73.48	18.79	11.92	1.64	-0.09	0.8
CS13-15	28.69	59.2	12.11	24.06	1.97	0.2	0.78
CS13-16	12.66	73.83	13.51	16.75	1.69	0.13	0.75
CS13-17	58.03	34.84	7.13	50.35	2.03	0.48	0.91
CS13-18	8.04	71.17	20.79	11.13	1.69	-0.14	0.84
CS13-19	13.92	69.44	16.64	15.25	1.78	0.02	0.72
CS13-20	43.51	50.4	6.1	41.52	1.84	0.3	1.24
CS13-21	33.42	54.22	12.36	26.31	2.08	0.21	0.77
CS13-22	12.39	71.36	16.24	13.87	1.73	-0.12	0.76
CS13-23	57.47	37.82	4.71	60.27	1.7	0.34	1.35
CS13-24	12.62	69.84	17.54	14.71	1.8	0.06	0.79
CS13-25	4.53	72	23.48	9.69	1.59	-0.08	0.85
CS13-26	52.24	42.47	5.29	49.53	1.71	0.4	1.27

Hokitika Data

Sample Name	Sand (wt. %)	Silt (wt. %)	Clay (wt. %)	Mean grain size (μm)	Standard Deviation	Skewness	Kurtosis
T14_M_01	19.59	71.15	9.26	24.60	2.29	-0.31	1.16
T14_M_10	1.55	80.32	18.14	9.35	1.32	-0.04	0.96
T14_M_20	5.93	77.24	16.83	9.99	1.7	-0.25	1.44
T14_M_30	1.12	78.06	20.82	8.53	1.3	-0.06	0.95
T14_M_40	2.11	76.19	21.70	8.72	1.38	-0.08	0.95
T14c_50	3.48	87.11	9.41	13.72	1.31	0.03	0.97
T14_M_60	1.09	77.00	21.91	7.95	1.55	-0.18	1.16
T14_M_70	0.23	80.94	18.83	7.92	1.11	-0.04	1
T14_L2_M_80	1.95	78.04	20.01	8.95	1.34	-0.05	0.96
T14_M_90	3.53	76.27	20.20	8.76	1.33	-0.08	0.99
T14_M_100	2.94	75.75	21.31	9.31	1.46	-0.09	0.92
T14_110	0.84	73.35	25.81	7.52	1.3	-0.09	0.93
T14_M_120	1.22	75.38	23.40	8.23	1.35	-0.06	0.92
T14_M_130	0.01	74.00	25.99	7.23	1.23	-0.06	0.92
T14_M_140	0.94	78.14	20.91	8.50	1.29	-0.03	0.94
T14_L1_M_150	7.35	74.99	17.66	10.13	1.73	-0.23	1.39
T14_M_160	4.44	76.77	18.79	9.37	1.4	-0.09	1.02
T14_M_170	1.40	79.25	19.35	8.97	1.3	-0.03	0.94
T14_L2_M_180	1.86	80.07	18.07	9.14	1.28	-0.03	0.97
T14_190	4.84	73.33	21.83	8.64	1.44	-0.12	1.04
T14_200	1.21	83.17	15.63	10.36	1.32	-0.01	0.92
T14_210	2.01	75.50	22.48	8.85	1.42	-0.06	0.9
T14_220	3.97	70.99	25.03	8.35	1.49	-0.14	0.97
T14_L1_230	9.74	65.37	24.89	9.52	1.97	-0.32	1.26
T14_240	1.74	74.25	24.01	8.32	1.4	-0.06	0.92
T14_250	6.11	68.33	25.56	8.62	1.6	-0.18	1
T14_260	1.18	68.91	29.91	7.07	1.38	-0.12	0.93
T14_M_270	8.04	70.07	21.88	9.65	1.66	-0.2	1.07
T14_280	1.66	75.94	22.40	8.23	1.33	-0.07	0.98
T14_L2_290	1.06	76.71	22.24	8.18	1.31	-0.05	0.96
T14_L2_300	1.31	80.59	18.10	9.38	1.32	-0.05	0.95
T14_L2_310	4.83	75.92	19.24	9.32	1.43	-0.13	1.04
T14_NL_320	3.02	78.02	18.97	9.80	1.43	-0.07	0.93

Appendix C: Mineralogical Data (XRD)

Sample	Calcite	Quartz	Muscovite	Labradorean	Kaolin	Orthoclase	Biotitic	Halite	Dolomite	Microcline	Siderite	Unknown	χ^2
CS01_1	38	20.5	14.1	9.9	4.9	2.8	2.6	2.4	2.2	2.1	0.3	0.2	3.11
CS01_2	42.1	23	13.3	5.2	4.6	3.9	3.2	2.4	1.7	0.3	0.2	0.1	2.81
CS01_3	31.6	28.4	14.2	9	4.2	3.8	3.4	2.6	2.1	0.6	0	0.1	3.76
CS01_4	26.4	25.3	19.4	7.2	6.6	5.3	5.1	3.3	1.4	0.1	0	-0.1	3.56
CS13_1	43.6	21.1	14.5	5.1	4.7	3.5	3.4	2.7	1.4	0	0	0	2.68
CS13_2	42.2	18.5	13	6.8	5.3	4.9	3.6	2.9	1.5	1.2	0	0.1	2.9
CS13_3	29.1	17.9	15.2	14.4	7.8	5.7	4.7	2.9	2.2	0	0	0.1	5.06
CS13_4	27.5	27.2	24.1	9.7	3.7	2.5	1.9	1.5	1	0.8	0	0.1	6.52
CS13_5	29.3	25	15.2	10.1	5.2	4.2	3.7	3	2.7	1.5	0	0.1	3.85
CS13_6	30.8	20	16.8	7.1	6.8	5.8	5.2	5.1	2.4	0	0	0	3.82
CS13_7	29.7	21.5	17.3	8.7	6.6	5.6	5.2	3.2	2.2	0	0	0	3.8
CS13_8	27.2	26.6	19.7	11.7	3.9	3.6	3.1	2.1	1	1	0	0.1	5.85
CS13_9	30.9	21.9	17.3	7.4	6.6	5.9	5.4	2.4	2.2	0	0	0	3.56
CS13_10	35.5	16.9	14.2	13.3	5.9	5.9	3.3	3.2	1.1	0.6	0	0.1	13.44
CS13_11	25.2	21.6	17.7	9	7.6	6.4	5.5	3.1	1.8	1.8	0.2	0.1	3.64
CS13_12	25.2	24	17.1	11.2	6.6	5.8	4.7	3.2	2.3	0	0	-0.1	4.63
CS13_13	21.2	19.6	16.5	15.4	12.4	7.1	3.1	2.1	1.7	0.9	0	0	7.81
CS13_14	32	23.9	14.3	6.4	5.2	4.8	4.7	4.5	2.5	1.6	0	0.1	3.58
CS13_15	24.4	21.4	18.4	12.4	7.9	5.9	5.1	2	1.7	0.6	0	0.2	5.79
CS13_16	24.3	20.9	18.1	15.1	6.8	5.7	5.6	2.4	1.1	0	0	0	7.03
CS13_17	30.9	24.1	14.1	10.8	4.7	4.6	3.9	3.3	2.9	0.5	0	0.2	3.31
CS13_18	28.5	28.3	18.8	6	5.5	4.3	4.3	2.4	0.8	0.6	0.5	0	2.89
CS13_19	32	27.8	18.5	5.5	4.7	4.1	3.4	2.9	0.8	0.2	0	0.1	3.17

CS13_20	33.5	18.8	12.3	10.3	6.6	6.4	4.9	3.9	2.2	1.2	0	-0.1	5.58
CS13_21	35.5	15.3	12.7	11.6	10.5	7.7	2.2	2	1.7	0.7	0	0.1	6.53
CS13_22	31.6	25.6	11.4	7.1	5.7	4.8	4.4	3.9	3.7	1.7	0	0.1	2.74
CS13_23	25.9	21.7	14.8	13.3	10.3	4.7	4.1	2	1.9	1.4	0	-0.1	7.7
CS13_24	26.9	20.3	15.7	14.3	7	4.4	4	3.6	3	0.9	0	-0.1	6.91
CS13_25	30.1	21.3	17.3	11.7	5.6	5.2	3.8	2.5	2	0.2	0	0.3	4.93
CS13_26	28.8	23.8	14.4	9.1	9	6	2.8	2.8	1.8	1.4	0	0.1	4.01

Appendix D: Major and trace element data

Major Elements

Sample	Na (wt. %)	Mg (wt. %)	Al (wt. %)	Si (wt. %)	K (wt. %)	Ca (wt. %)	Ti (wt. %)	Mn (wt. %)	Fe (wt. %)	Sr (wt. %)	Ba (wt. %)
CS01-1	3.776	1.645	15.979	4.178	5.862	-1.443	0.815	0.020	1.933	0.020	0.059
CS01-2	1.899	1.300	15.049	8.070	5.532	-3.570	0.315	0.023	2.161	0.020	0.016
CS01-3	3.546	1.574	15.378	4.271	6.171	-1.577	0.827	0.017	1.730	0.018	0.078
CS01-4	3.869	1.754	15.745	2.091	6.097	-0.588	0.960	0.019	2.298	0.020	0.090
CS13-1	1.880	1.808	14.813	5.820	4.833	-2.215	0.675	0.011	1.781	0.019	0.048
CS13-2	2.697	2.050	14.135	4.794	4.644	-1.756	0.824	0.014	2.001	0.019	0.054
CS13-3	4.116	1.921	11.925	4.604	3.234	-1.747	0.504	0.021	1.718	0.016	0.032
CS13-4	6.951	1.213	11.026	3.848	2.706	-1.142	0.589	0.021	1.376	0.018	0.035
CS13-5	2.851	1.680	13.358	2.388	4.755	-0.729	0.894	0.014	1.527	0.018	0.069
CS13-6	9.998	1.090	14.006	2.843	4.384	-1.040	0.843	0.016	1.755	0.018	0.063
CS13-7	4.754	1.623	15.144	4.989	5.321	-1.508	0.769	0.024	2.818	0.020	0.059
CS13-8	2.359	1.592	13.272	3.179	4.906	-1.250	0.940	0.018	1.815	0.018	0.065
CS13-9	5.235	1.419	15.109	2.878	5.719	-0.958	0.959	0.017	2.010	0.019	0.079
CS13-10	3.061	0.805	10.268	6.040	3.963	-1.024	0.557	0.019	1.081	0.021	0.064
CS13-11	2.387	1.946	16.378	4.771	6.123	-1.299	0.998	0.022	2.542	0.021	0.065
CS13-12	3.395	1.805	13.496	3.217	4.964	-1.133	0.730	0.022	1.915	0.019	0.066
CS13-13	2.813	1.397	12.566	2.599	4.869	-0.960	0.788	0.016	1.340	0.019	0.071
CS13-14	1.334	0.953	12.580	12.279	4.619	-4.894	0.626	0.015	1.713	0.013	0.001
CS13-15	6.333	1.065	12.910	2.004	4.410	-0.746	0.654	0.016	1.446	0.018	0.067
CS13-16	2.627	1.351	13.642	2.643	4.976	-0.761	0.854	0.017	2.018	0.018	0.058
CS13-19	1.816	0.949	8.040	3.287	3.330	-1.284	0.501	0.011	1.060	0.011	0.032
CS13-20	2.631	1.401	12.561	6.953	4.612	-2.785	0.827	0.022	1.764	0.018	0.037
CS13-21	4.474	1.346	14.005	3.275	4.975	-1.325	0.841	0.016	2.097	0.019	0.057
CS13-22	12.293	1.005	13.519	3.865	3.620	0.158	0.627	0.014	1.453	0.021	0.043

CS13-23	6.751	0.669	9.815	1.951	3.258	-0.779	0.491	0.014	1.133	0.016	0.045
CS13-24	5.307	1.021	13.777	4.771	4.711	-2.034	0.780	0.010	1.470	0.017	0.051

Trace Elements

Sample	B (ppb)	P (ppb)	Cu (ppb)	Zn (ppb)	Rb (ppb)	Sr (ppb)	Zr (ppb)	Ba (ppb)	La (ppb)	Ce (ppb)
CS01-1	3.5	407.7	198.9	-39.5	21.0	10.8	9.1	40.2	4.0	7.5
CS01-2	-1.2	390.4	9.4	-29.6	9.5	4.4	3.8	16.3	1.7	3.0
CS01-3	8.4	451.3	1.3	-49.9	17.2	10.4	6.7	38.3	3.8	7.3
CS01-4	16.2	442.4	2.0	-46.0	40.4	23.6	15.5	100.8	8.5	16.2
CS13-1	11.7	420.0	0.3	-49.8	12.4	7.4	6.8	18.9	3.0	5.5
CS13-2	5.7	376.1	8.1	-51.9	14.1	9.2	10.5	28.5	4.1	8.0
CS13-3	3.7	383.1	0.2	-52.5	8.0	7.4	5.6	14.9	2.9	5.7
CS13-4	-1.7	408.4	0.7	-36.4	8.9	10.4	7.2	27.4	4.0	8.0
CS13-5	9.1	453.5	0.4	-48.9	29.4	19.8	17.1	74.8	7.7	15.6
CS13-6	5.9	396.6	0.2	-51.4	18.7	13.4	11.2	48.4	6.0	11.7
CS13-7	0.9	410.7	0.4	-38.2	13.9	8.7	7.5	35.9	3.7	7.3
CS13-8	5.6	380.3	0.1	-52.4	17.7	11.9	11.4	41.3	6.5	12.5
CS13-9	7.4	425.3	1.9	-37.8	28.1	16.4	11.2	66.1	6.6	12.8
CS13-10	3.1	408.5	-0.2	-52.1	13.4	14.1	7.5	43.9	6.2	12.6
CS13-11	1.9	419.8	1.1	-35.1	20.4	11.3	10.2	48.6	4.7	9.0
CS13-12	4.0	428.8	0.8	-49.5	17.8	12.5	9.0	47.6	5.2	10.8
CS13-13	5.2	374.4	0.0	-52.3	21.5	14.7	10.5	61.4	6.3	12.5
CS13-14	-0.1	411.8	13.7	-52.8	5.3	2.3	2.8	0.7	1.4	2.7
CS13-15	5.6	404.5	0.2	-51.4	23.2	16.7	11.5	69.5	6.8	13.6
CS13-16	6.7	450.7	2.6	-34.4	25.6	16.4	13.8	64.0	6.4	12.5
CS13-19	3.4	358.7	86.1	-52.3	13.2	7.6	7.9	20.1	3.2	6.1
CS13-20	3.5	406.3	188.8	-51.4	7.9	6.1	5.4	13.5	2.7	5.1
CS13-21	7.8	366.1	0.1	-52.1	18.0	11.3	9.9	39.8	4.5	8.5
CS13-22	3.3	397.5	0.2	-47.4	9.0	11.0	7.6	22.2	3.9	7.9
CS13-23	6.8	396.5	0.5	-52.2	15.2	15.0	13.0	44.5	6.7	13.5
CS13-24	3.1	395.2	1.3	-53.0	12.3	7.5	6.7	21.9	3.1	6.0

Trace Elements (cont'd).

Sample	Pr (ppb)	Nd (ppb)	Sm (ppb)	Eu (ppb)	Gd (ppb)	Yb (ppb)	Hf (ppb)	Pb (ppb)	Th	U
CS01-1	0.9	2.9	0.5	0.1	0.4	0.2	0.6	-0.2	1.2	0.3
CS01-2	0.4	1.2	0.3	0.0	0.2	0.2	0.4	-0.6	0.7	0.2
CS01-3	0.9	2.8	0.5	0.1	0.4	0.2	0.7	-0.3	1.1	0.3
CS01-4	1.9	7.0	1.2	0.2	1.0	0.4	1.2	0.8	2.4	0.6
CS13-1	0.7	2.0	0.3	0.1	0.3	0.2	0.4	-0.6	0.8	0.2
CS13-2	0.9	3.3	0.5	0.1	0.4	0.2	0.6	-0.5	1.2	0.4
CS13-3	0.7	2.4	0.5	0.1	0.4	0.2	0.4	-0.6	1.0	0.3
CS13-4	1.0	3.5	0.7	0.1	0.6	0.2	0.5	-0.4	1.3	0.3
CS13-5	1.8	6.1	1.2	0.2	1.0	0.4	0.9	0.4	2.3	0.6
CS13-6	1.4	4.8	0.9	0.2	0.7	0.6	0.6	0.6	1.9	0.5
CS13-7	0.9	2.8	0.4	0.1	0.4	0.2	0.4	-0.3	1.1	0.3
CS13-8	1.5	5.2	0.8	0.1	0.7	0.3	0.5	-0.1	1.8	0.5
CS13-9	1.4	5.3	0.8	0.2	0.7	0.3	0.6	0.3	1.8	0.5
CS13-10	1.5	5.5	1.1	0.2	1.0	0.3	0.9	0.0	1.8	0.4
CS13-11	1.0	3.4	0.6	0.1	0.5	0.3	0.5	-0.3	1.4	0.3
CS13-12	1.2	4.4	0.8	0.1	0.7	0.3	0.7	0.8	1.5	0.4
CS13-13	1.4	5.3	1.0	0.1	0.7	0.4	0.7	0.1	1.8	0.4
CS13-14	0.3	1.1	0.2	0.0	0.2	0.1	0.2	-0.9	0.4	0.1
CS13-15	1.5	5.8	1.0	0.2	0.8	0.4	0.6	0.2	2.0	0.5
CS13-16	1.4	5.2	0.8	0.1	0.6	0.3	0.7	0.0	1.9	0.5
CS13-19	0.7	2.4	0.5	0.1	0.4	0.2	0.5	-0.5	1.0	0.3
CS13-20	0.6	2.1	0.4	0.1	0.3	0.2	0.3	-0.5	0.7	0.2
CS13-21	1.0	3.7	0.6	0.1	0.5	0.2	0.5	-0.2	1.3	0.4
CS13-22	1.0	3.2	0.6	0.1	0.6	0.2	0.5	-0.5	1.4	0.3
CS13-23	1.5	5.7	1.0	0.2	0.8	0.3	1.1	0.1	2.0	0.5
CS13-24	0.7	2.4	0.4	0.1	0.4	0.1	0.5	-0.5	0.8	0.2

Appendix E: U isotope data

Var Data

Sample name	(234U/238U)	2σ
CS01_1	0.905	0.001
CS01_2	0.922	0.002
CS01_3	0.961	0.006
CS01_4	0.931	0.002
CS13_1	0.880	0.001
CS13_2	0.898	0.002
CS13_3	0.926	0.002
CS13_4	0.960	0.001
CS13_5	0.904	0.002
CS13_6	0.923	0.001
CS13_7	0.960	0.001
CS13_8	0.933	0.001
CS13_9	0.943	0.001
CS13_10	0.972	0.002
CS13_11	0.901	0.001
CS13_12	0.930	0.001
CS13_13	0.929	0.002
CS13_14	0.927	0.001
CS13_15	0.943	0.001
CS13_16	0.911	0.001
CS13_17	0.916	0.002
CS13_18	0.926	0.002
CS13_19	0.926	0.001
CS13_20	0.920	0.002
CS13_21	0.908	0.002
CS13_22	0.941	0.002
CS13_23	0.938	0.002
CS13_24	0.905	0.001
CS13_25	0.925	0.002
CS13_26	0.925	0.001

Hokitika Data

Sample Name	($^{234}U/^{238}U$)	2σ
T14_M_01	1.000	0.007
T14_M_20	0.992	0.004
T14_M_30	0.981	0.007
T14_M_40	0.998	0.007
T14c_50	0.979	0.008
T14_M_60	0.968	0.004
T14_M_70	1.000	0.007
T14_L2_M_80	0.992	0.006
T14_M_90	0.993	0.006
T14_M_100	0.976	0.010
T14_110	0.992	0.007
T14_M_120	0.992	0.012
T14_M_130	0.990	0.007
T14_M_140	0.996	0.005
T14_M_170	0.984	0.007
T14_L2_M_180	0.989	0.007
T14_190	1.001	0.007
T14_200	0.991	0.005
T14_210	0.980	0.007
T14_220	0.966	0.011
T14_L1_230	0.902	0.004
T14_240	0.975	0.005
T14_250	0.978	0.007
T14_260	0.992	0.008
T14_M_270	0.988	0.006
T14_280	0.999	0.009
T14_L2_290	0.986	0.006
T14_L2_300	0.983	0.006
T14_L2_310	0.960	0.001
T14_NL_320	0.974	0.005
GSP-2	1.048	0.005
QLO-1	1.007	0.005
Blank	1.123	0.090

Appendix F: U isotope method evaluation data

Var Data

Sample	($^{234}U/^{238}U$)	2σ
Secondary Standard (U005A)	0.625	0.003
Rock standard blank (GSP2)	0.989	0.004
Sequential leaching blank	1.003	0.013
CS13_14 (1) carbonate leached	0.928	0.003
CS13_14 (2) carbonate leached	0.921	0.003
CS13_11 carbonate leached	0.874	0.003
CS13_14 (1) FeMnOx leached	0.873	0.004
CS13_14 (2) FeMnOx leached	0.872	0.004
CS13_11 FeMnOx leached	0.923	0.002
CS13_14 (1) organics leached	0.960	0.003
CS13_14 (2) organics leached	0.990	0.004
CS13_11 organics leached	0.973	0.004
CS13_14 (1) HF/HCl etch 2hr	0.929	0.003
CS13_14 (2) HF/HCl etch 2hr	0.949	0.002
CS13_11 HF/HCl etch 2hr	0.948	0.004
CS13_14 (1) HF/HCl etch 4hr	0.909	0.003
CS13_14 (2) HF/HCl etch 4hr	0.944	0.004
CS13_11 HF/HCl etch 4hr	0.949	0.004
CS13_14 (1) HF/HCl etch 6hr	0.920	0.003
CS13_14 (2) HF/HCl etch 6hr	0.931	0.003
CS13_11 HF/HCl etch 6hr	0.949	0.004
CS13_14 (1) HF/HCl etch 8hr	0.918	0.004
CS13_14 (2) HF/HCl etch 8hr	0.932	0.003
CS13_11 HF/HCl etch 8hr	0.939	0.002
CS13_14 (1) initial	0.977	0.004
CS13_14 (2) initial	0.964	0.003
CS13_11 initial	0.964	0.003

Hokitika Data

Sample Name	($^{234}U/^{238}U$)	2σ
T14_M_170 exchangeables leached	1.101	0.011
T14_M_170 carbonates leached	0.99	0.006
T14_M_170 FeMnOx leached	0.968	0.002
T14_M_170 organics leached	0.977	0.008
T14_M_170 2hrs HF/HCl etch	0.991	0.004
T14_M_170 4hrs HF/HCl etch	0.998	0.009
T14_M_170 6hrs HF/HCl etch	0.992	0.008
T14_M_170 8hrs HF/HCl etch	0.998	0.003
T14_190 exchangeables leached	1.017	0.05
T14_190 2hrs HF/HCl etch	0.993	0.003
T14_190 2hrs HF/HCl etch	0.994	0.002
T14_190 4hrs HF/HCl etch	0.996	0.009
T14_190 6hrs HF/HCl etch	1.001	0.005
T14_190 8hrs HF/HCl etch	1.017	0.05
QLO1 Rock Standard	1.006	0.003